

# Exploring Logistic Functions as Robust Alternatives to Hill Functions in Genetic Network Modeling

M. Belgacem Ismail

ismail.belgacem.81@gmail.com

Mezaourou, Ghazaouet, Tlemcen, Algeria

## Abstract

Gene regulatory networks and related biological systems exhibit sigmoidal response dynamics, which are traditionally modeled using Hill functions. These functions capture cooperative molecular binding through fractional exponents. However, when Hill coefficients assume non-integer values, a ubiquitous occurrence in experimental parameter fitting, these functions lose differentiability at low expression levels, creating singularities that compromise numerical stability, complicate bifurcation analysis, and impede control-theoretic applications. We present a systematic framework that replaces Hill functions with logistic functions throughout biological network modeling, utilizing increasing logistic functions for activation and decreasing logistic functions for repression. Logistic functions preserve sigmoidal switching characteristics while offering decisive mathematical advantages: global infinite differentiability, closed-form self-referential derivatives that significantly simplify Jacobian computations, analytically invertible forms enabling feedback linearization, and intrinsic representation of non-zero basal expression without *ad hoc* modifications. We establish rigorous theoretical foundations through existence and uniqueness theorems with explicit Lipschitz bounds, demonstrating that logistic-based systems possess globally Lipschitz continuous vector fields, guaranteeing unique solutions and uniform boundedness in positive invariant rectangles. We develop systematic parameter estimation methodologies with biologically motivated threshold selection that preserve local input-output sensitivity, validated through comprehensive case studies including genetic oscillators, positive autoregulation in *Escherichia coli*, and two-gene networks exhibiting chaos and extreme events. Numerical simulations with experimentally derived parameters reveal quantitative advantages: in positive autoregulation, logistic models enable noise-driven escape from low-expression traps through basal production, while Hill-based models remain irreversibly trapped, directly relevant to systems like the *gal* operon and bacterial bistable circuits. We demonstrate that logistic functions respond to absolute concentrations rather than logarithmic fold changes, aligning with empirical evidence from bacterial gene regulation, mammalian transcription factor studies, and NF- $\kappa$ B signaling, where regulatory decisions depend on exact molecule counts per cell. We outline control-theoretic advantages, including continuous controllability even at zero expression levels (which is absent in Hill models), seamless integration with model predictive control through closed-form inverses, and superior numerical stability in sliding mode implementations. Extensions to the logit transformation lay the foundations for inferring gene regulatory networks from single-cell RNA-seq data, leveraging strict log-likelihood concavity for guaranteed global convergence and native handling of zero-inflated dropout events. Additional applications span immunological dynamics (T-cell activation thresholds, cytokine feedback), hematopoiesis with delay-induced oscillations (characteristic equation simplification for Hopf bifurcations in cyclic neutropenia), and environmental systems (microbial growth in bioreactors). By delivering models that are simultaneously biologically realistic, analytically tractable, and computationally robust, the logistic framework advances precision modeling capabilities for synthetic biology circuit design, therapeutic intervention strategies, metabolic engineering optimization, and genome-scale network analysis.

# 1 Introduction

Our core idea is straightforward: we propose replacing the classical Hill-type sigmoidal functions, the traditional choice across biological modeling, with logistic functions, which furnish substantially improved analytical tractability. This substitution delivers tangible benefits: mathematical analysis becomes more transparent and rigorous, parameter estimation from experimental measurements becomes more robust, and the foundation for synthesizing feedback control systems and state observers becomes practical where previously it was intractable. The framework applies across a diverse spectrum of biological domains: gene regulatory networks, cellular proliferation dynamics, hematopoietic tissue formation, epidemiological disease transmission, immunological responses, pharmacodynamic drug action, neural circuit dynamics, tumor growth progression, and microbial bioprocess engineering, among numerous other contexts. Beyond theoretical advances, this framework has immediate practical implications for synthetic biology and biotechnology. Logistic-based models enable robust design of genetic circuits with predictable behavior under noisy cellular conditions, facilitate real-time control of engineered biosynthetic pathways through model predictive control strategies, and provide computationally efficient frameworks for genome-scale metabolic engineering, where thousands of regulatory interactions must be simulated simultaneously.

Gene regulatory networks orchestrate cellular decision-making through coupled differential equation systems. We have explored numerous modeling strategies to identify approaches that simultaneously achieve biological fidelity and analytical tractability, enabling both system understanding and control design. The references [1, 2, 3, 4] document this rich history of methodological development. The central challenge is formidable: biological networks exhibit strong nonlinear coupling across many interacting components, operate simultaneously across disparate timescales, and resist decomposition into independent subsystems. Hill functions have dominated this landscape for decades, becoming the *de facto* standard for encoding activation and inhibition dynamics in genetic networks [5, 6, 7, 8, 9]. Their enduring appeal derives from genuine strengths that capture cooperative molecular binding, threshold-like regulatory transitions, and the empirically observed sigmoidal response curves. Yet beneath this success lies a subtle mathematical fragility: the fractional exponents essential to Hill function definitions, while mechanistically motivated, create analytical obstacles that multiply rapidly in high-dimensional systems [10]. A natural question thus arises: why not employ step functions that toggle abruptly between on and off states? The answer reveals the fundamental inadequacies of naïve simplification. Step functions are mathematically undefined at the threshold values corresponding to regulatory switches, which precludes the rigorous definition of solutions across these critical transitions [6, 11]. Piecewise-linear approximations of sigmoidal responses, while analytically tractable for qualitative analysis in certain parameter regimes [12, 13], inherit these discontinuities and require sophisticated mathematical frameworks to handle switching behaviors rigorously. Beyond technical pathology, step functions encode unrealistic biology: they presume instantaneous, all-or-nothing switching. Biological reality is gentler; regulatory transitions unfold gradually, with genes responding smoothly across a range of inducer concentrations rather than at a single magic threshold. A sigmoidal function with moderate steepness better captures this empirical behavior. Yet extremely steep sigmoidal responses corresponding to large Hill coefficients  $n$  are themselves often biologically implausible and computationally hazardous. Rigorous analysis of two-dimensional systems with steep sigmoidal nonlinearities reveals that while qualitative dynamics may converge across functional forms as steepness increases, numerical integration becomes increasingly unstable and sensitive to perturbations [14]. In practice, synthetic biologists who engineer genetic circuits face this trade-off directly: achieving switch-like responses requires high cooperativity, but numerical instabilities with large Hill coefficients ( $n > 5$ ) complicate circuit optimization and parameter tuning in computational design platforms like Cello and Genetdes [15, 16, 17]. The logistic framework resolves this tension by providing tunable steepness through the parameter  $\lambda$  with linear scaling properties that maintain numerical stability even for sharp transitions.

The Hill coefficient  $n$  itself merits careful examination. Operationally, experimentalists measure promoter activity over a range of inducer concentrations, fit sigmoidal curves to experimental data, and extract the Hill coefficient  $n$  as a quantitative measure of response steepness and local input–output sensitivity. This data-driven estimation captures the empirical response without requiring the imposition of detailed mechanistic assumptions. Nevertheless,  $n$  often admits a mechanistic interpretation as well: under cooperative

binding conditions, where multiple transcription factors or ligands must interact or where allosteric effects amplify the response,  $n$  approximates the number of interacting binding sites or the degree of cooperativity. The lac operon exemplifies this principle: the Hill coefficient  $n \approx 2-3$  reflects tetramer-mediated repression and DNA looping by LacI, enabling smooth IPTG-dependent induction rather than abrupt phase transitions [18, 19, 20, 21, 22]. Such a mechanistic understanding directly informs synthetic biology applications: engineered toggle switches and oscillators in *E. coli* and yeast rely on precisely tuned cooperative binding (typically  $n = 2-4$ ) to achieve bistable memory devices, programmable cellular timers, and biosensors with sharp dose-response thresholds [23, 24, 25]. The logistic framework presented here provides a mathematically tractable alternative for designing and optimizing these circuits, without sacrificing the sigmoidal characteristics essential for switch-like behavior. Across naturally occurring and engineered gene regulatory networks, Hill coefficients typically cluster in the range  $n = 1$  to 4, capturing realistic molecular interactions without invoking extreme ultrasensitivity. This moderate range proves instructive. Hemoglobin's cooperative oxygen binding ( $n \approx 2.8$ ) achieves sufficient steepness for efficient oxygen loading in the lungs and unloading in tissue, yet remains gradual enough to prevent catastrophic threshold behavior that would destabilize oxygen homeostasis [10, 22, 21]. Similarly, transcriptional regulatory networks across biology employ Hill coefficients in this range ( $n = 1-4$ ), where dimer or tetramer formation of transcription factors generates robust, tunable responses [26, 10, 27, 28, 29, 30, 31]. Rare exceptions exist; certain signaling cascades exhibit  $n > 4$ , producing sharp, switch-like responses, yet these exceptional cases incur a cost: heightened computational instability and biological implausibility in most regulatory contexts [10, 26, 27]. The Hill coefficient  $n$  in biochemical and gene regulatory models can also take values between 0 and 1, which typically indicates negative cooperativity, where the binding of one ligand or transcription factor hinders subsequent bindings, leading to a shallower response curve compared to non-cooperative systems [32, 33, 34]. Beyond providing analytical advantages for modeling known regulatory architectures, logistic functions offer compelling benefits for *inferring* unknown gene regulatory networks from experimental data. The logit transformation, which is the inverse of the logistic function, maps probabilities to log-odds ratios, forming the mathematical foundation of logistic regression. This enables principled probabilistic inference of regulatory interactions from binary or binarized expression data. This framework proves particularly valuable for analyzing single-cell RNA sequencing (scRNA-seq) datasets, which exhibit extreme sparsity and pervasive dropout events where expressed genes incorrectly appear unexpressed due to low molecule counts and stochastic capture inefficiencies. The logistic function's smooth, bounded structure ensures numerical stability when handling zero-inflated data, while its analytically tractable derivatives enable efficient gradient-based optimization for parameter estimation. The strict concavity of the log-likelihood function ensures convergence to a unique global maximum, thereby avoiding the local optima that plague Hill-based formulations. Moreover, seamless integration with elastic net regularization enables simultaneous feature selection and coefficient shrinkage in high-dimensional settings where potential regulatory interactions vastly outnumber observations. These advantages position logistic regression as a promising methodology for genome-scale network reconstruction from single-cell data, though comprehensive validation and experimental benchmarking remain important directions for future investigation. Complicating matters further, experimental fitting often yields non-integer Hill coefficients when cooperative mechanisms are incomplete or heterogeneous, in which case  $n$  functions as a purely phenomenological parameter extracted from data rather than reflecting a clear molecular mechanism.

To circumvent these difficulties and resolve discontinuities at regulatory thresholds, alternative approaches have emerged, most notably, the use of ramp function approximations. This strategy models the transition between inactive and active regulatory states as a smooth, linear change across an interval, requiring the specification of two threshold values (representing the onset and offset of the ramp) rather than a single inflection point. While conceptually appealing, this method trades one set of complications for another: two thresholds introduce additional parameter burden, and the assumed linearity within the transition region often lacks biological justification [8, 7, 35]. We propose a more direct resolution: abandon the Hill framework and adopt logistic functions, which provide superior mathematical structure, analytical tractability, and the biological advantages elaborated throughout this paper.

In this paper, we propose a more direct path forward: systematically replace both increasing and decreasing Hill functions with their logistic counterparts, which deliver equivalent sigmoidal response profiles while

offering superior mathematical structure suited to biological network modeling. Logistic functions have established themselves as versatile tools across statistics and machine learning [36, 37, 38, 39]. Their applicability extends beyond traditional statistical inference into complex networked systems. In network engineering, for example, logistic functions model control dynamics within virtual network topologies, enabling swift reconfiguration as traffic demands fluctuate across IP-over-wavelength-routed WDM infrastructure [40]. In approximation theory, logistic functions serve as activation functions in feedforward neural networks, where they establish sharp error bounds for function approximation, with convergence rates characterized by their smoothness properties [41]. This demonstrates their utility in proving that approximation errors remain bounded by established limits.

Within the gene regulatory network literature, Samuilik et al. [42] investigated logistic function representations for GRN modeling. However, their approach borrowed strategies from network engineering contexts, employing a single increasing logistic function form. This choice reflects a compromise: GRNs operate under distinct constraints, gene concentrations remain positive, and regulatory thresholds carry specific biological meaning. Yet, modeling both activation and repression within a unified increasing logistic framework, with weights encoding regulatory direction, necessarily sacrifices precision. Subsequent studies have perpetuated this formulation [42, 43, 44, 45, 46, 47, 48]. Yet, this compromise carries a cost: the approach fails to adequately preserve the distinct sigmoidal dynamics of activation versus repression, and it obscures biological realism, particularly when regulatory circuits require an explicit separation of activatory and inhibitory pathways. Our investigation takes a fundamentally different direction. Rather than forcing both regulatory modes into a single increasing sigmoid, we distinguish sharply between increasing and decreasing logistic functions, deploying each where biologically appropriate. This formulation preserves biological interpretability: a gene activated by one regulator and repressed by another is naturally represented by an increasing sigmoid for the activator and a decreasing sigmoid for the repressor, enabling transparent construction of composite regulatory logic (AND gates, OR gates, AND-NOT mechanisms) that would be obscured in single-function approaches [42].

This investigation examines logistic functions as a mathematically principled alternative to Hill functions within genetic network modeling, with particular emphasis on analytical tractability, computational feasibility, and their potential integration with control-theoretic methods and observer synthesis. Logistic functions are a biologically realistic alternative to Hill functions for modeling gene regulatory networks and related biological systems. Hill-type functions, despite their prevalence in gene regulatory and biochemical modeling, carry inherent analytical burdens: they resist closed-form analysis and forfeit differentiability when Hill coefficients assume non-integer values, a common occurrence in empirical parameter estimation. We systematically replace Hill nonlinearities with logistic functions, which yield models that are globally smooth ( $C^\infty$ ) and possess analytically invertible closed forms. We rigorously establish the existence and uniqueness of equilibrium points in logistic-based dynamical systems through our main theoretical result, which proves global existence, smoothness, and boundedness of solutions, complemented by explicit Lipschitz bounds that guarantee numerical stability. We provide rigorous theoretical foundations, demonstrate systematic replacement strategies, catalog comprehensive mathematical and computational advantages, establish biological realism through basal expression modeling, develop classical parameter estimation methodologies with detailed case studies, and outline pathways for control-theoretic applications and extensions to diverse biological domains. While certain ambitious applications remain as future work, the framework presented here provides a solid mathematical foundation and a practical modeling toolkit that advances the field beyond the limitations of the Hill function.

The practical advantages of our framework for increasing and decreasing logistic functions extend to industrial biotechnology and therapeutic applications. In metabolic engineering, where production pathways involve dozens of regulated enzymes, the logistic formulation's computational efficiency should enable rapid *in silico* screening of genetic modifications and dynamic control strategies for optimizing biofuel, pharmaceutical, and biochemical production [49, 50]. In therapeutic contexts, the framework should facilitate model-based design of engineered T-cells with tunable activation thresholds for cancer immunotherapy and provides mathematical foundations for optogenetic control of insulin secretion in diabetes treatment [51, 52, 53]. The enhanced numerical stability and analytical tractability directly translate to faster design-build-test cycles

in these applications.

The paper’s structure reflects a progression from mathematical foundations to biological applications. First, we derive the equivalent logistic forms for gene regulatory network modeling, establishing the systematic replacement strategy for both activation and repression dynamics. The increasing logistic function replaces the increasing Hill function, while the decreasing logistic function replaces the decreasing Hill function. Critically, we establish the parameter relationship that preserves local input-output sensitivity at the half-maximal point, ensuring functional equivalence between the two frameworks while maintaining biological interpretability.

We then systematically catalog the mathematical and computational advantages of logistic functions over their Hill counterparts. We demonstrate that logistic functions possess: (i) closed-form derivatives with elegant self-referential structure, significantly simplifying Jacobian computations for stability analysis; (ii) analytically invertible forms, enabling feedback linearization and rapid threshold calculations; (iii) global infinite differentiability across the entire domain, eliminating the singularities that plague Hill functions with non-integer exponents near the origin; (iv) well-behaved linear approximations via hyperbolic identities and Taylor expansions, facilitating perturbation analysis; and (v) superior computational efficiency, avoiding the power operations that introduce numerical instability in Hill formulations. For non-integer Hill coefficients-ubiquitous in experimental parameter fitting, the Hill derivative diverges to infinity as concentration approaches zero, creating singularities that cause numerical integration failures, compromised stability analysis through ill-conditioned Jacobians, and limitations in control applications. We demonstrate through concrete analysis how the exponential structure of logistic functions maintains smooth, bounded behavior throughout the biologically relevant domain, with uniform bounds on derivatives ensuring well-conditioned numerical algorithms.

Subsequently, we develop the core modeling framework for classical logistic-based gene regulatory networks. Beginning with non-cooperative networks, where each gene responds to a single regulator, we present a general dynamical model with sign parameters that encode regulatory direction. The canonical genetic oscillator, a two-gene negative feedback loop, serves as our primary illustrative example. Through explicit Jacobian analysis exploiting the self-referential derivative form, we establish local asymptotic stability conditions and demonstrate that this two-dimensional system cannot exhibit Hopf bifurcations in the absence of time delays. The framework naturally extends to arbitrarily large multi-gene networks, preserving analytical advantages even in high-dimensional settings. Our formulation distinguishes sharply between increasing and decreasing logistic functions, deploying each where biologically appropriate to maintain regulatory interpretability. For parallel regulation, we construct the regulatory function as a product structure, naturally accommodating any combination of regulatory inputs while enabling transparent construction of composite regulatory logic, including AND gates, OR gates, and AND-NOT mechanisms. A detailed comparative analysis of alternative formulations is presented, focusing on the unique increasing weighted logistic function approach proposed by Samuilik and colleagues, which aggregates all regulatory inputs into a single weighted sum that is passed through one increasing logistic function per gene. We rigorously establish that our product-of-logistics formulation offers superior biological interpretability through regulator-specific thresholds that can be determined independently of experimental dose-response curves, explicit encoding of activation versus repression through the function form rather than the weight sign, and a direct correspondence between mathematical parameters and measurable biological quantities. Importantly, we demonstrate through concrete analysis that the Samuilik repression formulation exhibits problematic behavior: the critical point occurs at negative concentrations, and the function remains very low across the entire biologically relevant domain, never approaching unity for repression. This analysis motivates our explicit use of decreasing logistic functions for repression, which naturally capture the expected biological behavior. We illustrate the framework’s richness through a comprehensive case study of a two-gene network with mutual activation and self-repression, originally studied using Hill-based delay differential equations. This system exhibits complex behaviors, including periodic oscillations, deterministic chaos, and extreme events. We reformulate the system using logistic functions throughout, preserving the extreme events while facilitating easier sensitivity analysis and providing a foundation for systematic control design.

Furthermore, we address a critical aspect of biological realism that Hill functions systematically neglect:

non-zero basal expression. Gene regulatory systems exhibit persistent basal activity; even under strong repression, promoters exhibit low-level transcription. The logistic function captures this naturally, maintaining a positive value even at zero activator concentration, ensuring continuous production even without activators. This non-zero output depends solely on the product of steepness and threshold parameters and requires no additional parameters, in stark contrast to Hill functions, where production vanishes at zero input. We demonstrate the practical consequences through two canonical examples. In the genetic oscillator, simulations under strong degradation and near-zero initial conditions reveal that the Hill model becomes trapped in a low-expression state, while the logistic model maintains positive production, enabling the system to escape the off-state and reach the expected equilibrium. The positive autoregulation example provides an extensive case study grounded in *Escherichia coli* physiology, using experimentally derived parameters. Through rigorous bifurcation analysis, we establish critical amplification values for bistability. With biophysically realistic parameters, both models predict monostability at the high state. However, numerical simulations show that the logistic model escapes the off-state in approximately 44 minutes due to basal production, while the Hill model remains trapped at low expression, unable to escape without external perturbation. This quantitatively validates the theoretical insight that the inherent basal expression of logistic models enables noise-driven recovery from near-zero states, directly relevant to the *gal* operon and related systems. For repression functions, logistic formulations offer complementary advantages. The decreasing logistic function yields tunable unrepresored rates that approach, but need not equal, unity, reflecting biological constraints such as resource limitations. We introduce a scaled logistic function that achieves exactly unit value at zero repressor concentration when desired, providing flexibility to match either idealized Hill behavior or realistic imperfections depending on the biological context.

Moreover, we outline the control advantages that logistic functions provide, emphasizing that the non-zero response at minimal expression levels ensures continuous controllability even when gene expression drops to zero, whereas Hill functions create controllability gaps. Multiple control strategies become tractable: multiplicative control, steepness modulation, sliding mode control, state-feedback control, and model predictive control. While this discussion provides a conceptual foundation and a strategic overview, detailed implementation and validation of these control strategies remain directions for future work.

Parameter estimation receives detailed treatment. The logistic function's mathematical properties prove particularly advantageous: global smoothness and analytically tractable derivatives should ensure that gradient-based optimization algorithms converge efficiently and reliably. Crucially, logistic functions naturally encode basal expression through the steepness and threshold parameters, enabling bidirectional inference. We demonstrate the parameter fitting methodology through a comprehensive analysis of the two-gene self-inhibitory and mutually activating network, matching both the basal expression rate and the local activation slope. We advocate for biologically motivated threshold selection where thresholds represent concentrations at which regulatory transitions occur. Numerical validation confirms a close agreement between the fully logistic system and the original formulation, establishing the effectiveness of the parameter matching strategy.

Furthermore, translating the mathematical advantages of logistic functions, closed-form inverses, global smoothness, convex optimization landscapes, and self-referential derivatives into practical GRN inference requires a coherent computational strategy that addresses the unique challenges of single-cell data: extreme sparsity, technical dropout, and the curse of dimensionality in genome-scale network reconstruction. We proposed a four-stage inference pipeline that synergistically combines preprocessing strategies to enhance data quality, temporal constraints to enforce causal ordering, regularized regression to leverage the logistic framework's computational strengths, and logic extraction to recover interpretable regulatory architectures. Each stage leverages specific mathematical properties established earlier, while preparing the data and intermediate results for subsequent stages, thereby creating an end-to-end workflow that spans from raw scRNA-seq measurements to validated, biologically interpretable regulatory networks.

We then discuss extensions beyond gene regulatory networks to immunology, epidemiology, and environmental systems. In immunology and hematopoiesis, logistic functions naturally encode T-cell activation thresholds, cytokine feedback loops, and the saturation of immune responses. We present the canonical hematopoiesis model, where the elegant self-referential derivative significantly simplifies the analysis of char-

acteristic equations for identifying critical delays that trigger Hopf bifurcations, manifesting clinically as cyclic neutropenia. In environmental engineering, logistic functions can replace Hill and Monod equations for microbial growth in bioreactors, while in epidemiology, they approximate age-related susceptibility curves. These extensions, while conceptually established, represent directions for future detailed investigation.

Finally, the discussion provides crucial insights into the relationship between Hill and logistic functions through the lens of input scaling. We demonstrate that the two functions are mathematically equivalent under a logarithmic change of variables. This equivalence reveals a fundamental distinction: logistic functions with linear input respond to absolute concentrations, while Hill functions assume logarithmic or relative scaling. We argue extensively that biological regulation typically depends on absolute concentrations rather than log-scaled ones, marshaling evidence from bacterial gene regulation, mammalian transcription factor studies, NF- $\kappa$ B signaling, and toxicology. This analysis justifies our choice of linear-input logistic functions as the appropriate framework for biological concentration responses, particularly for capturing promoter leakiness and low-expression dynamics.

## 2 Derivation of the Equivalent Logistic Forms for Gene Regulatory Network Modeling.

Establishing rigorous equivalence between Hill and logistic formulations requires careful construction.

**Construction of the increasing form.** For activation dynamics, we begin with the increasing standard logistic function, as detailed in [54, 41, 55]:

$$f(s) = \frac{1}{1 + e^{-s}}.$$

This canonical form is centered at  $s = 0$ , where the function attains the value 1/2, and exhibits unit steepness in the exponential argument. To adapt this function for gene regulation, we must introduce two modifications:

1. **Adjustable steepness:** We incorporate a parameter  $\lambda > 0$  to control the transition sharpness, yielding

$$f(s, \lambda) = \frac{1}{1 + e^{-\lambda s}}.$$

Larger values of  $\lambda$  produce steeper sigmoids, analogous to higher Hill coefficients  $n$  in cooperative binding.

2. **Threshold alignment:** Since biological regulation responds to absolute concentration levels rather than deviations from zero, we shift the inflection point to the regulatory threshold  $\theta$  by substituting  $s = x - \theta$ . This translation ensures the function is centered at the biologically meaningful concentration  $x = \theta$ .

Therefore, for activation dynamics, we define here  $f^+(x, \theta, \lambda) = f(x - \theta, \lambda)$ , where the argument  $s = x - \theta$  ensures the desired monotonicity: as the regulator concentration  $x$  increases, so does  $s$ , and consequently  $f^+(x, \theta, \lambda)$  increases strictly monotonically from values near zero (when  $x \ll \theta$ ) to values approaching unity (when  $x \gg \theta$ ).

**Construction of the decreasing form.** For repression, we require a function that decreases with increasing regulator concentration. We achieve this by reversing the sign in the exponential. Specifically, we define here the standard decreasing logistic function by :

$$f(s, \lambda) = \frac{1}{1 + e^s},$$

Similarly, we introduce steepness through  $\lambda$  and shift the inflection point to  $\theta$ , yielding

$$f^-(x, \theta, \lambda) = \frac{1}{1 + e^{\lambda(x-\theta)}}.$$

The positive coefficient in the exponential ensures strict monotonic decrease: as  $x$  rises above  $\theta$ , the denominator grows exponentially, driving the function value toward zero. Equivalently, we may write this as

$$f^-(x, \theta, \lambda) = \frac{1}{1 + e^{-\lambda(\theta-x)}},$$

making explicit that repression responds to the signed deviation  $\theta - x$  rather than  $x - \theta$ .

In summary: The **activation** is modeled by the increasing Hill function  $h^+(x, \theta, n) = \frac{x^n}{x^n + \theta^n}$ , now replaced by the increasing logistic function  $f^+(x, \theta, \lambda) = \frac{1}{1 + e^{-\lambda(x-\theta)}}$ . The **repression** is modeled by the decreasing Hill function  $h^-(x, \theta, n) = \frac{\theta^n}{x^n + \theta^n}$ , now replaced by the decreasing logistic function  $f^-(x, \theta, \lambda) = \frac{1}{1 + e^{\lambda(x-\theta)}} = \frac{1}{1 + e^{-\lambda(\theta-x)}}$ . In both cases, the parameters  $n$  and  $\lambda$  govern the steepness of the sigmoidal response, quantifying how sharply the regulatory function transitions from its lower to upper asymptote. The threshold parameter  $\theta$  marks the concentration at which the regulatory effect is half-maximal, serving as the inflection point of the sigmoid curve.

Replacing Hill functions with logistic functions preserves essential biological realism: adjustable steepness (via  $\lambda$ , analogous to the Hill coefficient  $n$ ), flexible thresholds ( $\theta$ ), and sigmoidal switching that phenomenologically captures cooperativity without requiring explicit multi-site binding mechanistic assumptions.

The logistic sigmoid for gene activation, expressed parametrically as  $f(x) = \frac{1}{1 + e^{-\lambda(x-\theta)}}$ , exhibits distinct mathematical advantages grounded in its fundamental structure. This formulation guarantees global infinite differentiability ( $C^\infty$ ) where all derivatives exist and remain continuous everywhere, including at critical boundary points such as the origin ( $x = 0$ ). For the increasing logistic function  $f(x) = \frac{1}{1 + e^{-\lambda(x-\theta)}}$  with  $\lambda > 0$ , strict monotonicity holds: the function increases from  $f(-\infty) = 0$  to  $f(+\infty) = 1$ , with first derivative  $f'(x) = \lambda f(x)(1 - f(x)) > 0$  everywhere. The second derivative  $f''(x) = \lambda^2 f(x)(1 - f(x))(1 - 2f(x))$  exhibits sign change at the inflection point  $x = \theta$  (where  $f(\theta) = 1/2$ ). Consequently, the function displays convexity for  $x < \theta$  (accelerating growth phase) and concavity for  $x > \theta$  (decelerating saturation phase), with maximum slope  $f'(\theta) = \lambda/4$  at the inflection point. This S-shaped (sigmoid) profile naturally captures threshold-activated gene expression, emulating the cooperative switching observed in biological gene regulation.

Conversely, for gene repression, the decreasing logistic function  $f^-(x) = \frac{1}{1 + e^{\lambda(x-\theta)}}$  shares these mathematical advantages due to its analogous structure. This formulation also ensures global infinite differentiability ( $C^\infty$ ), with all derivatives existing and maintaining continuity across the entire domain, including at pivotal points such as the inflection threshold ( $x = \theta$ ). The decreasing logistic function  $f^-(x) = \frac{1}{1 + e^{\lambda(x-\theta)}}$  also exhibits strict monotonic decrease from  $f^-(-\infty) = 1$  to  $f^-(+\infty) = 0$ , with first derivative  $f'^-(x) = -\lambda f^-(x)(1 - f^-(x)) < 0$  for all  $x$ . The second derivative  $f''^-(x) = \lambda^2 f^-(x)(1 - f^-(x))(1 - 2f^-(x))$  changes sign at inflection point  $x = \theta$  (where  $f^-(\theta) = 1/2$ ). The function is concave for  $x < \theta$  (decelerating descent from maximum expression) and convex for  $x > \theta$  (accelerating approach to minimal expression), with maximum slope magnitude  $|f'^-(\theta)| = \lambda/4$  at the inflection point. This decreasing sigmoidal curve naturally represents repressive regulation, where an increasing repressor concentration progressively silences target gene expression through a smooth, biologically realistic transition.

### 3 Properties and Analytical Advantages in Gene Regulatory Network Modeling

This section establishes the mathematical foundation justifying the logistic-based formulation, which features the explicit selection of decreasing and increasing functions for GRN modeling, particularly in large-scale systems where analytical tractability and computational efficiency supersede concerns about mechanistic binding details. Logistic and Hill functions both generate smooth sigmoidal response curves with tunable steepness and threshold behavior. However, logistic functions achieve this biological fidelity while circumventing the

analytical pathologies inherent to Hill formulations: fractional exponents that complicate symbolic manipulation, power-law singularities at boundary points, and ill-conditioned numerical behavior. Logistic functions provide globally smooth, analytically invertible models with well-established mathematical properties, rendering them particularly well-suited for systems biology. Their pervasive smoothness and differentiability make them ideally suited for modeling biological networks, where analytical rigor is paramount.

We consider the increasing form  $f^+(x, \theta, \lambda) = \frac{1}{1+e^{-\lambda(x-\theta)}}$  (See above for more detailed derivations) and the decreasing form  $f^-(x, \theta, \lambda) = \frac{1}{1+e^{\lambda(x-\theta)}} = \frac{1}{1+e^{-\lambda(\theta-x)}}$  (See above for more detailed derivations), which are parametrized versions of the standard increasing logistic function  $f(s) = \frac{1}{1+e^{-s}}$  (see [54, 41, 55]) and the standard decreasing logistic function  $f(s) = \frac{1}{1+e^s}$  (defined above). These increasing and decreasing parametric logistic functions possess a constellation of mathematically elegant and computationally useful properties. We enumerate these key properties:

- **Closed-Form Derivative with Self-Referential Structure:** The derivatives admit remarkably elegant closed forms. For the increasing function,  $\frac{\partial f^+}{\partial x} = \lambda \frac{e^{-\lambda(x-\theta)}}{(1+e^{-\lambda(x-\theta)})^2}$ , which simplifies via the self-referential property:  $\frac{\partial f^+}{\partial x} = \lambda f^+(x, \theta, \lambda)(1 - f^+(x, \theta, \lambda))$ . For the decreasing function,  $\frac{\partial f^-}{\partial x} = -\lambda \frac{e^{\lambda(x-\theta)}}{(1+e^{\lambda(x-\theta)})^2}$ , which simplifies to  $\frac{\partial f^-}{\partial x} = -\lambda f^-(x, \theta, \lambda)(1 - f^-(x, \theta, \lambda))$ . These elegant forms substantially accelerate analytical work in multiple ways. First, Jacobian matrices in stability analysis are simplified to simple algebraic operations, rather than requiring the evaluation of cumbersome power-law terms. The self-referential structure means that computing the derivative requires only knowledge of the function's value itself, without the need for complex rational expressions or fractional exponents. Consequently, eigenvalue analysis, perturbation expansions, and bifurcation studies become analytically tractable in dimensions where Hill functions would necessitate numerical approximation. The bounded nature of these derivatives provides an additional advantage: since  $f^+(x) \in (0, 1)$ , the product  $f^+(1 - f^+)$  is always bounded by 1/4, ensuring  $|\frac{\partial f^+}{\partial x}| \leq \lambda/4$ . This uniform bound holds across the entire domain, guaranteeing that the system's Jacobian remains well-conditioned and avoiding the derivative blow-ups that plague Hill functions at the origin for non-integer coefficients.
- **Symmetry Property Around the Inflection Point:** The parametric logistic functions exhibit a fundamental symmetry:  $f^+(x, \theta, \lambda) = 1 - f^-(x, \theta, \lambda)$ , and conversely  $f^-(x, \theta, \lambda) = 1 - f^+(x, \theta, \lambda)$ , centered at the inflection point  $x = \theta$  where both functions equal 1/2. This symmetry provides a natural probabilistic interpretation, as the functions balance positive and negative deviations from the threshold symmetrically, facilitating the transformation of mixed activation-repression networks into unified mathematical formulations. The logistic framework achieves both regulatory modes through simple sign changes in the argument, preserving the same mathematical structure and enabling elegant unified analysis of complex regulatory architectures.
- **Analytically Invertible Closed Form:** The inverse functions possess elementary closed forms. For the increasing function, solving  $y = f^+(x, \theta, \lambda)$  yields  $x = \theta + \frac{1}{\lambda} \ln\left(\frac{y}{1-y}\right)$  for  $y \in (0, 1)$ , equivalently written as  $x = \theta - \frac{1}{\lambda} \ln\left(\frac{1}{y} - 1\right)$ . For the decreasing function, solving  $y = f^-(x, \theta, \lambda)$  yields  $x = \theta + \frac{1}{\lambda} \ln\left(\frac{1-y}{y}\right)$ , equivalently  $x = \theta + \frac{1}{\lambda} \ln\left(\frac{1}{y} - 1\right)$ . This invertibility is indispensable for control-theoretic applications, enabling feedback linearization transformations that convert nonlinear gene regulatory dynamics into linear systems through exact coordinate changes. In model predictive control (MPC) for synthetic biology, the closed-form inverse enables the rapid computation of control inputs that achieve desired regulatory outputs, thereby streamlining the online optimization required for MPC implementation. Additionally, the inverses facilitate parameter estimation by converting implicit model-fitting problems into linear regression on a log-odds scale, and enable rapid threshold calculations from steady-state data. The logit transformation  $\text{logit}(y) = \ln\left(\frac{y}{1-y}\right)$  forms the foundation of logistic regression, a powerful tool for inferring gene regulatory networks from binary expression data. By contrast, Hill functions of the form  $h(x) = \frac{x^n}{K^n + x^n}$  admit an explicit inverse  $h^{-1}(y) = K \left(\frac{y}{1-y}\right)^{1/n}$

only in closed form, yet this formulation introduces power-law nonlinearities. For non-integer  $n$ , which commonly arise in empirical fits to experimental data, the fractional exponent  $1/n$  complicates both symbolic manipulation and numerical evaluation, particularly when combined with optimization algorithms requiring repeated inverse evaluations.

- **Global Infinite Differentiability ( $C^\infty$ ):** The parametric logistic functions are infinitely differentiable ( $C^\infty$ ) across their entire domain, with all derivatives continuous everywhere, including boundary points. This universality contrasts sharply with Hill functions when Hill coefficients  $n$  assume non-integer values, a ubiquitous occurrence in experimental data fitting. For non-integer  $n$ , Hill derivatives become singular or infinite at the origin ( $x = 0$ ), creating numerical instability and precluding rigorous stability or bifurcation analysis. The  $C^\infty$  property of logistic functions has profound implications for observer design and state estimation in gene regulatory networks. When reconstructing unmeasured gene expression levels from partial measurements, observer algorithms rely on computing Jacobian matrices at each time step. The guaranteed smoothness of logistic derivatives ensures these Jacobian computations remain numerically stable across the entire state space, including the biologically critical low-expression regimes where Hill functions exhibit pathological behavior. For nonlinear systems, observability, which represents the ability to reconstruct hidden states from measured outputs, depends on the rank of the observability matrix constructed from successive Lie derivatives. Hill functions with cooperative repression ( $n > 1$ ) yield zero derivatives at the origin, causing the observability matrix to lose rank precisely where robust state estimation is most crucial under basal conditions, where expression levels naturally fluctuate near zero.
- **Well-Behaved Linear Approximation:** The parametric logistic functions satisfy exact hyperbolic identities:  $f^+(x, \theta, \lambda) = \frac{1}{2} + \frac{1}{2} \tanh\left(\frac{\lambda(x-\theta)}{2}\right)$  and  $f^-(x, \theta, \lambda) = \frac{1}{2} - \frac{1}{2} \tanh\left(\frac{\lambda(x-\theta)}{2}\right)$ . Applying the Taylor expansion  $\tanh(z) \approx z + \mathcal{O}(z^3)$  for small  $z$  yields the linear approximations:  $f^+(x, \theta, \lambda) \approx \frac{1}{2} + \frac{\lambda(x-\theta)}{4}$  and  $f^-(x, \theta, \lambda) \approx \frac{1}{2} - \frac{\lambda(x-\theta)}{4}$  for small deviations from  $x = \theta$ . These transparent linear forms facilitate perturbation theory, bifurcation analysis around equilibria, and analytical approximations in regimes where nonlinearities remain moderate.

These mathematical properties collectively enable rigorous local stability computations such as Jacobian matrix evaluations in feedback-regulated circuits while simultaneously supporting global dynamical analysis via Lyapunov function construction, all while preserving the sigmoidal switching behavior that phenomenologically captures cooperative regulatory mechanisms. Hill functions, by contrast, rely fundamentally on non-integer exponents whose fractional powers create insurmountable analytical obstacles: integration becomes intractable, stability analysis suffers from singularities at boundary points, parameter fitting to experimental data yields non-integer Hill coefficients that destroy differentiability, and observer design encounters rank-deficient observability matrices. Logistic functions circumvent these pathologies entirely through their global infinite differentiability ( $C^\infty$ ), computational efficiency arising from exponential rather than power-law structure, provision of closed-form derivatives and analytically invertible expressions, and maintenance of full-rank observability across the entire biologically relevant domain.

To crystallize these comparative advantages, we employ the following, using the increasing Hill and logistic functions as our primary illustrative case study, thereby establishing a framework that extends naturally to repressive regulation. The decreasing Hill function,  $h^-(x, \theta, n) = \frac{\theta^n}{x^n + \theta^n}$ , is replaced by its logistic counterpart,  $f^-(x, \theta, \lambda) = \frac{1}{1 + e^{\lambda(x-\theta)}}$ . The mathematical properties and analytical advantages for the decreasing case mirror those of the increasing logistic formulation; consequently, the fundamental principles governing mathematical tractability, stability analysis, observer design, and control design remain essentially identical. We therefore proceed with a detailed analysis of the increasing case, with the understanding that decreasing regulatory modes follow by straightforward analogy, thereby maintaining rigor while economizing on exposition.

### 3.1 Mathematical Pathologies of Hill Functions at the Origin

Hill functions, conventionally formulated as  $h^+(x, \theta, n) = \frac{x^n}{\theta^n + x^n}$  for gene activation, emerge from mechanistic equilibrium analysis of ligand-receptor binding kinetics, yet have transcended their original biophysical context to become the standard regulatory nonlinearity across gene regulatory network (GRN) modeling. Within GRN frameworks, Hill functions encode cooperative binding effects through the Hill coefficient  $n > 0$ , which simultaneously quantifies two critical properties: the degree of molecular cooperativity (the number of interacting binding sites or the strength of allosteric effects) and the steepness of the sigmoidal regulatory response. The dissociation constant  $\theta > 0$  represents the inducer or ligand concentration at which the response reaches half-maximal, functioning as a biological threshold that gates regulatory activation [10, 56].

Mathematical tractability depends critically on the nature of the Hill coefficient. When  $n$  takes positive integer values, Hill functions maintain global infinite differentiability ( $C^\infty$ ) across the entire domain, including at boundary points such as the origin  $x = 0$ , enabling smooth analytical manipulations, Taylor expansions, and stable numerical implementations. Yet this analytical grace vanishes in practical parameter estimation from real biological data. When Hill models are fitted to experimental measurements of gene expression versus inducer concentration, the resulting Hill coefficients frequently assume non-integer values [57, 10, 58, 59], a ubiquitous phenomenon reflecting incomplete cooperativity, heterogeneous binding site occupancy, or complex allosteric mechanisms that resist simple integer-valued interpretations. This transition from integer to non-integer Hill coefficients precipitates a catastrophic loss of mathematical structure: differentiability collapses specifically at the origin  $x = 0$ , generating singularities that render the system mathematically ill-posed and computationally unstable, thereby introducing formidable obstacles to rigorous analysis, numerical simulation, observer design, and control implementation.

For non-integer Hill coefficients, the loss of differentiability at the origin exhibits distinct pathological behavior depending on the specific range of  $n$ . When  $0 < n < 1$ , the fractional exponent in the Hill function's derivative causes the first derivative to diverge to infinity as  $x \rightarrow 0^+$ , creating a singularity with infinite slope where the function exhibits a sharp cusp-like profile at the origin that destroys smoothness. For  $1 < n < 2$ , the first derivative remains finite at  $x = 0$ , but higher-order derivatives (such as the second derivative) become unbounded due to negative exponents in the derivative expressions, rendering the function only finitely differentiable, specifically,  $C^{\lfloor n \rfloor}$  rather than  $C^\infty$ , where  $\lfloor n \rfloor$  denotes the floor function, the largest integer not exceeding  $n$ , which tells us the highest derivative order that remains continuous. This cascade of differentiability loss from undefined first derivatives through bounded-but-unbounded higher derivatives percolates through every downstream analytical and computational task: integration of differential equations becomes numerically intractable as ODE solvers encounter stiffness and reject adaptively small time steps near the origin; stability analysis via linearization suffers from ill-conditioned Jacobian matrices with singular or near-singular entries; bifurcation studies lose rigor when Taylor expansions around equilibria become impossible; observer design encounters rank-deficient observability matrices that prevent state reconstruction from partial measurements; and large-scale numerical simulations accumulate errors catastrophically in low-expression regimes where the singularities concentrate [56, 60]. Hill functions pose numerical challenges in gradient-based methods when non-integer exponents result in origin singularities.

To understand the fundamental limitations of Hill functions, consider the standard activation form  $h^+(x, \theta, n) = \frac{x^n}{\theta^n + x^n}$ . Near  $x = 0$ , the substitution  $t = x^n/\theta^n$  reveals that  $h^+(x, \theta, n) = \frac{t}{1+t} = t - t^2 + t^3 - \dots$ , yielding leading behavior proportional to  $x^n$  for small  $x$ . The derivatives exhibit increasingly severe singularities as we approach the origin. The first derivative

$$h'(x) = \frac{n\theta^n x^{n-1}}{(\theta^n + x^n)^2}$$

behaves asymptotically as  $h'(x) \sim \frac{n}{\theta^n} x^{n-1}$  as  $x \rightarrow 0^+$ . Similarly, the second derivative satisfies  $h''(x) \sim \frac{n(n-1)}{\theta^n} x^{n-2}$  near the origin. More generally, the  $m$ -th derivative  $h^{(m)}(x)$  is proportional to  $x^{n-m}$  ( $h^{(m)}(x) \propto x^{n-m}$ ) as  $x \rightarrow 0^+$ , with prefactor given by the falling factorial  $n(n-1) \cdots (n-m+1) = \Gamma(n+1)/\Gamma(n-m+1)$ .

**Critical consequences for non-integer Hill coefficients.** These asymptotic forms create severe problems when  $n$  is non-integer, a ubiquitous situation in experimental parameter estimation:

- **For  $0 < n < 1$ :** The first derivative diverges,  $h'(x) \rightarrow \infty$  as  $x \rightarrow 0^+$ , creating a vertical tangent or cusp-like singularity at the origin. The function is not differentiable at  $x = 0$ . This infinite slope creates insurmountable numerical difficulties for optimization algorithms, ODE solvers, and observer design methods that rely on gradient information. In control applications, the unbounded derivative prevents reliable linearization around low-expression equilibria, undermining feedback controller synthesis.
- **For  $1 < n < 2$ :** While  $h'(0) = 0$  exists and is finite, the second derivative explodes:  $h''(x) \rightarrow \infty$  as  $x \rightarrow 0^+$ , indicating unbounded curvature. This limits the function to  $C^1$  (once continuously differentiable) at the origin, preventing the use of Newton-Raphson methods, Hessian-based optimization, and second-order sensitivity analysis. Bifurcation studies become intractable near low-expression steady states because they require the computation of second derivatives, which are essential for detecting saddle-node bifurcations or Hopf bifurcations.
- **For  $n \in (k, k + 1)$  where  $k \geq 1$ :** Derivatives of order  $m > [n]$  diverge at the origin. The Hill function is only  $C^{[n]}$  at  $x = 0$ , not  $C^\infty$ . This finite differentiability class restricts the applicability of advanced analytical techniques that require arbitrary-order derivatives, such as center manifold theory, normal form analysis, and high-order perturbation methods.

Away from the origin on any domain  $(\delta, \infty)$  with  $\delta > 0$ , the function remains analytic as a rational composition of smooth terms. However, the origin-specific pathologies persist and cannot be circumvented by restricting the domain, as biological systems frequently operate in or pass through low-expression regimes. While the function itself is well-defined and continuous at  $x = 0$  with  $h^+(0) = 0$ , the higher-order smoothness failure stems directly from the fractional power-law terms, introducing singularities that cascade through derivatives.

Consider some concrete cases: when  $n \in (0, 1)$ , we get an infinite slope at zero; when  $n \in (1, 2)$ , the slope vanishes but curvature explodes; and for  $n \in (k, k + 1)$  with  $k \geq 1$ , all derivatives beyond the  $k$ -th diverge at the origin. These pathologies become particularly problematic in cooperative regulatory systems, where empirical Hill coefficients commonly fall within the range  $n \approx 1.5$  to  $n \approx 3.5$ , creating second- and third-order derivative singularities that destabilize numerical methods.

These undefined higher derivatives create serious complications for dynamical analysis. They interfere with Jacobian calculations at equilibrium points, which are essential for determining local stability through eigenvalue analysis. They obscure the bifurcation structure by preventing the construction of normal forms that require smooth coordinate changes. They invalidate Taylor series expansions around zero, eliminating a primary tool for local approximation. They complicate Lyapunov exponent computations, which require derivatives of the flow map. In observer design, they cause the observability matrix, constructed from successive Lie derivatives of the output function, to lose rank at the origin for  $n > 1$ , rendering hidden states unobservable precisely in the low-expressivity regimes where robust state estimation is most crucial. The resulting analytical blind spots can mask important dynamics such as oscillations, multistability, noise-induced transitions, or behaviors induced by time delays that would otherwise be accessible through standard techniques.

### 3.1.1 Practical Consequences for Modeling and Analysis

This loss of infinite differentiability at the origin creates substantial obstacles across multiple domains:

**Numerical integration failures.** When solving ODEs that model gene regulatory networks, these singularities can cause numerical solvers to fail, exhibit stiffness, or need excessively small time steps near low-concentration regimes (such as basal expression levels). This leads to computational inefficiency, numerical instability, and inaccuracies in large-scale simulations involving many interacting genes. Adaptive step-size algorithms may repeatedly reject time steps, resulting in a significant increase in computational cost. Stiffness ratios, the ratio of the fastest to slowest timescales, can become arbitrarily large near the origin, forcing implicit solvers designed for stiff equations to increase their per-step computational burden.

In high-dimensional GRN models with hundreds of genes, these numerical pathologies compound, potentially rendering simulation infeasible within reasonable computational budgets.

**Compromised stability analysis.** Computing Jacobians for equilibria, performing bifurcation studies, constructing Taylor expansions, and calculating Lyapunov exponents all require well-behaved derivatives. The undefined (higher) derivatives complicate these derivations, potentially masking or distorting subtle dynamic behaviors such as oscillations, multistability, or delay-induced phenomena. For instance, determining the stability of an equilibrium point  $x^*$  near the origin requires computing the Jacobian matrix  $J(x^*)$  and analyzing its eigenvalues. If components of  $x^*$  are small and Hill functions with non-integer  $n$  govern the dynamics, the Jacobian entries may be undefined, infinite, or numerically unreliable, preventing rigorous stability assessment. Bifurcation analysis for identifying parameter values where qualitative changes in dynamics occur becomes especially problematic, as standard continuation methods rely on smooth parameter-dependent Jacobians that Hill functions cannot provide near the origin.

**Control theory limitations.** Observer design and control applications, particularly techniques relying on higher-order approximations, feedback linearization, or pole placement, are severely impeded by this lack of smoothness. Observer design for state estimation from partial measurements requires computing the observability matrix, which depends on successive Lie derivatives of the output function. For Hill functions with  $n > 1$ , the vanishing derivative at the origin causes the observability matrix to lose rank, making it impossible to reconstruct unmeasured gene expression levels when concentrations are low, particularly in the regime where measurement noise and dropout events are most problematic in single-cell experiments. Feedback linearization techniques that rely on exact coordinate transformations fail when the nonlinear function lacks a smooth inverse. Model predictive control (MPC), which requires repeated solution of optimization problems involving the system model, encounters numerical difficulties when the model exhibits singularities in its derivatives. Systems may display ill-conditioned responses or require ad-hoc regularizations near zero, ultimately limiting the scalability, robustness, and reliability of models for complex biological networks. The logistic function circumvents all these issues through its exponential structure, which remains  $C^\infty$  everywhere, ensuring smooth Jacobians, well-conditioned observability matrices, and tractable linearization procedures across the entire biologically relevant domain.

**Parameter estimation challenges.** Fitting Hill models to experimental data becomes problematic when non-integer  $n$  values provide the best fit. Standard nonlinear least-squares algorithms (Levenberg-Marquardt, Gauss-Newton) rely on computing gradients and, often, Hessians of the residual function with respect to parameters. When the model involves Hill functions evaluated near zero, which is common in time-series data capturing gene expression dynamics from off to on states, the derivative singularities propagate into the parameter gradients, causing optimization algorithms to stall, converge slowly, or reach incorrect local minima. Confidence intervals and parameter uncertainty estimates derived from the inverse Fisher information matrix become unreliable when the model's Hessian is ill-conditioned. By contrast, the smooth structure of logistic functions ensures stable parameter estimation even from sparse, noisy data.

### 3.2 Analytical Tractability: Integration and Series Expansions

Beyond smoothness, the logistic function offers superior analytical properties. Its antiderivative has a closed form:

$$\begin{aligned} \int f(x) dx &= (x - \theta) + \frac{1}{\lambda} \ln(1 + e^{-\lambda(x-\theta)}) + C \\ &= \frac{1}{\lambda} \ln(1 + e^{\lambda(x-\theta)}) + C. \end{aligned} \tag{1}$$

which is both computationally efficient and enables exact solutions for transient dynamics in simple GRN motifs such as auto-repressors or feedforward loops. This closed-form antiderivative proves invaluable when solving differential equations using the separation of variables method or when computing integrals arising

in moment calculations for stochastic models. Definite integrals over bounded domains can be evaluated numerically with high precision using standard quadrature methods without encountering the convergence issues that plague Hill function integrals. In specialized contexts, such as computing partition functions in thermodynamic models of gene regulation or evaluating cumulative distribution functions in non-equilibrium statistical mechanics, the logistic integral relates to the dilogarithm function  $\text{Li}_2(z)$ , a well-studied special function with efficient numerical implementations.

The Taylor series expansion around the inflection point  $x = \theta$  provides excellent local approximations:

$$f(x) = \frac{1}{2} + \frac{\lambda}{4}(x - \theta) - \frac{\lambda^3}{48}(x - \theta)^3 + \frac{\lambda^5}{480}(x - \theta)^5 + \mathcal{O}((x - \theta)^6).$$

This rapidly converging series facilitates Jacobian-based stability analysis, higher-order perturbation expansions in bifurcation studies, and reduced-order modeling of multi-gene interactions. The coefficients decay factorially, ensuring that low-order truncations provide accurate approximations in a substantial neighborhood of the inflection point. These analytical tractabilities should prove particularly valuable in stochastic GRN simulations, where the smooth, differentiable form integrates seamlessly into Gillespie algorithms for low-copy-number regimes, thereby minimizing discretization errors and variance in propensity evaluations (see [61] for more details). The series structure also enables symbolic computation packages to derive analytical expressions for derived quantities such as eigenvalues, Lyapunov functions, and normal forms that would require purely numerical methods for Hill-based models.

### 3.2.1 The Integration Problem for Hill Functions

In stark contrast to the logistic function's elementary antiderivative, the Hill function lacks closed-form antiderivatives for general  $n$ . The integral

$$\int \frac{\xi^n}{\theta^n + \xi^n} d\xi$$

poses significant analytical challenges that escalate rapidly with increasing complexity of the Hill coefficient  $n$ .

**Case  $n = 1$ : Michaelis-Menten Kinetics.** For the simplest non-trivial case, we compute:

$$\int \frac{\xi}{\theta + \xi} d\xi = \int \frac{(\theta + \xi) - \theta}{\theta + \xi} d\xi \quad (2)$$

$$= \int \left(1 - \frac{\theta}{\theta + \xi}\right) d\xi \quad (3)$$

$$= \xi - \theta \ln |\theta + \xi| + C. \quad (4)$$

**Case  $n = 2$ : Cooperative Binding.** The complexity escalates for  $n = 2$ . We begin by algebraic manipulation:

$$\int \frac{\xi^2}{\theta^2 + \xi^2} d\xi = \int \left(1 - \frac{\theta^2}{\theta^2 + \xi^2}\right) d\xi \quad (5)$$

$$= \xi - \theta^2 \int \frac{1}{\theta^2 + \xi^2} d\xi. \quad (6)$$

The remaining integral requires the standard arctangent formula  $\int \frac{1}{a^2 + x^2} dx = \frac{1}{a} \arctan\left(\frac{x}{a}\right) + C$ :

$$\int \frac{\xi^2}{\theta^2 + \xi^2} d\xi = \xi - \theta^2 \cdot \frac{1}{\theta} \arctan\left(\frac{\xi}{\theta}\right) + C \quad (7)$$

$$= \xi - \theta \arctan\left(\frac{\xi}{\theta}\right) + C. \quad (8)$$

This expression involves both algebraic and inverse trigonometric functions, significantly complicating symbolic integration in dynamical systems analysis.

**General Case: Series Representation via Substitution.** For arbitrary  $n$ , we employ the substitution  $u = \xi/\theta$ , which yields  $d\xi = \theta du$ :

$$\int \frac{\xi^n}{\theta^n + \xi^n} d\xi = \theta \int \frac{u^n}{1 + u^n} du. \quad (9)$$

To evaluate this integral, we decompose the integrand:

$$\frac{u^n}{1 + u^n} = 1 - \frac{1}{1 + u^n}. \quad (10)$$

For  $|u^n| < 1$  (which corresponds to  $|\xi| < \theta$  in the original variable), we apply the geometric series:

$$\frac{1}{1 + u^n} = \sum_{k=0}^{\infty} (-1)^k u^{nk}. \quad (11)$$

This expansion is valid within the radius of convergence and allows term-by-term integration:

$$\int \frac{1}{1 + u^n} du = \int \sum_{k=0}^{\infty} (-1)^k u^{nk} du \quad (12)$$

$$= \sum_{k=0}^{\infty} (-1)^k \int u^{nk} du \quad (13)$$

$$= \sum_{k=0}^{\infty} (-1)^k \frac{u^{nk+1}}{nk+1} \quad (14)$$

$$= u - \frac{u^{n+1}}{n+1} + \frac{u^{2n+1}}{2n+1} - \frac{u^{3n+1}}{3n+1} + \dots \quad (15)$$

Substituting back:

$$\int \frac{u^n}{1 + u^n} du = \int \left( 1 - \frac{1}{1 + u^n} \right) du \quad (16)$$

$$= u - \sum_{k=0}^{\infty} (-1)^k \frac{u^{nk+1}}{nk+1} \quad (17)$$

$$= u - \left( u - \frac{u^{n+1}}{n+1} + \frac{u^{2n+1}}{2n+1} - \frac{u^{3n+1}}{3n+1} + \dots \right) \quad (18)$$

$$= \frac{u^{n+1}}{n+1} - \frac{u^{2n+1}}{2n+1} + \frac{u^{3n+1}}{3n+1} - \dots \quad (19)$$

Returning to the original variable  $\xi = \theta u$ :

$$\int \frac{\xi^n}{\theta^n + \xi^n} d\xi = \theta \sum_{k=1}^{\infty} (-1)^{k+1} \frac{u^{kn+1}}{kn+1} + C = \sum_{k=1}^{\infty} (-1)^{k+1} \frac{\xi^{kn+1}}{\theta^{kn}(kn+1)} + C. \quad (20)$$

**Connection to Special Functions.** For non-integer  $n$ , this series cannot be summed in terms of elementary functions. Instead, the antiderivative requires hypergeometric functions  ${}_2F_1$  or incomplete beta functions  $B_z(a, b)$ . Specifically, through the substitution  $v = u^n$  (so  $du = \frac{1}{n}v^{1/n-1}dv$ ), we obtain

$$\int \frac{u^n}{1 + u^n} du = \frac{1}{n} \int \frac{v^{1/n}}{1 + v} dv, \quad (21)$$

which is  $\frac{1}{n+1}v^{1+1/n} {}_2F_1\left(1, 1 + \frac{1}{n}; 2 + \frac{1}{n}; -v\right) + C$  after further manipulation [62].

**Computational and Analytical Implications.** The complexity of these integrals has several profound consequences:

- **Computationally expensive to evaluate:** Numerical evaluation requires adaptive quadrature methods (such as Gauss-Kronrod rules) with careful error control. For non-integer  $n$ , each function evaluation may require iterative computation of special functions, multiplying computational cost by factors of 10–100 compared to elementary operations.
- **Not amenable to symbolic manipulation:** The lack of closed forms prevents derivation of analytical formulas for equilibrium points (which require solving  $\int f(x) dx = g(x)$  type equations), basin boundaries in multistable systems, or bifurcation curves where parameter-dependent integrals determine stability transitions.
- **Limited qualitative insights:** Without explicit closed forms, the dependence on parameters  $(\theta, n)$  remains opaque. Asymptotic analysis near boundaries or perturbation theory for small parameter variations becomes intractable, preventing the kind of intuitive understanding that closed-form solutions provide.
- **Numerical instability near  $\xi = 0$ :** The derivative singularities for non-integer  $n$  at the origin (discussed in Section 3.1) propagate into integration routines. When  $0 < n < 1$ , the integrand's derivative  $\frac{\partial}{\partial \xi} \left( \frac{\xi^n}{\theta^n + \xi^n} \right) \sim \xi^{n-1}$  diverges as  $\xi \rightarrow 0^+$ , causing adaptive integrators to refine step sizes excessively, leading to inefficiency or failure.
- **Series convergence issues:** The power series representation converges only for  $|\xi| < \theta$ . For  $\xi > \theta$  (supra-threshold concentrations common in gene regulation), alternative representations or numerical methods are mandatory. The rate of convergence deteriorates as  $\xi \rightarrow \theta^-$ , requiring  $O(1/\epsilon)$  terms to achieve accuracy  $\epsilon$ , making practical summation infeasible for high precision.

**Impact on Systems Biology Applications.** In applications requiring repeated integration, parameter sweeps that explore  $10^3$ – $10^5$  parameter combinations, Monte Carlo simulations with  $10^4$ – $10^6$  samples, and Bayesian inference via Markov chain Monte Carlo with  $10^5$ – $10^7$  likelihood evaluations, the cumulative computational cost of numerically integrating Hill functions becomes prohibitive. Each integration may consume  $10^2$  to  $10^4$  function evaluations, depending on the required accuracy and  $n$ -value.

By contrast, logistic functions possess closed-form antiderivatives:

$$\int \frac{1}{1 + e^{-\lambda(x-\theta)}} dx = x + \frac{1}{\lambda} \ln(1 + e^{-\lambda(x-\theta)}) + C, \quad (22)$$

evaluable via elementary operations (one exponential, one logarithm, one division) with  $O(1)$  cost per evaluation. This enables orders-of-magnitude speedups: what might require hours or days for Hill-based inference can be completed in minutes or hours with logistic formulations, directly impacting the feasibility of genome-scale network inference and real-time control applications.

This analytical burden motivates the adoption of the logistic framework, where mathematical tractability directly translates to practical feasibility for modern systems biology applications that demand rigorous statistical inference and real-time control.

### 3.3 Closed-Form Derivatives and Inverses

Logistic functions possess remarkably concise closed-form expressions for both derivatives and inverses, making them highly suitable for control design, bifurcation analysis, and symbolic computation. The derivative's self-referential form

$$f'(s) = \lambda f(s)(1 - f(s))$$

simplifies analytical derivations significantly, particularly in stability analysis of ODE systems. Crucially, this avoids fractional powers, reducing symbolic complexity. When computing the Jacobian matrix for a multi-gene network, each entry involving a logistic regulatory function simplifies to an algebraic expression in terms of the current state, avoiding the rational functions with power-law terms that arise for Hill models. This simplification propagates through eigenvalue calculations: the characteristic polynomial's coefficients become simpler algebraic expressions, often enabling symbolic computation of stability boundaries in parameter space that would require purely numerical methods for Hill-based models.

The inverse also admits an elementary closed form. For activation,

$$f^{-1}(y) = \theta + \frac{1}{\lambda} \ln \left( \frac{y}{1-y} \right),$$

and for repression,

$$g^{-1}(y) = \theta - \frac{1}{\lambda} \ln \left( \frac{y}{1-y} \right).$$

These closed-form inverses should enable powerful control-theoretic techniques. Feedback linearization can transform nonlinear GRN dynamics into linear systems amenable to classical linear control methods, and model predictive control (MPC) should become tractable for synthetic biology designs, thereby enhancing robustness to parameter uncertainties [63, 64, 65]. In feedback linearization, one computes a state-dependent coordinate transformation that eliminates nonlinearities; having an explicit inverse function is often essential for constructing such transformations. In MPC, one repeatedly solves optimization problems involving the system model; smooth, invertible nonlinearities should significantly improve optimizer convergence and robustness.

Moreover, the steepness parameter  $\lambda$  provides linear, predictable tuning, promoting numerical stability even at high values. This contrasts sharply with the Hill coefficient  $n$ , which introduces nonlinear sensitivity that often causes numerical instability at large values, particularly in large-scale simulations or when dealing with delay differential equations. When  $n \gg 1$ , Hill functions become increasingly switch-like, with near-vertical transitions that challenge ODE solvers requiring small time steps. The logistic function's exponential structure, by contrast, maintains smooth transitions even for large  $\lambda$ , with the steepness increasing linearly rather than exhibiting the factorial-like growth in derivative magnitude characteristic of high-order power laws.

### 3.3.1 Hill Functions' Derivatives and Inverses Issues

While Hill functions exhibit smooth asymptotic behavior away from the origin, their response is highly sensitive to the Hill coefficient  $n$ , yielding complex curve shapes that increase computational complexity. Hill derivatives involve fractional powers, for instance:

$$h^{+'}(x) = \frac{nx^{n-1}\theta^n}{(x^n + \theta^n)^2},$$

which is substantially more complex symbolically than the logistic's  $f'(s) = \lambda f(s)(1 - f(s))$  with  $s = (x - \theta)$  for activation. The Hill derivative requires evaluating two power functions and a rational function, whereas the logistic derivative requires one exponential and simple arithmetic. This complexity difference multiplies when computing higher derivatives, multivariable gradients in high-dimensional systems, or derivatives with respect to parameters for sensitivity analysis.

Critically, while the Hill function  $h^+(x, \theta, n) = \frac{x^n}{x^n + \theta^n}$  itself remains well-defined at  $x = 0$  with  $h^+(0) = 0$ , its derivative  $h^{+'}(x)$  exhibits singular behavior at the origin for non-integer Hill coefficients. Specifically,  $h^{+'}(x) = \frac{n\theta^n x^{n-1}}{(x^n + \theta^n)^2}$  diverges to infinity as  $x \rightarrow 0^+$  when  $0 < n < 1$ , creating numerical instabilities in gradient-based optimization algorithms and compromising the conditioning of Jacobian matrices required for stability analysis and linearization. For  $1 < n < 2$ , while  $h^{+'}(0) = 0$  exists and is finite, the second derivative  $h^{''}(x) \sim x^{n-2}$  becomes unbounded as  $x \rightarrow 0^+$ , limiting the function to  $C^{[n]}$  differentiability rather than

$C^\infty$  smoothness. These limitations pose substantial challenges in high-dimensional biological networks: for instance, analyzing a 50-gene regulatory network where each gene responds to multiple regulators requires computing a  $50 \times 50$  Jacobian matrix at equilibrium. When equilibrium points occur near basal expression states (low concentrations), Hill-based models with empirically fitted non-integer coefficients encounter ill-conditioned or rank-deficient Jacobians due to the accumulated singularities, whereas logistic-based models maintain well-conditioned numerical stability through their globally bounded derivatives  $|f'(x)| \leq \lambda/4$ , facilitating reliable parameter estimation, eigenvalue computation, and observer synthesis even in genome-scale networks.

The inversion problem is equally severe. The increasing Hill function  $h(x) = \frac{x^n}{\theta^n + x^n}$  lacks a general closed-form inverse for arbitrary  $n$ . For integer values, the inverse can be written in complex expressions, for example, when  $n = 2$ ,

$$h^{-1}(y) = \theta \sqrt{\frac{y}{1-y}},$$

which still involves a square root (irrational function). For  $n = 3$ , the inverse involves cube roots and more complex algebraic manipulations. However, these forms are not universally applicable and become increasingly cumbersome for higher integer values of  $n$ . For non-integer  $n$  (e.g.,  $n \approx 1.39$  from empirical fits [10]), no elementary inverse exists. The formal inverse

$$h^{-1}(y) = \theta \left( \frac{y}{1-y} \right)^{1/n}$$

requires computing fractional powers, which are multi-valued complex functions for non-integer exponents when the argument becomes negative, introducing branch cuts and numerical ambiguities. This necessitates numerical inversion, introducing approximation errors that hinder exact linearization and limit the precision of real-time control. Iterative methods, such as the Newton-Raphson method, can be used to compute the inverse numerically; however, this approach introduces computational overhead and potential convergence failures, particularly near  $y = 0$  or  $y = 1$ , where the derivative of the Hill function becomes small.

Furthermore, Hill's power-law form introduces stiffness and complex constraint handling, making MPC computationally intensive and less robust to uncertainties compared to the logistic function's bounded, smooth, and differentiable form. In MPC implementations for synthetic biology, where one must solve constrained optimization problems at each control cycle, potentially in real-time, the logistic function's closed-form inverse and smooth gradients translate directly into faster and more reliable optimization convergence. The bounded output range  $[0, 1]$  also simplifies constraint handling, as logistic-based models naturally respect physical bounds without requiring explicit inequality constraints.

### 3.4 Linear Approximations and Perturbation Analysis

The logistic function's steepness parameter  $\lambda$  enables linear, predictable tuning, ensuring robust and interpretable model behavior. Logistic functions of the form  $1/(1 + e^{-\lambda(x-\theta)})$  admit multiple useful linear approximations that facilitate different aspects of analysis:

- **Near the origin ( $x \approx 0$ ):** For small  $x$ , the function can be approximated as

$$f(x) \approx \frac{1}{1 + e^{\lambda\theta}} + \frac{\lambda e^{\lambda\theta}}{(1 + e^{\lambda\theta})^2} x.$$

This linear approximation captures basal expression levels (represented by the constant term) and sensitivity to small increases in concentration (represented by the linear coefficient). It proves essential for analyzing low-expression regimes, where genes operate near their minimum activity, which is common in developmental biology before induction, in metabolic pathways with constitutive low-level expression, and in negative feedback loops that maintain repressed states.

- **Around the threshold ( $x \approx \theta$ ):** The function exhibits a steep transition, with linear approximation

$$f(x) \approx \frac{1}{2} + \frac{\lambda}{4}(x - \theta).$$

This midpoint linearization characterizes the switch-like behavior characteristic of cooperative regulation, with slope  $\lambda/4$  quantifying the responsiveness to concentration changes near the half-maximal point. It provides the foundation for local stability analysis of equilibria positioned near thresholds.

- **For small steepness ( $\lambda \ll 1$ ):** The entire sigmoid can be approximated linearly across a broader range,

$$f(x) \approx \frac{1}{2} + \frac{\lambda(x - \theta)}{4} + O(\lambda^2),$$

valid for  $|x - \theta|$  of order unity. This global linear approximation applies to weakly cooperative systems or when regulatory interactions are mild, allowing for a purely linear analysis of network dynamics and significantly simplifying stability assessment, frequency response analysis, and control design.

- **Exponential approximation:** For  $x \ll \theta$  and large  $\lambda\theta$ , we have

$$f(x) \approx e^{\lambda(x-\theta)},$$

capturing the exponential decay of gene expression far below the threshold. This approximation connects logistic models to exponential growth/decay models commonly used in enzyme kinetics, proving useful when analyzing transient dynamics far from the steady state.

These approximations should prove particularly useful near equilibrium points in dynamical systems, enabling perturbation methods, bifurcation analysis, and closed-form solutions in GRN ordinary differential equation (ODE) models. In feedback loops, the linear regimes simplify Jacobian computations for local stability, while the overall smoothness enhances global Lyapunov stability analysis and numerical tractability compared to Hill functions, which may introduce singularities or complex fractional derivatives. For example, the linear approximation around the equilibrium yields a Jacobian matrix with explicit algebraic entries proportional to  $\lambda$ . Eigenvalue analysis then reduces to solving a quadratic equation with coefficients that depend linearly on  $\lambda$ , enabling the analytical determination of stability boundaries. For Hill-based models, the corresponding Jacobian entries involve power-law terms with exponent  $n - 1$ , yielding characteristic equations that typically resist closed-form solution for non-integer  $n$ .

Such approximations preserve biological realism in saturation and cooperativity effects, with recent studies demonstrating improved scalability in stochastic simulations and control-theoretic designs [48, 65, 66]. The linear approximations also facilitate teaching and conceptual understanding, as they provide intuitive interpretations of regulatory strength (slopes) and thresholds (intercepts) that connect directly to experimental observables.

### 3.4.1 The Approximations Problem for Hill Functions

The simplicity of these linear approximations stands in stark contrast to Hill function approximations. The Hill function  $h^+(x, \theta, n) = \frac{x^n}{x^n + \theta^n}$  admits the expansion around small  $n$ :  $h^+(x, \theta, n) \approx \frac{1}{2} + \frac{n}{4} \ln\left(\frac{x}{\theta}\right) + O(n^2)$ , which introduces logarithmic dependence on  $x$ . This logarithmic term substantially complicates analysis, particularly near  $x = 0$ , since  $\ln(x/\theta) \rightarrow -\infty$  as  $x \rightarrow 0^+$ . The divergence introduces singular behavior in the approximation, rendering it ill-defined or numerically unstable near the origin, precisely where many biological systems operate under basal conditions or in response to weak signals. Furthermore, the logarithmic scaling implies that Hill functions respond to *relative* changes (fold-changes) in the input signal, whereas logistic functions respond to *absolute* differences, a distinction with profound implications for capturing biological regulatory mechanisms. The Hill function's behavior near the origin stands in sharp contrast.

Around  $x = 0$ , the Hill function exhibits power-law behavior rather than linear behavior:  $h^+(x, \theta, n) \approx \frac{x^n}{\theta^n} + O\left(\left(\frac{x}{\theta}\right)^{2n}\right)$ , indicating that the function vanishes at the origin with increasing flatness for larger values of the Hill coefficient  $n$ . This power-law structure introduces additional complexity, as the behavior of the first derivative at  $x = 0$  depends critically on the value of  $n$ :

- For  $n > 1$  (the typical cooperative case):  $\frac{dh^+(x)}{dx}\Big|_{x=0} = 0$ , meaning the function has zero slope at the origin.
- For  $n = 1$  (Michaelis-Menten kinetics):  $\frac{dh^+(x)}{dx}\Big|_{x=0} = \frac{1}{\theta}$ , giving a non-zero but finite slope.
- For  $0 < n < 1$ :  $\frac{dh^+(x)}{dx}\Big|_{x=0} \rightarrow \infty$ , leading to an infinite slope at the origin.

This variability in derivative behavior requires careful handling in both analytical work and numerical simulations, especially for the commonly encountered case of moderate  $n > 1$ , where cooperative binding effects are significant.

Around the midpoint  $x = \theta$ , the Hill exhibits remarkably similar linear approximations:  $h^+(x, \theta, n) \approx \frac{1}{2} + \frac{n}{4\theta}(x - \theta) + O((x - \theta)^2)$ . However, a crucial difference emerges: the Hill function's slope also depends inversely on the threshold parameter  $\theta$ , making it sensitive to the threshold scale in a way that the logistic function's slope which depends only on  $\lambda$  is not. This difference has practical implications for parameter interpretation and system robustness to threshold variations. These approximations become functionally equivalent when parameters are appropriately matched through the relationship  $\lambda = n/\theta$ . This matching ensures the functions have identical slopes at the midpoint, enabling similar local stability analysis in dynamical models.

### 3.5 Computational Efficiency and Numerical Stability

Computationally, logistic functions are fundamentally simpler: the exponential form is efficient to evaluate, avoiding the power operations in Hill functions that introduce numerical instability for non-integer exponents. Modern processors include optimized instructions for exponential function evaluation, whereas arbitrary-power operations  $x^n$  for non-integer  $n$  require logarithm-exponential compositions ( $x^n = e^{n \ln x}$ ) that are slower and accumulate floating-point rounding errors, especially for small  $x$  where  $\ln x$  has large negative values.

For Hill-based models, ODE solvers may fail, exhibit stiffness, or require excessively small time steps near low-concentration regimes (basal expression levels), causing inefficiency and instability in large-scale simulations. The derivative singularities force adaptive time-stepping algorithms to repeatedly reject steps, reducing effective integration speed. Implicit methods designed for stiff systems require solving nonlinear equations at each time step, and these Newton iterations may fail to converge when Jacobians are ill-conditioned due to Hill function derivatives near the origin.

In pharmacodynamics, a field with substantial overlap with GRN modeling, the four-parameter model with increasing and decreasing logistic curves should offer more stable parameter estimates than the Hill equation, particularly when fitting noisy data [59, 58]. This stability arises because logistic functions avoid the multicollinearity issues in Hill parameterizations, where  $n$  and  $\theta$  can correlate strongly, changes in  $n$  can be partially compensated by changes in  $\theta$ , leading to an elongated, ridge-like parameter likelihood surface that confounds optimization [59, 67]. The logistic parameterization, by separating steepness ( $\lambda$ ) from threshold ( $\theta$ ) in a more orthogonal manner, should yield better-conditioned parameter estimation problems with narrower confidence intervals.

For large-scale GRNs involving hundreds of genes, prioritizing analytical insights over molecular details becomes essential. Logistic functions reduce complexity by abstracting binding kinetics while maintaining realism in feedback loops and saturation effects. In flexible GRN inference models, logistic functions can transform linear transcription factor activities to capture expression saturation, where the output plateaus despite increasing input (see [67]). This limitation in linear models is naturally addressed by the logistic upper asymptote. The computational savings compound in high-dimensional systems: simulating a 100-gene network over developmental time scales might require evaluating regulatory functions millions of times,

and the per-evaluation speed-up of logistic over Hill functions should translate to substantial reductions in wall-clock time.

Furthermore, these increasing and decreasing logistic functions should be integrated seamlessly with modern automatic differentiation frameworks used in machine learning and optimization. Libraries such as TensorFlow, PyTorch, and JAX offer highly optimized implementations of the logistic sigmoid and its derivatives, enabling efficient gradient-based parameter inference and optimal control synthesis. Hill functions, by contrast, often require custom implementations with careful handling of edge cases (zero or near-zero inputs, non-integer exponents), reducing portability and performance.

### 3.6 Stochastic Simulations and Empirical Validation

In stochastic GRN contexts, Hill functions often require corrections to account for fluctuations in small molecule counts, as direct insertion into master equations approximates deterministic rates poorly [56, 57]. The chemical master equation describes probability distributions over discrete molecule counts, and propensity functions (reaction rates) must be properly adjusted when transitioning from deterministic concentration models. Hill functions, derived from equilibrium assumptions for macroscopic concentrations, can overestimate or underestimate stochastic reaction rates when molecule counts are low (1-100 molecules per cell), as they fail to account for discrete fluctuations and finite-number effects.

Logistic functions, being inherently smooth, support better integration with stochastic simulations (e.g., Gillespie algorithms) and reduce variance in propensity rates. Their structure also aids control theory applications, such as designing observers for state estimation in feedback networks, where smoothness ensures well-posed optimization problems. The Gillespie algorithm requires repeatedly evaluating propensity functions and computing their sum. The bounded derivatives of logistic functions ensure that these propensities vary smoothly with the system state, reducing the variance of time-step estimates and improving the statistical efficiency of stochastic trajectories. Hill functions' sharp transitions and derivative singularities, by contrast, can introduce artificial stiffness in stochastic simulations, forcing smaller time steps than physically necessary.

Empirical studies reconstructing GRNs from single-cell data demonstrate that neural network approximations, which often embed sigmoids like logistic functions, overlap significantly with Hill-based topologies, validating functional equivalence while offering superior scalability [68, 67]. For instance, in *Xenopus* mesoderm induction, logistic-based models can refine core topologies around genes like Brachyury, accurately capturing moderate activin signaling thresholds [67]. Single-cell RNA-seq data exhibits extreme sparsity (most entries are zero due to dropout or true absence of expression), and inference methods must handle this gracefully. Logistic regression built on the logit transformation of logistic functions provides a principled probabilistic framework for inferring regulatory interactions from binary or binarized expression data, outperforming Hill-based approaches that struggle with the discrete, sparse nature of single-cell measurements.

This framework consolidates logistic functions as theoretically sound, especially in noisy or large datasets, though validation against primary biological data remains essential to balance abstraction with realism. The key is that logistic functions provide a "sweet spot": sufficient biological realism to capture sigmoidal dose-response relationships and cooperative regulation, yet sufficient mathematical tractability to enable rigorous analysis, efficient computation, and robust control design advantages that become increasingly critical as systems biology moves toward genome-scale models and precision control of synthetic circuits.

### 3.7 Biological Realism: Absolute Scales and Basal Expression

A fundamental distinction between Hill and logistic functions lies in their input scaling. Hill functions respond to log-scaled inputs (equivalent to logistic under  $x \rightarrow e^x$ ), emphasizing relative changes. Mathematically, the Hill function  $h(x) = \frac{x^n}{x^n + \theta^n}$  can be rewritten in terms of the ratio  $x/\theta$ :

$$h(x) = \frac{(x/\theta)^n}{(x/\theta)^n + 1},$$

showing that it depends only on the fold-change  $x/\theta$ , not absolute concentrations. A tenfold increase from 1 to 10 molecules per cell produces the same change in the Hill function as a tenfold increase from 100 to 1000 molecules, a characteristic response of logarithmic behavior.

In contrast, logistic functions use absolute scales, which better capture thresholds defined by absolute transcription factor counts in GRNs. Gene regulation often depends on whether the number of transcription factor molecules exceeds a critical threshold for promoter occupancy, such as 50 molecules per cell for half-maximal activation, regardless of the fold change from previous states. The logistic function  $f(x) = \frac{1}{1+e^{-\lambda(x-\theta)}}$  with  $\theta = 50$  naturally encodes this absolute threshold, with the response depending on the arithmetic difference  $x - \theta$  rather than the ratio  $x/\theta$ .

Empirical evidence supports the concept of absolute concentration scaling in many regulatory contexts. Bacterial gene regulation studies show that absolute protein copy numbers determine binding kinetics, threshold behaviors, and expression levels, with regulatory decisions based on exact molecule counts per cell [69]. Mammalian transcription factor studies demonstrate that precise modulation of TF levels yields gene expression responses dependent on absolute dosages [70]. NF- $\kappa$ B activity responds to absolute differences in cytokine concentrations rather than fold changes [71]. While fold-change detection exists in certain sensory systems (bacterial chemotaxis, photoreceptor adaptation), it is not universal in gene regulation.

At extremes, the scaling difference becomes critical. Hill functions drop to zero at  $x = 0$  (no basal activity), which risks model trapping in off-states where the system cannot escape low-expression steady states without an external perturbation. Logistic functions maintain tunable non-zero basal expression ( $> 0$ ), providing realism for leaky systems. In fitting biological data (e.g., dose-response curves), the 4-parameter logistic (4PL) model often outperforms the Hill model due to its stable parameter estimates and avoidance of singularities for non-integer  $n$ . The 4PL model includes explicit upper and lower asymptote parameters, naturally accommodating non-zero baselines without requiring ad hoc offsets that compromise the mathematical structure of the Hill function.

Biological systems rarely exhibit true zero expression. Even under full repression, promoters display leakiness, stochastic transcription initiation events producing 0.1-1 mRNA molecules per cell in bacteria [19], or 1-10 transcripts per million (TPM) in mammalian cells [72]. This persistent basal activity serves critical functions: it reduces phenotypic noise by shifting expression distributions from multimodal to unimodal, prevents irreversible trapping in off-states during stochastic fluctuations, and enables rapid induction responses by maintaining the transcriptional machinery in a primed state. The logistic function captures this fundamental biology naturally through its non-zero output at  $x = 0$ :

$$f^+(0, \theta, \lambda) = \frac{1}{1 + e^{\lambda\theta}} > 0,$$

which can be tuned via the product  $\lambda\theta$  without introducing additional parameters. Hill functions, with their strict zero at the origin, require artificial modifications to represent this ubiquitous biological phenomenon.

### 3.8 Advantages for Activation and Repression

The logistic model offers a superior approach for controlling both basal gene expression in the absence of activators and the unrepresed rate in the absence of repressors. By leveraging adjustable parameters, it can fine-tune non-zero baseline outputs, effectively capturing:

- Leaky promoter activity, where transcription occurs at low rates even without bound activators due to stochastic formation of pre-initiation complexes or incomplete nucleosome occlusion.
- Stabilization of low-expression states in biological systems like GAL networks (yeast galactose metabolism) or auto-regulatory circuits where negative feedback maintains basal expression below induction thresholds.
- Biological imperfections such as resource limits (finite RNA polymerase availability) or noise (stochastic binding/unbinding events) that prevent perfect repression even with saturating repressor concentrations.

- Near-maximal expression without extra modifications in systems lacking regulators, where the logistic's saturation naturally approaches but need not equal unity, reflecting polymerase saturation or competition for transcriptional resources.

This contrasts with the Hill function, which yields zero output without activators and a fixed maximum without repressors, requiring artificial offsets that compromise accuracy, regulation, and flexibility. Adding a constant  $\varepsilon$  to a Hill function, a common workaround for modeling basal expression introduces several problems: it shifts the entire response curve upward, causing outputs to exceed unity at high concentrations unless renormalized; it adds an extra parameter lacking clear biological interpretation; it breaks the mathematical relationship between parameters and binding constants; and it complicates derivative calculations needed for stability analysis.

The decreasing logistic function offers distinct advantages over its decreasing Hill counterpart, particularly in capturing decay dynamics from high to low expression levels. While the increasing logistic emphasizes activation through buildup from near-zero to saturation, the decreasing form excels in repression by providing tunable unrepresed rates at low repressor concentrations (near  $x = 0$ ). This tunability, achieved via parameters  $\theta$  (threshold) and  $\lambda$  (steepness), allows the function value at  $x = 0$  to approach, but not rigidly equal, 1, which can be adjusted below 1 to reflect biological constraints, such as resource limitations or incomplete promoter activation. For the decreasing logistic  $f^-(x) = \frac{1}{1+e^{\lambda(x-\theta)}}$ , we have

$$f^-(0) = \frac{1}{1+e^{-\lambda\theta}},$$

which approaches 1 as  $\lambda\theta \rightarrow \infty$  but can be set to any value in  $(0.5, 1)$  by appropriate parameter choices. For instance, setting  $\lambda = 4$  and  $\theta = 3$  yields  $f^-(0) \approx 0.99999$ , nearly perfect repression. Setting  $\lambda = 1$  and  $\theta = 1$  gives  $f^-(0) \approx 0.73$ , modeling substantial resource limitations.

In contrast, the decreasing Hill function always yields exactly 1 at  $x = 0$  ( $h^-(0) = 1$ ), assuming ideal maximal expression without repressor. This rigidity often necessitates the use of artificial offsets or additional terms to model realistic imperfections, which can potentially lead to parameter instability or overfitting during data fitting. The Hill function's all-or-none character at the boundaries, strict zeros for activation at  $x = 0$  and strict ones for repression at  $x = 0$ , reflects its origin in equilibrium binding models that neglect stochastic fluctuations, finite-size effects, and competing cellular processes.

### 3.9 Preserving Cooperativity While Gaining Tractability

The Hill coefficient ( $n$ ) quantifies the degree of cooperativity and is obtained by fitting Hill functions directly to gene expression data, such as promoter activity versus inducer concentration [73, 74]. The cooperativity, a hallmark of Hill's mechanistic origin in ligand-receptor binding, can be preserved in logistic formulations. The steepness parameter  $\lambda$  controls the sharpness of the sigmoidal transition, analogous to the Hill coefficient  $n$ . When  $n$  is estimated directly from gene expression data, the corresponding logistic parameter can be matched to preserve local input-output sensitivity. Specifically, the logistic steepness parameter can be scaled as  $\lambda = n/\theta$  to faithfully preserve the local input-output sensitivity of the Hill model. This relationship emerges from matching the derivatives at the half-maximal point. For the Hill function  $h^+(x) = \frac{x^n}{x^n + \theta^n}$ , the derivative at  $x = \theta$  is

$$h^+'|_{x=\theta} = \frac{nx^{n-1}\theta^n}{(x^n + \theta^n)^2}|_{x=\theta} = \frac{n\theta^{n-1}\theta^n}{(2\theta^n)^2} = \frac{n}{4\theta}.$$

For the logistic function  $f^+(x) = \frac{1}{1+e^{-\lambda(x-\theta)}}$ , the derivative at  $x = \theta$  is

$$f^+'|_{x=\theta} = \lambda f(\theta)(1 - f(\theta)) = \lambda \cdot \frac{1}{2} \cdot \frac{1}{2} = \frac{\lambda}{4}.$$

Equating these slopes yields  $\lambda = n/\theta$ , ensuring identical local responsiveness to concentration changes near the activation threshold. The same result holds for the repression logistic function.

The sigmoidal switching behavior emulates cooperativity phenomenologically without requiring explicit multi-site binding assumptions. This smooth structure supports control design and analysis in feedback regulatory networks while maintaining biological realism. The key insight is that cooperativity manifests macroscopically as steepness of the dose-response curve, whether this steepness arises from multiple binding sites (Hill's mechanistic interpretation) or from other sources of ultrasensitivity (allosteric conformational changes, phosphorylation cascades, competition for limiting factors) may be secondary for systems-level modeling. The logistic function captures the phenomenology, characterized by a sigmoidal input-output relationship with tunable steepness, without committing to specific molecular mechanisms.

For control-theoretic applications, methods such as Linear Quadratic Regulation (LQR), feedback linearization, and observer design benefit from the manageable system representations provided by logistic functions, which outperform Hill functions in terms of computational efficiency and stability. LQR requires solving Riccati equations involving the system's Jacobian; logistic models yield Jacobians with a simpler algebraic structure, thereby accelerating the solution. Feedback linearization requires computing coordinate transformations involving the inverse of the nonlinear function; the closed-form inverse of logistic functions enables exact linearization. Observer design requires the observability matrix to have full rank; logistic functions maintain this rank even at low concentrations where Hill functions fail.

### 3.10 Optimal Balance of Fidelity and Tractability

The increasing and decreasing logistic functions' integrability, smoothness, and closed-form expressions offer significant advantages over the Hill function in terms of analytical and computational efficiency. These properties enable the generation of qualitative insights, approximate solutions, and efficient stochastic simulations, while preserving biological realism in capturing sigmoidal repression and steady-state behavior.

Logistic functions strike an optimal balance, upholding biological fidelity in sigmoidal switching and cooperativity while prioritizing analytical and computational tractability. This makes them ideal for prioritizing insights in complex, noisy GRNs, though empirical validation against molecular data ensures alignment with mechanistic details. The substitution preserves key biological features such as cooperativity thresholds and sigmoidal switching while reducing computational complexity, making the increasing and the decreasing logistic functions particularly well suited for large-scale gene regulatory networks where analytical insights are prioritized over exact molecular binding details, particularly when:

- **Molecular binding details are less critical than overall regulatory logic:** In systems biology and synthetic biology, the focus often shifts from understanding precise binding constants and cooperative interaction parameters to designing robust regulatory circuits, predicting phenotypic outcomes, or controlling cellular behavior. These logistic functions provide sufficient detail to capture regulatory logic (activation/repression, thresholds, saturation) without the mechanistic complexity that Hill functions import from equilibrium thermodynamics.
- **Large-scale networks prioritize computational tractability:** Genome-scale GRN models involving thousands of genes and tens of thousands of regulatory interactions demand computationally efficient formulations. The exponential evaluation cost of Hill functions with non-integer exponents becomes prohibitive in such settings, whereas the simple exponential structure of logistic functions enables rapid simulation. In parameter inference from single-cell RNA-seq datasets with millions of cells, the computational savings multiply: fitting a logistic-based model might take hours, while a Hill-based model could require days or weeks.
- **Noisy or incomplete data preclude precise mechanistic parameterization:** Single-cell transcriptomics, the dominant technology for profiling gene expression, exhibits severe technical noise dropout events where expressed genes appear as zero, amplification biases, and batch effects. When data quality limits parameter identifiability, the additional mechanistic parameters in Hill models (binding constants, cooperativity coefficients) cannot be reliably estimated and may overfit noise. Logistic models, with their simpler parameterization and robust numerical properties, extract maximal information from limited data without overfitting.

- **Control and observer design require smooth, invertible nonlinearities:** Synthetic biology increasingly aims to engineer predictable, controllable cellular behaviors: biosensors with specified dose-response curves, oscillators with tunable frequencies, toggle switches with designated thresholds. Model-based control and observer design algorithms require non-linear models with well-behaved mathematical properties: smooth derivatives for gradient-based optimization, closed-form inverses for feedback linearization, and full-rank observability matrices for state estimation. Logistic functions provide these properties; Hill functions with non-integer exponents generally do not.
- **Integration with machine learning frameworks is desired:** Modern approaches to GRN inference and control increasingly leverage machine learning (neural networks for learning regulatory functions from data), reinforcement learning for optimal control policy synthesis, Gaussian processes for uncertainty quantification. These frameworks rely on automatic differentiation, which requires smooth, efficiently evaluable functions. Logistic sigmoids integrate seamlessly, as they are primitive operations in all major deep learning libraries. Hill functions require custom implementations that carefully handle edge cases, which reduces portability and performance.
- **Biological interpretability of low-expression dynamics is paramount:** Understanding how genes behave at basal expression levels, such as before induction, in differentiated cells maintaining repressed developmental programs, or in metabolic pathways with constitutive low activity, requires models that accurately represent non-zero baselines. Logistic functions encode this naturally; Hill functions, on the other hand, require ad hoc modifications that obscure interpretation.

In summary, while Hill functions retain value when the specific molecular mechanism of cooperative binding is the focus of investigation such as in biophysical studies determining the number of binding sites or allosteric coupling constants, logistic functions provide a superior foundation for systems biology, synthetic biology, and computational biology applications where the goals are understanding network-level behavior, predicting cellular phenotypes, designing robust controllers, or inferring regulatory architectures from noisy high-throughput data. The choice is not about biological realism versus mathematical convenience, but about matching the model’s complexity to the question being asked and the data available to answer it. For the vast majority of GRN modeling applications in modern biology, logistic functions provide the appropriate level of abstraction, capturing essential regulatory features while enabling the rigorous analysis and efficient computation that complex biological systems require.

## 4 Modeling and Analysis of Classical Logistic-Based Models

This paper centers on a fundamental reformulation: we model gene activation through *increasing* logistic functions and gene repression through *decreasing* logistic functions. Our overarching objective is to establish that logistic functions constitute not merely a viable alternative to Hill functions in classical genetic network modeling, but in many respects a *superior* one offering enhanced analytical tractability, numerical stability, and biological realism.

### 4.1 The Core Replacement Strategy

Our central task is to systematically replace Hill functions with their logistic counterparts in gene regulatory network (GRN) models, while rigorously preserving the characteristic sigmoidal dynamics that define regulatory transitions. This substitution must be executed with care to ensure functional equivalence under biologically relevant conditions. Specifically, we propose the following mappings:

- **For activation:** The increasing Hill function  $h^+(x, \theta, n) = \frac{x^n}{x^n + \theta^n}$  is replaced by the increasing logistic function  $f^+(x, \theta, \lambda) = \frac{1}{1 + e^{-\lambda(x-\theta)}}$ . See above for more detailed derivations.
- **For repression:** The decreasing Hill function  $h^-(x, \theta, n) = \frac{\theta^n}{x^n + \theta^n}$  is replaced by the decreasing logistic function  $f^-(x, \theta, \lambda) = \frac{1}{1 + e^{\lambda(x-\theta)}} = \frac{1}{1 + e^{-\lambda(\theta-x)}}$ . See above for more detailed derivations.

To ensure a close approximation between the Hill and logistic functions, the steepness parameters can be matched by equating the maximum slopes at the inflection points. For the increasing functions, the maximum derivative of the Hill function is  $n/(4\theta)$ , while for the logistic it is  $\lambda/4$ . Thus, setting  $\lambda = n/\theta$  provides a good match in transition sharpness. A similar matching applies to the decreasing forms.

## 4.2 Non-Cooperative Gene Regulatory Networks

In the simplest regulatory scenarios, where each gene responds to a single regulator without cooperative binding effects, the logistic framework takes a particularly streamlined form. Here, gene  $i$  is regulated by the expression level of gene  $x_j$  through a single logistic function, with the regulatory direction (activation or repression) encoded by a sign parameter. The general dynamical model is:

$$\dot{x}_i = \kappa_i \frac{1}{1 + e^{-\sigma_i \lambda (x_j - \theta_i)}} - \gamma_i x_i, \quad i = 1, \dots, n, \quad (23)$$

where:

- $x_i$  denotes the expression level (e.g., protein concentration) of gene  $i$ ,
- $x_j$  is the concentration of the regulatory species (for example,  $j = i - 1$  in a sequential regulatory cascade, or any other gene index in the network),
- $\kappa_i > 0$  is the maximal production rate,
- $\gamma_i > 0$  is the degradation rate,
- $\lambda > 0$  controls the steepness of the regulatory response,
- $\theta_i > 0$  is the regulatory threshold,
- $\sigma_i \in \{+1, -1\}$  encodes the regulatory sign:  $\sigma_i = +1$  for activation and  $\sigma_i = -1$  for repression.

This formulation embeds both activation and repression within a unified structure, with the sole distinction being the sign  $\sigma_i$  that inverts the exponential argument.

**Example 1** (The Genetic Oscillator: A Canonical Test Case). *Genetic oscillators represent one of the most fundamental and ubiquitous motifs in biological networks, governing phenomena from circadian rhythms to cell cycle progression. In their simplest incarnation, such oscillators comprise two genes forming a negative feedback loop: the first gene activates the second, which in turn inhibits the first, creating a cyclical pattern of expression (Fig. 1).*



Figure 1: Architecture of a two-gene negative feedback loop. Gene A activates gene B (blue arrow), while gene B represses gene A (red bar).

*Deploying our logistic formulation, the dynamics of this system are governed by the coupled ordinary differential equations:*

$$\begin{aligned} \dot{x}_1 &= \kappa_1 \frac{1}{1 + e^{-\lambda(\theta_2 - x_2)}} - \gamma_1 x_1, \\ \dot{x}_2 &= \kappa_2 \frac{1}{1 + e^{-\lambda(x_1 - \theta_1)}} - \gamma_2 x_2, \end{aligned} \quad (24)$$

where  $\kappa_1, \kappa_2$  are the maximal production rates,  $\gamma_1, \gamma_2$  are the degradation rates,  $\lambda$  determines the steepness of both regulatory responses, and  $\theta_1, \theta_2$  are the respective threshold concentrations. Note that gene 1 is repressed by gene 2 (hence the argument  $\theta_2 - x_2$ , which decreases as  $x_2$  rises), while gene 2 is activated by gene 1 (argument  $x_1 - \theta_1$ , which increases with  $x_1$ ).

Numerical simulations of this system with parameter values  $\lambda = 3$ ,  $\kappa_1 = 3$ ,  $\gamma_1 = 0.25$ ,  $\kappa_2 = 4$ ,  $\gamma_2 = 0.5$ ,  $\theta_1 = 4$ ,  $\theta_2 = 3$ , starting from initial conditions  $x_1(0) = x_2(0) = 1$ , are depicted in Fig. 2. The system exhibits damped oscillations approaching the equilibrium approximately at  $(x_1^*, x_2^*) \approx (3.87, 3.25)$ .

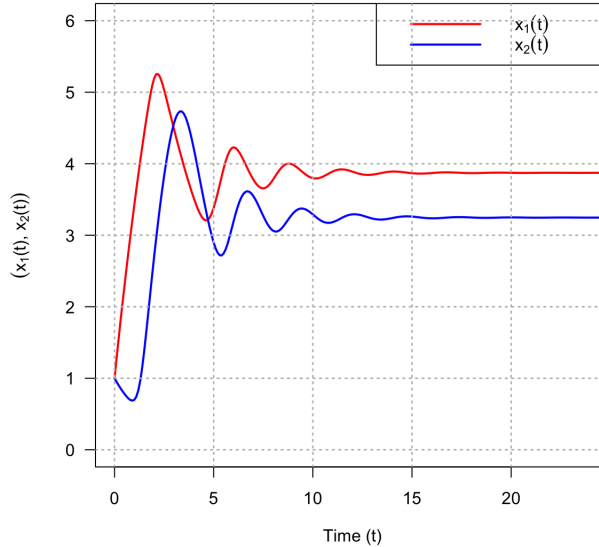


Figure 2: Temporal evolution of the two-gene oscillator system (24). Parameters:  $\lambda = 3$ ,  $\kappa_1 = 3$ ,  $\gamma_1 = 0.25$ ,  $\kappa_2 = 4$ ,  $\gamma_2 = 0.5$ ,  $\theta_1 = 4$ ,  $\theta_2 = 3$ ; initial conditions  $x_{01} = x_{02} = 1$ .

**Jacobian Matrix and Local Stability Analysis.** To analyze the stability properties of this system, we linearize the dynamics around an equilibrium point  $(x_1^*, x_2^*)$  satisfying the steady-state conditions

$$\kappa_1 f_1(x_2^*) = \gamma_1 x_1^*, \quad \kappa_2 f_2(x_1^*) = \gamma_2 x_2^*,$$

where we write  $f_1(x_2) = \frac{1}{1+e^{-\lambda(\theta_2-x_2)}}$  and  $f_2(x_1) = \frac{1}{1+e^{-\lambda(x_1-\theta_1)}}$  for compactness.

The Jacobian matrix at equilibrium is:

$$J = \begin{pmatrix} -\gamma_1 & \kappa_1 f'_1(x_2^*) \\ \kappa_2 f'_2(x_1^*) & -\gamma_2 \end{pmatrix}.$$

A key advantage of the logistic formulation manifests immediately in the derivatives. For the repression function  $f_1$ , we have

$$f'_1(x_2) = \frac{d}{dx_2} \left( \frac{1}{1+e^{-\lambda(\theta_2-x_2)}} \right) = -\lambda f_1(x_2)(1-f_1(x_2)) < 0,$$

exploiting the characteristic self-referential form of the logistic derivative. The negative sign arises because  $f_1$  decreases as  $x_2$  increases. Similarly, for the activation function  $f_2$ :

$$f'_2(x_1) = \lambda f_2(x_1)(1-f_2(x_1)) > 0.$$

These expressions are remarkably simple and require no fractional exponents or complex algebraic manipulations, a direct consequence of the logistic function's exponential structure.

**Eigenstructure.** The characteristic polynomial of  $J$  is:

$$\chi(\mu) = (\mu + \gamma_1)(\mu + \gamma_2) - \kappa_1 \kappa_2 f'_1(x_2^*) f'_2(x_1^*).$$

Expanding this expression, we obtain the trace and determinant:

$$\text{tr}(J) = -(\gamma_1 + \gamma_2) < 0,$$

$$\det(J) = \gamma_1 \gamma_2 + \kappa_1 \kappa_2 \lambda^2 f_1(x_2^*) (1 - f_1(x_2^*)) f_2(x_1^*) (1 - f_2(x_1^*)) > 0.$$

The trace is manifestly negative due to the positive degradation rates. The determinant is positive because all terms are non-negative: the product  $f(1 - f)$  attains its maximum value of  $1/4$  at the inflection point but remains strictly positive throughout the interior of the unit interval.

**Local Asymptotic Stability.** The Routh-Hurwitz criterion for a  $2 \times 2$  matrix guarantees local asymptotic stability when  $\text{tr}(J) < 0$  and  $\det(J) > 0$ , conditions that are satisfied here for all biologically meaningful parameter values. The nature of the approach to equilibrium depends on the discriminant:

$$\Delta = (\text{tr}(J))^2 - 4 \det(J).$$

When  $\Delta < 0$ , the eigenvalues form a complex conjugate pair with negative real part  $\text{Re}(\mu) = -(\gamma_1 + \gamma_2)/2 < 0$ , producing damped oscillations where the system spirals into the equilibrium in a decaying sinusoidal manner.

**Bifurcation Landscape.** A natural question arises: Can this system undergo a Hopf bifurcation, transitioning from a stable equilibrium to sustained periodic oscillations as the parameters vary?

For a Hopf bifurcation to occur in a two-dimensional system, we require  $\text{tr}(J) = 0$  (the sum of eigenvalues vanishing so they become purely imaginary) while maintaining  $\det(J) > 0$  (ensuring complex conjugates rather than real roots). However, in our model:

$$\text{tr}(J) = -(\gamma_1 + \gamma_2),$$

which is fixed and strictly negative for any positive degradation rates  $\gamma_1, \gamma_2 > 0$ . No variation of the remaining parameters:  $\lambda$ ,  $\kappa_i$ , or  $\theta_i$ , can force the trace to vanish.

**Remark 1.** The ordinary differential equation model (24), in the absence of time delays, cannot exhibit Hopf bifurcations. In future work, we plan to introduce delays to achieve sustained limit cycles, particularly for the genetic oscillator. Sustained limit cycles emerge only when we incorporate delay differential equations to account for transcription, translation, or transport lags. This highlights the importance of delays in generating persistent oscillations, as seen in real biological clocks.

### 4.3 Extension to Multi-Gene Regulatory Networks

The logistic-based formulation extends naturally to arbitrarily large networks, preserving its analytical and computational advantages even in high-dimensional settings. A distinguishing feature of our modeling philosophy is the *explicit differentiation* between increasing and decreasing logistic functions: we deploy each form precisely where it is biologically appropriate, thereby maintaining clear regulatory interpretability. This stands in contrast to some alternative formulations that attempt to unify all regulatory interactions through a single increasing functional form, potentially obscuring biological meaning. Our framework accommodates *logical rules* governing how multiple regulators collectively orchestrate gene expression. These rules capture combinatorial effects such as:

- **OR logic** (additive activation): multiple activators independently promote expression, with the gene responding when *any* activator is present;

- **AND logic** (synergistic activation or repression): gene expression requires the *simultaneous* presence (or absence) of multiple regulators;
- **Hybrid combinations:** more complex regulatory architectures involving mixtures of AND, OR, and NOT gates.

For cooperative regulation via such logical combinations, see the pioneering work by Albert and Othmer [75].

**General Multi-Gene Formulation.** Consider a gene regulatory network comprising  $n$  genes, where  $x_i(t)$  denotes the concentration of the protein product of gene  $i$  at time  $t$ . Each gene's dynamics obey a balance equation between synthesis and degradation:

$$\dot{x}_i = \kappa_i f_i(x_1, \dots, x_n) - \gamma_i x_i,$$

where the regulatory function  $f_i : \mathbb{R}^n \rightarrow \mathbb{R}$  synthesizes the influences from all relevant activators and repressors in the network. As an illustrative and biologically prevalent case, we examine **parallel regulation**, wherein multiple transcription factors simultaneously exert independent regulatory effects, with some activating and others repressing on the target gene's promoter. In this architecture, the regulatory function takes a product structure:

$$f_i(x_1, \dots, x_n) = \prod_{j \in \mathcal{A}_i} \frac{1}{1 + e^{-\lambda(x_j - \theta_{ij})}} \cdot \prod_{k \in \mathcal{R}_i} \frac{1}{1 + e^{-\lambda(\theta_{ik} - x_k)}}, \quad (25)$$

where:

- $\mathcal{A}_i$  is the set of indices  $j$  corresponding to gene  $i$ 's activators,
- $\mathcal{R}_i$  is the set of indices  $k$  corresponding to gene  $i$ 's repressors,
- each factor in the first product is an increasing logistic (activation term),
- each factor in the second product is a decreasing logistic (repression term).

The complete dynamical system governing the network is thus:

$$\dot{x}_i = \kappa_i \left( \prod_{j \in \mathcal{A}_i} \frac{1}{1 + e^{-\lambda(x_j - \theta_{ij})}} \cdot \prod_{k \in \mathcal{R}_i} \frac{1}{1 + e^{-\lambda(\theta_{ik} - x_k)}} \right) - \gamma_i x_i. \quad (26)$$

This formulation naturally accommodates any combination of activators and repressors acting on each gene, with the thresholds  $\theta_{ij}$  and  $\theta_{ik}$  allowing gene-specific and regulator-specific tuning of sensitivity. Biologically, this product form models independent binding sites, where full activation requires all activators to be bound and all repressors to be unbound, akin to AND logic.

**Example 2** (A Two-Node Network with Mutual Activation and Self-Repression). *To illustrate the richness of dynamics achievable with logistic-based models, we consider a two-gene regulatory network studied by Vinoth et al. [76]. This system exhibits complex behaviors, including periodic oscillations, deterministic chaos, and extreme events, abrupt, large-amplitude spikes in protein concentration reminiscent of "rogue waves" in nonlinear dynamics. Such concentration spikes have been hypothesized to correlate with biological disruptions in disease contexts, for instance, abnormal protein accumulation in neurodegenerative disorders. The network comprises two proteins,  $A$  and  $B$ , with the following regulatory architecture:*

- **Mutual activation:** Protein  $A$  activates gene  $B$ , and protein  $B$  activates gene  $A$ .
- **Cooperative self-repression:** Each gene represses its own expression via multimeric binding (e.g., dimers or tetramers), traditionally captured by a Hill coefficient  $n > 1$ .

- **Time delays:** The system incorporates delays  $\tau_1, \tau_2, \tau_{12}, \tau_{21}$  representing transcription/translation lags or signaling delays.

These delays interact with the cooperative nonlinearities to produce a rich bifurcation structure, resulting in bistability, oscillatory bursting, and even chaotic dynamics under specific parameter regimes. The regulatory architecture is depicted schematically in Fig. 3.

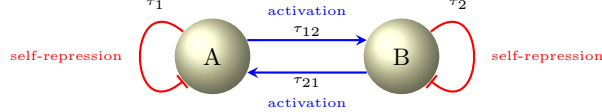


Figure 3: Regulatory topology of the two-gene network. Red lines with bars indicate cooperative self-repression; blue arrows represent mutual activation. Delays  $\tau_1, \tau_2$  govern self-repression lags, while  $\tau_{12}, \tau_{21}$  represent cross-activation delays due to transcription/translation or signal propagation.

**The Original Formulation.** In the original study [76], the model employs additive linear activation combined with Hill-type repression. The delay differential equations (DDEs) for protein concentrations  $A(t)$  and  $B(t)$  are:

$$\begin{aligned}\frac{dA(t)}{dt} &= (g_A + g_{AB}B(t - \tau_{12})) \frac{1}{1 + \left(\frac{A(t - \tau_1)}{A_0}\right)^n} - k_A A(t), \\ \frac{dB(t)}{dt} &= (g_B + g_{BA}A(t - \tau_{21})) \frac{1}{1 + \left(\frac{B(t - \tau_2)}{B_0}\right)^n} - k_B B(t),\end{aligned}$$

where:

- $g_A, g_B$  are basal production rates,
- $g_{AB}, g_{BA}$  quantify the strength of mutual activation,
- $k_A = \gamma_A, k_B = \gamma_B$  are degradation rates,
- $A_0, B_0$  are repression thresholds,
- $n$  is the Hill coefficient encoding cooperativity in self-repression.

All parameter values follow [76]: basal production  $g_A = g_B = 50$  nM/min, cross-activation strengths  $g_{AB} = g_{BA} = 3$  nM/min, degradation rates  $\gamma_A = k_A = 0.20$  min<sup>-1</sup>,  $\gamma_B = k_B = 0.24$  min<sup>-1</sup>, repression thresholds  $A_0 = 100$  nM and  $B_0 = 4$  nM.

**The Logistic Reformulation.** We reformulate this system using logistic functions to preserve the essential sigmoidal regulatory responses while enhancing analytical tractability. The key idea is to replace, for instance:

- The Hill repression term  $\frac{1}{1+(A/A_0)^n}$  with a decreasing logistic function  $f^-(A, A_0, \lambda)$ .
- The linear activation term  $(g_A + g_{AB}B)$  with a scaled increasing logistic function to introduce saturation at high concentrations, which adds biological realism by preventing unbounded production.

The reformulated delay differential equations become:

$$\dot{A}(t) = \kappa_1 f^+(B(t - \tau_{12}), \theta_B, \lambda) f^-(A(t - \tau_1), A_0, \lambda) - \gamma_A A(t), \quad (27)$$

$$\dot{B}(t) = \kappa_2 f^+(A(t - \tau_{21}), \theta_A, \lambda) f^-(B(t - \tau_2), B_0, \lambda) - \gamma_B B(t). \quad (28)$$

Written out explicitly:

$$\dot{A}(t) = \frac{\kappa_1}{1 + e^{-\lambda(B(t - \tau_{12}) - \theta_B)}} \cdot \frac{1}{1 + e^{\lambda(A(t - \tau_1) - A_0)}} - \gamma_A A(t), \quad (29)$$

$$\dot{B}(t) = \frac{\kappa_2}{1 + e^{-\lambda(A(t - \tau_{21}) - \theta_A)}} \cdot \frac{1}{1 + e^{\lambda(B(t - \tau_2) - B_0)}} - \gamma_B B(t). \quad (30)$$

Here,  $\kappa_1, \kappa_2$  are maximal production rates (to be calibrated to approximate the linear activation range),  $\lambda$  controls the steepness of all logistic responses, and  $\theta_A, \theta_B$  are activation thresholds for the cross-regulatory interactions. The precise mapping from the original parameters to the logistic parameters can be established through Taylor expansion matching or least-squares fitting to the original dynamics (details in subsequent sections on parameter estimation). This reformulation not only maintains the extreme events but also facilitates easier sensitivity analysis due to the logistic derivatives.

**Theorem 1** (Global Existence, Smoothness, and Boundedness). *Let  $\mathbf{x}(t) = (x_1(t), \dots, x_n(t))^\top \in \mathbb{R}^n$  denote the state vector of gene expression levels, and consider the general logistic-based regulatory network:*

$$\dot{x}_i(t) = \kappa_i f_i(\mathbf{x}(t)) - \gamma_i x_i(t), \quad i = 1, \dots, n, \quad (31)$$

where each regulatory function  $f_i : \mathbb{R}^n \rightarrow \mathbb{R}$  is defined as a product:

$$f_i(\mathbf{x}) = \prod_{m=1}^{M_i} g_{i,m}(x_{j(i,m)}),$$

with each factor given by the logistic function:

$$g_{i,m}(s) = \frac{1}{1 + \exp[-\lambda_{i,m} \sigma_{i,m}(s - \theta_{i,m})]}.$$

Here, the parameters satisfy:

- $\lambda_{i,m} > 0$  (steepness),
- $\theta_{i,m} \in \mathbb{R}$  (threshold),
- $\sigma_{i,m} \in \{+1, -1\}$  (regulatory sign: +1 for activation, -1 for repression),
- $\kappa_i \geq 0$  (maximal production rate),
- $\gamma_i > 0$  (degradation rate).

The index  $j(i, m)$  maps the  $m$ -th regulatory input of gene  $i$  to its corresponding state variable.

Then the system (31) possesses the following fundamental properties:

1. **Infinite Smoothness.** The vector field  $\mathbf{F} : \mathbb{R}^n \rightarrow \mathbb{R}^n$  defined by

$$F_i(\mathbf{x}) = \kappa_i f_i(\mathbf{x}) - \gamma_i x_i$$

is of class  $C^\infty$  (infinitely differentiable) on all of  $\mathbb{R}^n$ .

2. **Global Lipschitz Continuity and Unique Global Solutions.** The vector field  $\mathbf{F}$  is globally Lipschitz continuous on  $\mathbb{R}^n$ . Consequently, for every initial condition  $\mathbf{x}(0) \in \mathbb{R}^n$ , there exists a unique solution  $\mathbf{x}(t)$  to (31) that is defined for all  $t \geq 0$ .

3. **Positive Invariance and Uniform Boundedness.** Define the rectangular region:

$$\mathcal{B} := \prod_{i=1}^n \left[ 0, \frac{\kappa_i}{\gamma_i} \right] \subset \mathbb{R}^n.$$

This set is positively invariant under the flow of (31). In particular, if  $\mathbf{x}(0) \in \mathbb{R}_+^n$  (all components nonnegative), then  $\mathbf{x}(t) \in \mathcal{B}$  for all  $t \geq 0$ . Thus, solutions remain nonnegative and uniformly bounded, with each component satisfying  $0 \leq x_i(t) \leq \kappa_i/\gamma_i$ .

*Proof.* The proof proceeds in three parts, establishing smoothness, Lipschitz continuity, and positive invariance in turn.

**Part (i): Infinite Smoothness.**

Each scalar logistic function

$$g_{i,m}(s) = (1 + e^{-\lambda_{i,m}\sigma_{i,m}(s-\theta_{i,m})})^{-1}$$

is a composition of the exponential function  $e^{-\lambda_{i,m}\sigma_{i,m}(s-\theta_{i,m})}$  (which is  $C^\infty$  in  $s$ ), the addition of 1, and inversion  $u \mapsto 1/u$  (which is  $C^\infty$  for  $u > 0$ ). Since  $1 + e^{-\lambda_{i,m}\sigma_{i,m}(s-\theta_{i,m})} > 1$  for all  $s \in \mathbb{R}$ , the denominator never vanishes, and thus  $g_{i,m} \in C^\infty(\mathbb{R})$ .

The regulatory function  $f_i(\mathbf{x}) = \prod_{m=1}^{M_i} g_{i,m}(x_{j(i,m)})$  is a finite product of  $C^\infty$  functions of the coordinates  $x_{j(i,m)}$ , hence  $f_i \in C^\infty(\mathbb{R}^n)$ .

Finally,  $F_i(\mathbf{x}) = \kappa_i f_i(\mathbf{x}) - \gamma_i x_i$  is a linear combination of  $C^\infty$  functions, so  $F_i \in C^\infty(\mathbb{R}^n)$ . Therefore, the entire vector field  $\mathbf{F} = (F_1, \dots, F_n)^\top$  is  $C^\infty$  on  $\mathbb{R}^n$ .

**Part (ii): Global Lipschitz Continuity.**

To establish global Lipschitz continuity, we bound the Jacobian matrix  $D\mathbf{F}(\mathbf{x})$  uniformly over all  $\mathbf{x} \in \mathbb{R}^n$ .

*Step 1: Derivative of a single logistic factor.* For any scalar logistic function  $g(s) = (1 + e^{-\lambda\sigma(s-\theta)})^{-1}$ , the derivative is:

$$g'(s) = \frac{\lambda\sigma e^{-\lambda\sigma(s-\theta)}}{(1 + e^{-\lambda\sigma(s-\theta)})^2} = \lambda\sigma g(s)(1 - g(s)).$$

Since  $g(s) \in (0, 1)$  for all  $s$ , we have  $g(1 - g) \leq 1/4$  (with equality at  $g = 1/2$ ), and thus:

$$|g'(s)| \leq \frac{\lambda}{4}.$$

*Step 2: Partial derivatives of the regulatory function.* The regulatory function  $f_i$  is a product of logistic factors. Applying the product rule:

$$\frac{\partial f_i}{\partial x_j} = \sum_{m: j(i,m)=j} \left( \prod_{q \neq m} g_{i,q} \right) g'_{i,m}.$$

For any  $m$  such that  $j(i,m) = j$ , we have:

$$\prod_{q \neq m} g_{i,q} \leq 1 \quad (\text{since each } g_{i,q} \in (0, 1)),$$

and  $|g'_{i,m}| \leq \lambda_{i,m}/4$ . Summing over all such  $m$ :

$$\left| \frac{\partial f_i}{\partial x_j} \right| \leq \sum_{m: j(i,m)=j} \frac{\lambda_{i,m}}{4} =: L_i^j.$$

*Step 3: Bound on the Jacobian entries.* The entries of the Jacobian  $D\mathbf{F}$  are:

$$\frac{\partial F_i}{\partial x_j}(\mathbf{x}) = \kappa_i \frac{\partial f_i}{\partial x_j}(\mathbf{x}) - \gamma_i \delta_{ij},$$

where  $\delta_{ij}$  is the Kronecker delta. Thus:

$$\left| \frac{\partial F_i}{\partial x_j}(\mathbf{x}) \right| \leq \begin{cases} \kappa_i L_i^j, & j \neq i, \\ \kappa_i L_i^j + \gamma_i, & j = i. \end{cases}$$

Taking the maximum over all entries, we obtain a uniform bound on the operator norm of the Jacobian:

$$\|D\mathbf{F}(\mathbf{x})\| \leq M := \max_{i=1,\dots,n} \left( \kappa_i \sum_{j=1}^n L_i^j + \gamma_i \right) < \infty.$$

By the mean value theorem,  $\mathbf{F}$  is globally Lipschitz with Lipschitz constant  $L_F = M$ . This guarantees the existence and uniqueness of solutions for all time via the Picard-Lindelöf theorem (extended to the global case).

*Remark on Second-Order Lipschitz Continuity.* For completeness, we note that the Jacobian  $D\mathbf{F}$  itself is globally Lipschitz (i.e., the Hessian  $D^2\mathbf{F}$  is uniformly bounded). This follows from bounding the second-order partial derivatives  $\partial^2 F_i / \partial x_k \partial x_j = \kappa_i \partial^2 f_i / \partial x_k \partial x_j$ , which involves products and second derivatives of logistic functions. For  $j \neq k$ , cross-partials contain terms of the form:

$$\frac{\partial^2 f_i}{\partial x_k \partial x_j} = \sum_{m \in \mathcal{M}_j} \sum_{p \in \mathcal{M}_k} \left( \prod_{r \neq m, p} g_{i,r} \right) g'_{i,p} g'_{i,m},$$

where  $\mathcal{M}_j = \{m : j(i, m) = j\}$ . Each such term is bounded by  $(\Lambda_i/4)^2$  with  $\Lambda_i = \max_m \lambda_{i,m}$ .

For  $j = k$ , we also encounter terms involving  $g''_{i,m}$ . The second derivative of a logistic function satisfies:

$$|g''(s)| = \lambda^2 |g(1-g)(1-2g)| \leq \lambda^2 \rho,$$

where  $\rho = \max_{g \in (0,1)} |g(1-g)(1-2g)| = \frac{\sqrt{3}}{18} \approx 0.096 < 1/4$ .

Thus, all second-order partials are uniformly bounded, implying  $\|D^2\mathbf{F}(\mathbf{x})\| \leq K < \infty$  for some constant  $K$ . Explicitly:

$$K = \max_{i,j,k} \left| \frac{\partial^2 F_i}{\partial x_k \partial x_j} \right| \leq \kappa_{\max} \cdot \max_i \left( |\mathcal{M}_i|^2 \frac{\Lambda_i^2}{16} + |\mathcal{M}_i| \Lambda_i^2 \rho \right),$$

where  $\kappa_{\max} = \max_i \kappa_i$ . This establishes that  $D\mathbf{F}$  is globally Lipschitz with constant  $L_{DF} = K$ .

### Part (iii): Positivity and Boundedness.

Since each logistic factor satisfies  $g_{i,m}(s) \in (0, 1)$  for all  $s \in \mathbb{R}$ , the product  $f_i(\mathbf{x})$  satisfies:

$$0 < f_i(\mathbf{x}) < 1 \quad \text{for all } \mathbf{x} \in \mathbb{R}^n.$$

Consequently,  $0 \leq \kappa_i f_i(\mathbf{x}) \leq \kappa_i$  for all  $\mathbf{x}$ .

*Nonnegativity.* Suppose at some time  $t_0$  we have  $x_i(t_0) = 0$  (one component reaches zero). Then:

$$\dot{x}_i(t_0) = \kappa_i f_i(\mathbf{x}(t_0)) - \gamma_i \cdot 0 = \kappa_i f_i(\mathbf{x}(t_0)) \geq 0.$$

Thus,  $x_i$  cannot become negative, the flow is directed inward at the boundary hyperplane  $\{x_i = 0\}$ .

*Upper boundedness.* Now suppose at some time  $t_1$  we have  $x_i(t_1) = \kappa_i / \gamma_i$ . Then:

$$\dot{x}_i(t_1) = \kappa_i f_i(\mathbf{x}(t_1)) - \gamma_i \cdot \frac{\kappa_i}{\gamma_i} = \kappa_i (f_i(\mathbf{x}(t_1)) - 1) \leq 0,$$

since  $f_i < 1$ . Thus,  $x_i$  cannot exceed  $\kappa_i/\gamma_i$ , the flow is directed inward at the hyperplane  $\{x_i = \kappa_i/\gamma_i\}$ . By the same argument applied to all components, the rectangular region

$$\mathcal{B} = \prod_{i=1}^n \left[ 0, \frac{\kappa_i}{\gamma_i} \right]$$

has the property that vector field  $\mathbf{F}$  points inward (or tangentially) on each face of  $\mathcal{B}$ . Thus, any trajectory starting inside  $\mathcal{B}$  (or on its boundary) remains in  $\mathcal{B}$  for all future time. In particular, if  $\mathbf{x}(0) \in \mathbb{R}_+^n$  (the nonnegative orthant), then  $\mathbf{x}(t) \in \mathcal{B} \subset \mathbb{R}_+^n$  for all  $t \geq 0$ .

This completes the proof.  $\square$

**Remark 2** (Implications of Global Lipschitz Continuity of the Jacobian). *The global Lipschitz continuity of the Jacobian  $D\mathbf{F}$  (established in the remark within the proof) has several important consequences for system analysis and control:*

1. **Well-posedness of variational equations:** Sensitivity analysis with respect to initial conditions or parameters is well-defined and numerically stable.
2. **Uniform bounds on solution sensitivity:** Perturbations in initial conditions grow at most exponentially (with rate bounded by  $L_F$ ), facilitating robust control design.
3. **Enhanced numerical stability:** Standard ODE solvers (e.g., Runge-Kutta methods) exhibit reliable convergence without requiring adaptive step-size reduction to handle stiffness or discontinuities.
4. **Facilitates control-theoretic tools:** Observer design, feedback linearization, and optimization algorithms that rely on Jacobian computations (e.g., Gauss-Newton methods for parameter estimation) benefit from the smooth, bounded derivative structure.

These properties contrast sharply with Hill function-based models, where non-integer exponents can introduce unbounded derivatives near  $x = 0$ , complicating both theoretical analysis and numerical implementation.

**Example 3** (Quantitative Lipschitz Bounds for the Two-Node Network). *Returning to the two-gene network from Example 2, we compute explicit Lipschitz constants. The system has the structure:*

- Each gene has  $M_1 = M_2 = 2$  regulatory inputs (one activator, one repressor).
- These regulators act on distinct state variables (gene 1 is regulated by gene 2 and itself; gene 2 by gene 1 and itself), so the maximum multiplicity of any single variable appearing in the product is  $r_i = 1$ .
- The steepness parameters are uniform:  $\lambda_{i,m} = \lambda = 2.5$  for all  $i, m$ .
- Production and degradation rates:  $\kappa_1 = 3$ ,  $\kappa_2 = 4$ ,  $\gamma_1 = 0.25$ ,  $\gamma_2 = 0.5$ .

**Computation of  $L_F$ :**

For each gene, the partial derivative bound per regulating variable is:

$$L_i^j = \frac{\lambda}{4} = \frac{2.5}{4} = 0.625.$$

Since each gene has 2 regulators:

$$\sum_j L_i^j = 2 \times 0.625 = 1.25.$$

The global Lipschitz constant for  $\mathbf{F}$  is:

$$M = \max \left( \kappa_1 \sum_j L_1^j + \gamma_1, \kappa_2 \sum_j L_2^j + \gamma_2 \right) = \max(3 \times 1.25 + 0.25, 4 \times 1.25 + 0.5) = \max(4, 5.5) = 5.5.$$

Thus,  $L_F = 5.5$ .

**Computation of  $L_{DF}$  (Lipschitz constant for the Jacobian):**

Using  $\Lambda_i = \max_m \lambda_{i,m} = 2.5$  and  $|\mathcal{M}_i| = 2$  (number of inputs per gene):

$$K \leq \kappa_{\max} \cdot \max_i \left( |\mathcal{M}_i|^2 \frac{\Lambda_i^2}{16} + |\mathcal{M}_i| \Lambda_i^2 \rho \right),$$

where  $\kappa_{\max} = \max(\kappa_1, \kappa_2) = 4$  and  $\rho = \frac{\sqrt{3}}{18} \approx 0.096$ .

Substituting:

$$K \leq 4 \left( 2^2 \cdot \frac{(2.5)^2}{16} + 2 \cdot (2.5)^2 \cdot 0.096 \right) = 4 \left( \frac{4 \times 6.25}{16} + 2 \times 6.25 \times 0.096 \right) = 4(1.5625 + 1.2) = 11.05.$$

Thus,  $L_{DF} \approx 11.05$ .

*Interpretation:* These Lipschitz constants are relatively tight for the given parameter regime. They reflect the low-multiplicity structure of the network (each regulator appears at most once in each product). In scenarios with higher multiplicity, such as when approximating higher Hill coefficients via repeated factors acting on the same variable, the bounds would scale with  $r_i^2$  and  $r_i$ , potentially yielding looser (but still finite and computable) estimates.

#### 4.4 Comparison with Alternative Formulations in the Literature

Our product-of-logistics model (26) enables transparent and biologically interpretable representation of complex regulatory interactions through explicit products of activation and repression terms, but it differs fundamentally from an alternative formulation proposed by Samuilik and colleagues [42]:

$$\dot{x}_i = \kappa_i \cdot \frac{1}{1 + e^{-\mu_i(\sum_{j=1}^n w_{ij}x_j - \theta_i)}} - \gamma_i x_i, \quad w_{ij} \in \mathbb{R}, \quad (32)$$

where:

- $\mu_i$  is a *gene-specific* steepness parameter (allowing different sigmoid sharpness for each gene),
- $\theta_i$  is a *single shared threshold* for gene  $i$  (rather than regulator-specific thresholds  $\theta_{ij}$ ),
- The weights  $w_{ij}$  are *real-valued* (allowing continuously graded regulatory strengths, not just  $\pm 1$ ).

##### Key Differences:

**1. Regulatory Structure.** The Samuilik model aggregates all regulatory inputs into a single weighted sum  $\sum w_{ij}x_j$  passed through one increasing logistic function per gene, modeling additive or competitive effects. In contrast, our product-of-logistics approach multiplies individual sigmoidal terms for each regulator, naturally capturing multiplicative interactions, such as AND logic, where multiple conditions must be satisfied simultaneously for a full regulatory effect.

**2. Threshold Structure.** The Samuilik model uses a single threshold  $\theta_i$  pooled across all regulators of gene  $i$ , whereas our model employs regulator-specific thresholds  $\theta_{ij}$ . The shared threshold approach may oversimplify interactions where different regulators have distinct sensitivity ranges or binding affinities. Our per-regulator thresholds allow fine-tuned modeling of independent regulatory sites.

**3. Biological Interpretability.** The product structure in our formulation directly corresponds to independent transcription factor binding: each logistic term represents the probability-like occupancy of a specific site (increasing for activators, decreasing for repressors). This enhances interpretability, as parameters map directly to measurable quantities, such as dissociation constants. In contrast, the Samuilik model's aggregated sum and shared threshold represent a composite input, whose biological meaning becomes less clear in networks with heterogeneous regulators.

**Illustrating the Problem: Mixed Activation and Repression.** In the [42] model, both activation and repression employ the same increasing logistic function  $\frac{1}{1+e^{-\mu_i s}}$  with  $s = (\sum w_{ij}x_j - \theta_i)$ . This approach uses a shared threshold  $\theta_i$  across all regulators of a gene, potentially oversimplifying interactions, and does not normalize inputs by individual thresholds, limiting biological interpretability and control over individual regulatory effects.

Consider repression. In our formulation (Eq. (25)), the inhibition regulatory function is:

$$f_1^-(x, \theta, \lambda) = \frac{1}{1 + e^{-\lambda(\theta-x)}}.$$

In contrast, the [42] inhibition function is:

$$f_2^-(x, \theta, \mu) = \frac{1}{1 + e^{-\mu(wx-\theta)}}, \quad w < 0.$$

We must compare  $f_2^-$  with the decreasing Hill function  $h^-(x, \theta, n) = \frac{\theta^n}{x^n + \theta^n}$ . Critics suggest that  $f_2^-$  may not preserve expected sigmoidal dynamics or biological realism, particularly because it inhibits gene expression even when  $x < \theta$ . Simulations comparing the decreasing Hill function with both alternative inhibition functions  $f_1^-$  and  $f_2^-$  appear in Fig. 4. Critical points, where the function changes most significantly (output equals 0.5 or the derivative is steepest), are particularly important. For  $f_2^-$ , the midpoint occurs when:

$$e^{\mu(-wx+\theta)} = 1 \implies \mu(-wx + \theta) = 0 \implies -wx + \theta = 0 \implies x = \frac{\theta}{w}.$$

This yields a critical point at  $x_c = \theta/w$ , which is negative when  $w < 0$ . The function  $f_2^-$  appears to be very low (almost flat) in the plot; this is not an error, but rather reflects the parameter choices. With  $w = -1$ ,  $\mu = \lambda = \frac{n}{\theta} = \frac{4}{3}$ ,  $\theta = 3$ :

$$f_2^-(x) = \frac{1}{1 + \exp\left(\frac{4}{3}(x+3)\right)}.$$

For  $x \geq 0$ , this yields  $f_2^-(x) \leq \frac{1}{1+\exp(4)} \approx 0.018$ , and the function remains very low (never approaching 1) over the entire biologically relevant domain.

To preserve the cooperativity (effective Hill coefficient  $n$ ) of the original Hill function when using a logistic form, we take  $\lambda = \frac{n}{\theta}$  in  $f_1^-(x, \theta, \lambda) = \frac{1}{1+e^{-\lambda(\theta-x)}}$ .

In contrast,  $f_1^-(x, \theta, \lambda)$  more closely resembles Hill function behavior, as illustrated in Fig. 4.

So, consider a scenario involving one activator and one repressor acting on gene  $i$ . In our framework (Eq. (26)), the regulatory function is:

$$f_i^{(1)}(x_1, x_2) = \frac{1}{1 + e^{-\lambda(x_1 - \theta_{i1})}} \cdot \frac{1}{1 + e^{-\lambda(\theta_{i2} - x_2)}}.$$

Here, the thresholds  $\theta_{i1}$  and  $\theta_{i2}$  can be determined independently from experimental dose-response curves for each regulator. In contrast, parameterizing the Samuilik regulatory function:

$$f_i^{(2)}(x_1, x_2) = \frac{1}{1 + e^{-\mu_i(w_{i1}x_1 + w_{i2}x_2 - \theta_i)}}$$

requires selecting appropriate values for  $\mu_i$ ,  $\theta_i$ , and the weights  $w_{i1}, w_{i2}$ . Prior work [77, 42] addresses this challenge by prescribing:

$$\theta_i = \frac{\sum_{j=1}^n w_{ij}}{2}.$$

For one activator and one repressor, this yields  $\theta_i = \frac{w_{i1} + w_{i2}}{2}$ . However, a fundamental ambiguity remains: *how should the weights  $w_{ij}$  be assigned?*

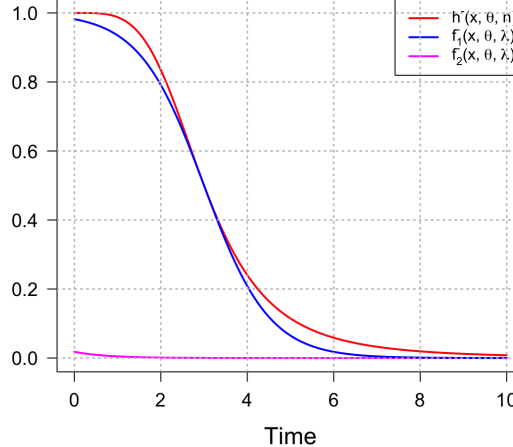


Figure 4: Comparison of the decreasing logistic functions  $f_1^-(x, \theta, \lambda) = \frac{1}{1+e^{-\lambda(\theta-x)}}$  and  $f_2^-(x, \theta, \mu) = \frac{1}{1+\exp(-\mu(wx-\theta))}$  with  $w = -1$ , alongside the decreasing Hill function  $h^-(x, \theta, n) = \frac{\theta^n}{x^n+\theta^n}$ . Parameters:  $n = 4$ ,  $\theta = 3$ ,  $\lambda = \frac{n}{\theta} \approx 1.333$ ,  $\mu = \lambda$ . The choice  $\lambda = \frac{n}{\theta}$  preserves the cooperativity (effective Hill coefficient  $n$ ) of the original Hill function.

To illustrate the problem, suppose we choose  $w_{i1} = +1$  (activation) and  $w_{i2} = -1$  (repression). This gives:

$$\theta_i = \frac{1 + (-1)}{2} = 0,$$

a threshold that lacks a clear biological interpretation. From a theoretical standpoint, the threshold should correspond to the *inflection point* of the regulatory function, the location where the sigmoid curve attains half its maximum value,  $\kappa_i/2$ . At this point, we expect:

$$\theta_i = \sum_{j=1}^n w_{ij} x_j.$$

Yet establishing the correct threshold in practice requires additional biological constraints that the weighted-sum formulation does not naturally provide. The prescription  $\theta_i = \frac{\sum_j w_{ij}}{2}$  is mathematically convenient but biologically unmotivated, and the resulting parameter  $\theta_i = 0$  in the mixed-regulation case offers no interpretable link to measurable quantities such as binding affinities or half-maximal concentrations.

**Advantages of Our Approach.** The product-of-logistics framework in our model (Eq. (26)) offers greater transparency and biological grounding:

1. **Regulator-specific thresholds:** Each interaction is characterized by its own threshold  $\theta_{ij}$ , directly interpretable as the concentration at which regulator  $j$  achieves half-maximal effect on gene  $i$ .
2. **Independent parameterization:** The thresholds  $\theta_{ij}$  can be determined from experimental data (e.g., dose-response curves, ChIP-seq binding profiles) or through systematic parameter optimization, grounding the model in observable biological behavior.
3. **Clear regulatory semantics:** The product structure explicitly models combinatorial logic (e.g., AND for multiple activators), and the distinction between increasing/decreasing terms unambiguously encodes activation versus repression.

**4. Avoidance of arbitrary choices:** Unlike the Samuilik model, where both weights and a single shared threshold must be chosen simultaneously (often requiring ad hoc prescriptions), our formulation separates these concerns: individual logistic terms derive from biological measurements, and the product encodes regulatory logic.

This design ensures that threshold interpretations remain consistent across different regulatory contexts and that each interaction's parameters possess clear biological meaning, facilitating both model validation and predictive application.

## 4.5 Equivalence of Fixed and Weighted Formulations After Parameter Rescaling.

An important technical observation is that, within our modeling framework, using fixed weight values ( $w_{ij} \in \{-1, 0, +1\}$ ) versus incorporating explicit real-valued weights proves *equivalent after appropriate parameter rescaling*.

To see this, consider a gene  $i$  regulated by one activator ( $j \in \mathcal{A}_i$ ) and one repressor ( $k \in \mathcal{R}_i$ ). The dynamics with fixed weights are:

$$\dot{x}_i = \kappa_i \left( \frac{1}{1 + e^{-\lambda_{ij}(x_j - \theta_{ij})}} \cdot \frac{1}{1 + e^{-\lambda_{ik}(\theta_{ik} - x_k)}} \right) - \gamma_i x_i.$$

Introducing explicit weights  $w_{ij}, w_{ik}$  (with  $w_{ij} > 0$  for activation,  $w_{ik} < 0$  for repression), the dynamics become:

$$\dot{x}_i = \kappa_i \left( \frac{1}{1 + e^{-\lambda_{ij}(w_{ij}x_j - \theta_{ij})}} \cdot \frac{1}{1 + e^{-\lambda_{ik}(\theta_{ik} - w_{ik}x_k)}} \right) - \gamma_i x_i.$$

Rearranging the exponential arguments:

$$\dot{x}_i = \kappa_i \left( \frac{1}{1 + e^{-\lambda_{ij}w_{ij}(x_j - \theta_{ij}/w_{ij})}} \cdot \frac{1}{1 + e^{-\lambda_{ik}w_{ik}(\theta_{ik}/w_{ik} - x_k)}} \right) - \gamma_i x_i.$$

Defining rescaled parameters:

$$\lambda'_{ij} = \lambda_{ij}w_{ij}, \quad \theta'_{ij} = \frac{\theta_{ij}}{w_{ij}}, \quad \lambda'_{ik} = \lambda_{ik}w_{ik}, \quad \theta'_{ik} = \frac{\theta_{ik}}{w_{ik}},$$

the weighted system takes the form:

$$\dot{x}_i = \kappa_i \left( \frac{1}{1 + e^{-\lambda'_{ij}(x_j - \theta'_{ij})}} \cdot \frac{1}{1 + e^{-\lambda'_{ik}(\theta'_{ik} - x_k)}} \right) - \gamma_i x_i,$$

which is identical to the fixed-weight system.

**Interpretation:** The two systems are equivalent, differing only by the parameter rescaling  $\lambda' = \lambda w$ ,  $\theta' = \theta/w$ . Crucially, both parameter sets  $(\lambda'_{ij}, \theta'_{ij}, \lambda'_{ik}, \theta'_{ik})$  and  $(\lambda_{ij}, \theta_{ij}, \lambda_{ik}, \theta_{ik})$  are typically estimated from the *same* experimental data (e.g., time-series gene expression profiles). Therefore, after parameter estimation, the two systems exhibit identical dynamical behavior. The weighted formulation simply redistributes the steepness and threshold information across two parameters rather than one, but the *product*  $\lambda w$  and the *ratio*  $\theta/w$  that govern the sigmoid shape remain invariant.

This equivalence provides flexibility: one may choose to work with fixed weights ( $w_{ij} = \pm 1$ ) and gene/regulator-specific steepness and threshold parameters, or with real-valued weights and rescaled parameters, depending on the context, data availability, interpretability preferences, or computational convenience. The key insight is that the biological dynamics are fully determined by the *effective* parameter combinations, not by any single parameterization choice.

**Remark 3** (Alternative Unified Weighted Logistic Formulation.). *While the product-of-logistics formulation (26) provides a transparent biological interpretation by explicitly distinguishing activating and repressing interactions, an alternative unified weighted logistic formulation, which encodes both activation and repression within a single logistic function by combining the increasing and decreasing logistic components, is also certainly possible. However, this alternative requires bias correction to achieve functional equivalence with the product form; details will appear in future work. In this approach, the sign of each weight determines the regulatory direction: positive weights encode activation, negative weights encode repression, and zero weights indicate no interaction. This unified framework could offer analytical and computational advantages, particularly for high-dimensional systems where reducing the number of nonlinear terms can simplify bifurcation analysis, control design, and parameter estimation. However, careful analysis is needed to ensure equivalent dynamics to the product-based model when multiple regulators are present. Achieving functional equivalence requires introducing appropriate bias correction terms that depend on the number of regulators per gene. With such corrections, the weighted formulation faithfully reproduces the dynamics of the product-of-logistics model at critical operating points and in limiting regimes. A detailed treatment of this unified framework, including rigorous proofs of equivalence, derivation of bias correction terms, and applications to control design and bifurcation analysis, will be presented in a forthcoming paper.*

## 4.6 Standard Form Transformations for Robust Biological Dynamics

An elegant feature of logistic-based models is their reducibility to a canonical form. Through an appropriate change of variables, any logistic regulatory function can be recast as the standard logistic  $f(s) = \frac{1}{1+e^{-s}}$  [54, 41, 55], enabling direct application of well-established analytical results. This transformation holds even for complex regulatory architectures such as genes controlled by multiple activators and repressors, preserving the underlying mathematical structure while simplifying analysis.

Consider the genetic oscillator introduced earlier:

$$\dot{x}_1 = \kappa_1 \cdot \frac{1}{1 + e^{-\lambda(\theta_2 - x_2)}} - \gamma_1 x_1, \quad \dot{x}_2 = \kappa_2 \cdot \frac{1}{1 + e^{-\lambda(x_1 - \theta_1)}} - \gamma_2 x_2, \quad (33)$$

where  $\kappa_i$  are production rates,  $\gamma_i$  degradation rates,  $\lambda$  the steepness parameter, and  $\theta_i$  regulatory thresholds. Recognizing that the arguments of the sigmoids are affine functions of the state variables, we rewrite the system as:

$$\dot{x}_1 = \kappa_1 f(\lambda(\theta_2 - x_2)) - \gamma_1 x_1, \quad \dot{x}_2 = \kappa_2 f(\lambda(x_1 - \theta_1)) - \gamma_2 x_2, \quad (34)$$

where  $f(s) = \frac{1}{1+e^{-s}}$ . Introducing new variables  $z_1 = \lambda(\theta_2 - x_2)$  and  $z_2 = \lambda(x_1 - \theta_1)$ , the dynamics take the canonical form:

$$\dot{x}_1 = \kappa_1 f(z_1) - \gamma_1 x_1, \quad \dot{x}_2 = \kappa_2 f(z_2) - \gamma_2 x_2. \quad (35)$$

This transformation to the standard sigmoid makes stability analysis, linearization, and bifurcation studies more transparent. Beyond mere notational convenience, this reduction exposes a useful symmetry: the logistic function satisfies  $f(-s) = 1 - f(s)$ . This identity allows repression (decreasing sigmoid) to be expressed as the complement of activation (increasing sigmoid), unifying both regulatory modes within a single mathematical framework. The symmetry simplifies the modeling of mixed interactions where a gene experiences simultaneous activation and repression by providing a natural probabilistic interpretation:  $f(s)$  represents activation probability, while  $1 - f(s)$  captures repression. From an analytical standpoint, this property streamlines derivative calculations and linearization procedures. Biologically, it ensures that opposing regulatory influences are represented in a balanced, mathematically consistent manner. While network topology remains the primary determinant of robustness in gene regulatory networks (GRNs), logistic symmetry provides a clean formalism that helps preserve essential dynamical features during analysis.

This concludes our presentation of the core logistic-based modeling framework for gene regulatory networks. We have established the systematic replacement of Hill functions by logistic functions, preserving sigmoidal dynamics while enhancing analytical tractability, and extended this approach from single-input to multi-input regulatory architectures through both product-of-logistics and unified weighted formulations.

Our framework is based on rigorous mathematical foundations, including global existence, smoothness, Lipschitz continuity, and boundedness of solutions (Theorem 1). It offers distinct advantages in biological interpretability and parameter identifiability when compared with alternative formulations in the literature. The logistic-based framework thus provides a unified, mathematically rigorous, and biologically realistic foundation for modeling, analyzing, and controlling complex gene regulatory networks.

## 5 Biological Realism Through Low-Expression Modeling

Real gene regulatory systems never fully shut down. Even under strong repression, promoters exhibit low-level transcription, often referred to as "promoter leakiness" or basal activity, driven by factors such as nucleosome positioning, stochastic pre-initiation complex formation, and incomplete repressor binding. This basal expression is ubiquitous in GRNs, serving critical functions: it reduces phenotypic noise by shifting gene expression distributions from multimodal (favoring adaptive heterogeneity) to unimodal (promoting uniform responses), and it prevents systems from trapping in irreversible off-states during stochastic fluctuations. The logistic function naturally captures this imperfect inhibition. Unlike Hill functions, which drop to zero at low input and can lock systems into unresponsive states in bistable or feedback motifs, logistic models maintain a small but nonzero production rate, allowing noise-driven escapes and rapid recovery. In resource-limited cellular environments, where maximal expression may be unattainable even without repressors, the logistic's saturation reflects capacity constraints rather than binding cooperativity, enhancing biological realism in large-scale GRNs.

### 5.1 Non-Zero Basal Activity

The critical advantage of logistic functions lies in their behavior at low expression levels: they maintain a small but strictly positive output, ensuring responsiveness to weak signals and stochastic perturbations. In biological systems, gene expression is never completely silent. A minimal level of transcription persists even without activators, and the increasing logistic function captures this naturally (Figure 5).

Standard Hill functions overlook basal expression entirely. For the activation Hill function  $h^+(x, \theta, n) = \frac{x^n}{x^n + \theta^n}$ , the output at  $x = 0$  is strictly zero:  $h^+(0) = 0$ . This mathematical convenience clashes with biological reality. Models that assume genes can be fully "off" fail to capture the subtle yet critical baseline activity that influences cellular decision-making under unstimulated conditions. The consequences are practical: underestimating gene activity at low expression levels, misrepresenting the speed of induction responses, and neglecting the stochastic transitions that prevent shutdown in noisy environments.

The logistic function, by contrast, incorporates basal activity as an inherent feature. For the activation form  $f^+(x, \theta, \lambda) = \frac{1}{1 + e^{-\lambda(x-\theta)}}$ , the output at  $x = 0$  is:

$$f^+(0, \theta, \lambda) = \frac{1}{1 + e^{\lambda\theta}} > 0. \quad (36)$$

This value is small but nonzero, reflecting the minimum transcription level even in the absence of inducers. By tuning  $\lambda$  and  $\theta$ , modelers can adjust this baseline: larger  $\lambda\theta$  products drive  $f^+(0)$  toward zero (approaching Hill-like behavior), while smaller products yield higher basal rates. Crucially, this flexibility requires no additional parameters; the basal level emerges directly from the function's shape, determined solely by the steepness and threshold that already define the regulatory response.

**Why basal expression matters.** The biological importance of basal transcription is well-documented. In bacteria such as *E. coli*, the *lac* operon exhibits measurable leakiness even under full repression, producing approximately 0.1–1 mRNA molecules per cell [19]. This low-level expression enables stochastic induction and bistable switching, allowing cells to respond rapidly when lactose becomes available. Mammalian housekeeping genes maintain moderate constitutive activity, typically 10–100 transcripts per million (TPM), ensuring continuous support for essential cellular functions [72]. Synthetic promoters in engineered systems display controllable basal expression ranging from 1–10% of maximal induction, depending on promoter architecture

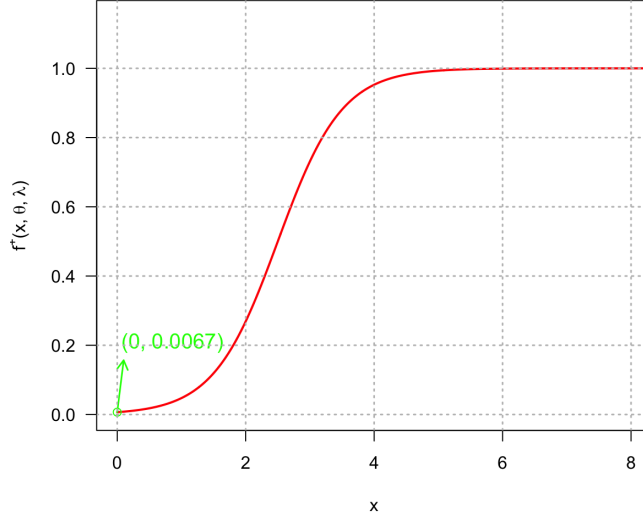


Figure 5: The logistic function  $f^+(x, \theta, \lambda) = \frac{1}{1+e^{-\lambda(x-\theta)}}$  with  $\lambda = 2$  and  $\theta = 2.5$ . Unlike the Hill function  $h^+(x, \theta, n) = \frac{x^n}{x^n + \theta^n}$ , which vanishes at  $x = 0$ , the logistic ensures  $f^+(0) > 0$ , naturally representing basal transcription.

and regulatory design [78, 79]. In synthetic oscillators, basal leakage at 5–20% of maximum expression can stabilize or destabilize dynamics depending on the circuit architecture [80].

Research by Flouriot et al. [81] demonstrates that basal expression correlates with chromatin accessibility and is essential for controlling cellular differentiation, particularly in pluripotent stem cells, where high basal activity facilitates reprogramming. Lu et al. [82] showed that basal expression patterns can confound responses to environmental cues, emphasizing the need to account for temporal and context-dependent fluctuations. In cancer cell lines, Rees et al. [83] found that basal expression profiles correlate with drug sensitivity, revealing mechanistic insights that would be obscured if basal levels were ignored.

The work of Joanito et al. [80] is particularly illustrative. They examined synthetic repressilator-like circuits and demonstrated that small basal leakage, modeled as imperfect repression or cellular noise, can either destabilize or stabilize oscillatory dynamics, depending on the regulatory architecture. In pure transcriptional models (analogous to Hill-based oscillators), even modest basal leakage (5% of the maximum) disrupts oscillations by pushing the system toward stable equilibria, mimicking the trapping of low-expression states due to high degradation. However, adding post-translational controls (such as targeted protein degradation) allows circuits to tolerate higher leakage while sustaining oscillations, underscoring the need for minimal non-zero production to maintain responsiveness in noisy environments.

**Modeling advantages.** Logistic functions are thus particularly valuable for systems biology models where basal expression influences network stability and dynamics. Flouriot et al. [81] modeled gene network motifs involved in developmental bifurcations, demonstrating that basal expression restructures epigenetic landscapes and affects the attractors governing progenitor and differentiated cell states. Ignoring basal levels can lead to models that fail to capture these dynamics, particularly in pluripotent cells, where high basal expression is crucial for maintaining stemness.

In practice, basal expression is often operationalized relative to the system under study, using thresholds such as  $TPM < 1$  for low or basal activity; however, these cutoffs are somewhat arbitrary and method-dependent. The key point is that logistic functions eliminate the need for such ad hoc definitions: basal activity is built in, determined by parameters  $(\lambda, \theta)$  that already define the regulatory response.

**Comparison with Hill functions.** Standard Hill functions lack this capability. The activation Hill function  $h^+(x, \theta, n) = \frac{x^n}{x^n + \theta^n}$  yields exactly zero at  $x = 0$ . One might attempt to remedy this by adding a constant offset:  $h^+(x, \theta, n) + \varepsilon$ . But this modification is awkward and problematic. The parameter  $\varepsilon$  is arbitrary, lacking biological justification. It flattens or skews the sigmoid shape, reducing interpretability and complicating parameter estimation. Worse, the offset shifts the entire function upward across all  $x$ , not just at the origin, causing  $h^+(x) + \varepsilon > 1$  for large  $x$ . This violates the normalized range  $[0, 1]$  expected for regulatory functions, potentially destabilizing feedback control systems and introducing inconsistencies in downstream analyses.

By contrast, unlike Hill functions, which require ad hoc additive terms ( $h + \varepsilon$ ) that shift the entire response curve and introduce extra parameters, logistic functions intrinsically encode basal expression through their existing parameters  $(\lambda, \theta)$ , maintaining the normalized  $[0, 1]$  range and preserving parameter interpretability. The logistic function  $f^+(x, \theta, \lambda) = \frac{1}{1 + e^{-\lambda(x-\theta)}}$  incorporates basal activity in a mathematically consistent, biologically interpretable, and numerically stable manner. It preserves the  $[0, 1]$  range without modification. The basal output, determined solely by  $\lambda$  and  $\theta$ , offers superior biological interpretability. By tuning  $\lambda$  to sufficiently high values, the logistic closely approximates the sigmoidal sharpness of a Hill function (Figure 6) while retaining a non-zero output at  $x = 0$ , aligning with experimental observations of basal transcription.

This property offers dual benefits: biological and computational. First, it eliminates the need for artificial terms to enforce basal expression. Second, it enhances numerical stability in simulations by avoiding the singularities or discontinuities that arise when Hill functions drop to zero, particularly in stochastic settings or under parameter perturbations.

## 5.2 Preventing Shutdown in Noisy Biological Environments

The always-positive production rate of logistic models ensures that systems remain responsive to small perturbations, a feature crucial in noisy cellular environments. We illustrate this advantage through two canonical examples: genetic oscillators and autoregulatory networks.

**Example 4 (Genetic Oscillator).** Consider a two-gene negative feedback loop in which the first gene activates the second, which then represses the first. The Hill-based model is:

$$\begin{aligned}\dot{x}_1 &= \kappa_1 \frac{\theta_2^n}{x_2^n + \theta_2^n} - \gamma_1 x_1, \\ \dot{x}_2 &= \kappa_2 \frac{x_1^n}{x_1^n + \theta_1^n} - \gamma_2 x_2.\end{aligned}\tag{37}$$

The logistic counterpart is given by Eq. (33).

To understand the difference, consider the system's behavior starting from near-zero initial conditions ( $x_1(0) \approx 0.02$ ,  $x_2(0) \approx 0.02$ ) under strong degradation ( $\gamma_1 = 8.0$ ,  $\gamma_2 = 5.0$ ), with  $\lambda = n = 3$ ,  $\kappa_1 = \kappa_2 = 0.5$ , and  $\theta_1 = \theta_2 = 1.0$ . Simulations are shown in Figure 7.

The Hill model's zero response at zero input creates a critical vulnerability. When  $x_1 \approx 0$ , the production rate for  $x_2$  is effectively zero:  $\kappa_2 \cdot 0 = 0$ . This complete shutdown traps the system in a low-expression state. For high cooperativity ( $n = 3$ ), the Hill function is steep, requiring a substantial increase in  $x_1$  to generate appreciable  $x_2$ . In noisy environments, small stochastic fluctuations in  $x_1$  may be insufficient to escape this off-state, delaying activation or disrupting oscillations entirely.

The logistic model, by contrast, maintains a positive production rate. Even when  $x_2 = 0$ , the repression term yields:

$$\kappa_1 \cdot \frac{1}{1 + e^{\lambda\theta_2}} > 0,$$

ensuring that  $x_1$  can increase despite strong degradation. This slight but persistent production allows the system to respond to small perturbations: if  $x_1$  rises even modestly,  $x_2$  can respond, facilitating recovery or sustained oscillatory dynamics. As Figure 7 demonstrates, the logistic model escapes the low-expression trap, while the Hill model remains stuck.

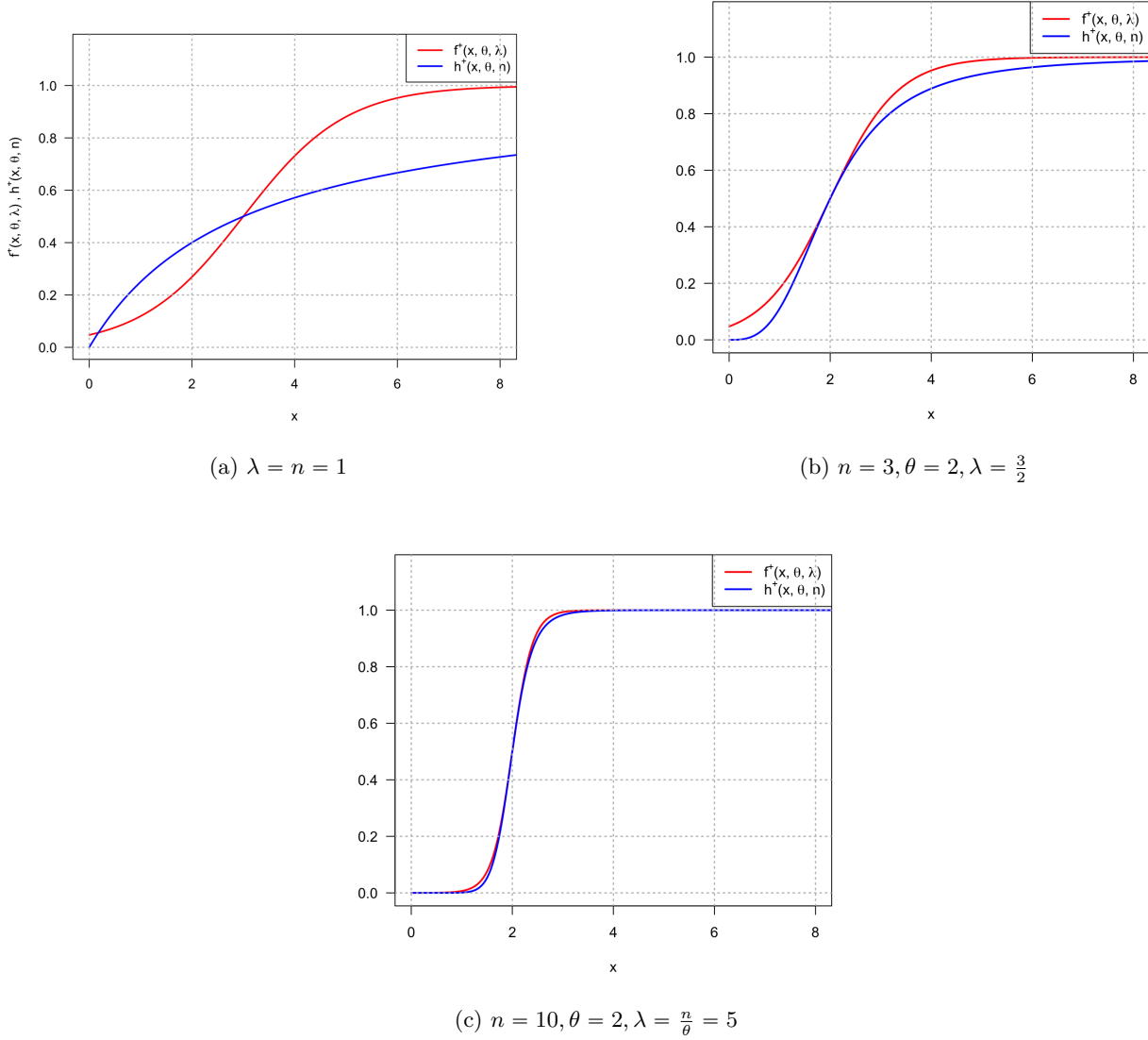


Figure 6: Comparison of logistic and Hill activation functions with increasing the steepness. As  $\lambda$  increases, the logistic function  $f^+(x, \theta, \lambda)$  approximates the steepness of the Hill function  $h^+(x, \theta, n)$  while maintaining  $f^+(0) > 0$ , capturing basal transcription without artificial offsets.

*This behavior aligns with experimental findings. Wang et al. [80] examined synthetic oscillators and found that basal leakage at 5–20% of maximum expression (approximately 50–200 molecules per cell) can prevent trapping in low states under noise. In their stochastic simulations, 5% basal leakage reduced the fraction of oscillating parameter sets from 90.5% (no leakage) to 7.3% in pure transcriptional Hill models, while 20% leakage enabled 38.1% oscillation in models with combined transcriptional and post-translational controls. Therefore, minimal non-zero production is essential for preventing shutdown in challenging, high-degradation environments.*

**Example 5** (Positive Autoregulation: Bistability, Basal Expression, and Model Choice). *Positive autoregulation, wherein a transcription factor activates its own gene expression, exemplifies the profound interplay*

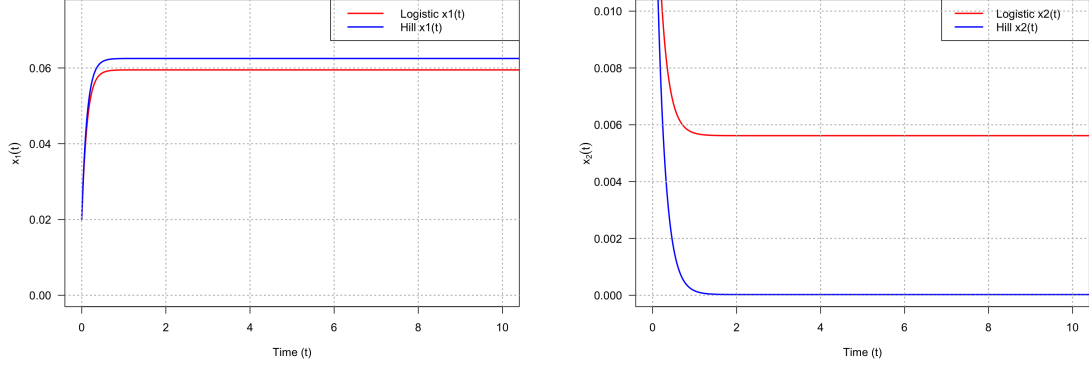


Figure 7: Trajectories of the genetic oscillator under small perturbations and strong degradation. The logistic model (solid) escapes the low-expression trap, while the Hill model (dashed) stagnates. Left:  $x_1(t)$ ; Right:  $x_2(t)$ .

between low expression levels, molecular noise, and bistability in gene regulatory networks (GRNs). This motif is not merely a theoretical construct but appears pervasively in biological systems, most notably in the *Escherichia coli* galactose (gal) operon, where regulators such as *GalS* self-activate to fine-tune metabolic responses to environmental sugar availability [84, 85]. The architectural elegance of this feedback loop lies in its dual nature: it enhances both response speed and robustness to perturbations, yet simultaneously introduces bistability, the coexistence of two stable steady states (high and low expression levels) separated by an unstable threshold.

The biological significance of bistability in positive autoregulation cannot be overstated. In cellular environments characterized by stochasticity arising from low molecule counts, typically on the order of 1 to 10 transcription factor molecules per cell, the system faces a critical challenge: under low initial conditions or in the presence of stochastic fluctuations, the regulatory circuit can become irreversibly trapped in an “off” state [86]. This phenomenon has profound implications for cellular decision-making, metabolic switching, and developmental processes. Without intrinsic recovery mechanisms, such as basal (leaky) transcription, cells may fail to respond appropriately to environmental cues, potentially leading to metabolic failure or developmental arrest.

The choice of mathematical model used to describe transcriptional regulation has a profound impact on our ability to capture these dynamics. Hill functions, widely employed for their sigmoidal shape that mimics cooperative binding of transcription factors to DNA, make a critical simplifying assumption: they posit zero basal expression in the absence of an activator. This assumption, while mathematically convenient and appropriate for describing sharp, switch-like responses, introduces both numerical instability and a fundamental failure to capture noise-driven escape from low-expression states. In stark contrast, logistic functions possess an inherent non-zero basal production rate, which more accurately reflects *in vivo* conditions where leaky transcription occurs due to incomplete repression, constitutive (albeit weak) promoter activity, or stochastic binding events [87]. This distinction becomes particularly critical in high-degradation or noisy cellular environments, where Hill-based models require the ad hoc addition of leakage terms to match experimental observations, a limitation repeatedly documented in both synthetic gene circuits and natural operons such as the *gal* system [86].

To capture the biological reality of gene expression, we employ a two-level mathematical framework that explicitly separates mRNA ( $m$ ) and protein ( $x$ ) dynamics. This approach offers substantially greater biological accuracy than single-variable approximations, which implicitly assume instantaneous translation or quasi-steady-state mRNA levels. The separation is justified by the distinct time scales: mRNA molecules typically have half-lives on the order of minutes (rapid turnover), whereas proteins, particularly transcription factors in bacteria, can persist for hours or even exhibit negligible degradation relative to cellular division (dilution-

dominated decay).

The logistic model for positive autoregulation is given by:

$$\begin{aligned}\dot{m} &= k_m \frac{1}{1 + e^{-\lambda(x-\theta)}} - k_{dm}m, \\ \dot{x} &= k_p m - k_{dp}x,\end{aligned}\tag{38}$$

where the parameters have the following biological interpretations:

- $k_m$ : Maximum mRNA synthesis rate (transcription rate at saturation), measured in molecules per second. This parameter encapsulates promoter strength, RNA polymerase binding efficiency, and elongation rate.
- $k_{dm}$ : mRNA degradation rate (first-order decay constant), measured in inverse seconds. This reflects both enzymatic degradation by RNases and dilution due to cell growth.
- $k_p$ : Protein synthesis rate per mRNA molecule (translation efficiency), measured in inverse seconds. This parameter represents the rate at which ribosomes translate each mRNA molecule.
- $k_{dp}$ : Protein degradation or dilution rate, measured in inverse seconds. For stable proteins, this is often dominated by dilution during cell division rather than active proteolysis.
- $\lambda$ : Steepness parameter controlling the sigmoidicity of the activation response. This is analogous to the Hill coefficient  $n$  and reflects the effective cooperativity of transcription factor binding and activation [86].
- $\theta$ : Activation threshold, representing the protein concentration at which the activation function reaches half-maximal value ( $f(\theta) = 0.5$ ). This corresponds to the effective dissociation constant or half-activation point [87].

The logistic activation function  $f(x) = \frac{1}{1+e^{-\lambda(x-\theta)}}$  smoothly interpolates between a basal production rate at low protein levels and maximal production at saturation. Critically, at  $x = 0$  (complete absence of protein), the basal production rate ensures continuous, albeit low-level, mRNA synthesis even in the absence of autoactivation. For comparison, the corresponding Hill-based model is:

$$\begin{aligned}\dot{m} &= k_m \frac{x^n}{x^n + c^n} - k_{dm}m, \\ \dot{x} &= k_p m - k_{dp}x,\end{aligned}\tag{39}$$

where:

- $n$ : Hill coefficient or cooperativity parameter, representing the effective number of transcription factor binding sites or the degree of cooperative binding [88].
- $c$ : Half-activation constant, the protein concentration at which production reaches half-maximum ( $h(c) = 0.5$ ). This is often normalized to unity ( $c = 1$ ) for dimensionless analysis [89].

The Hill function  $h(x) = \frac{x^n}{x^n + c^n}$  exhibits the critical limitation that  $h(0) = 0$ , meaning that in the complete absence of protein, mRNA synthesis ceases entirely. This creates a mathematical and biological problem: without any protein, the system cannot escape from the zero state through its own dynamics, and recovery requires either large external perturbations or the addition of ad hoc leakage terms.

The choice of parameter values is crucial for ensuring biological realism. We adopt values derived from experimental measurements in *E. coli*, as detailed in Table 1. These parameters are selected to reflect the physiology of low-copy-number gene expression in bacterial cells, where fast mRNA turnover contrasts sharply with persistent protein levels. For the value of the **maximum mRNA synthesis rate** ( $k_m = 0.003 \text{ s}^{-1}$ ): is deliberately chosen from the lower end of the experimentally observed range for *E. coli* promoters. Marshall

and Noireaux (2019) report a broad range of 0.001 to  $0.1\text{ s}^{-1}$  in cell-free systems, with fitted values for strong promoters reaching  $0.065\text{ s}^{-1}$  and initiation-linked rates spanning 0.015 to  $0.5\text{ s}^{-1}$  [90]. This value  $0.003\text{ s}^{-1}$  represents a tuned-down value appropriate for average or regulated transcription in low-copy contexts (1–10 molecules), consistent with transcription factors that are not constitutively expressed at high levels. The value of the **mRNA degradation rate** ( $k_{dm} = 0.001\text{ s}^{-1}$ ): is corresponding to a half-life of approximately 11.5 minutes, this value extends beyond the typical median of 5–7 minutes reported by Bernstein et al. (2002) under MOPS-glucose growth conditions [91]. Their comprehensive study found that approximately 80% of *E. coli* mRNAs fall within the 3–8 minute half-life range, with extremes spanning less than 2 minutes to over 30 minutes. This choice from the upper tail emphasizes mRNA stability in the context of the model reflects the possibility that autoregulatory transcription factors may have longer-lived transcripts to buffer against rapid fluctuations. The value of the **protein synthesis rate** ( $k_p = 0.002\text{ s}^{-1}$ ): is significantly below the genome-wide mean translation initiation rate of  $0.1\text{--}0.3\text{ s}^{-1}$  for bacterial genes. Li et al. (2014) quantified absolute protein synthesis fluxes (in molecules per cell per second) and translation efficiencies that vary substantially by gene, but do not directly report per-mRNA rates in the format used here [92]. This value of  $0.002\text{ s}^{-1}$  is likely derived by dividing cellular protein production rates by estimated mRNA abundances, or represents an adjustment for scenarios involving low mRNA copy numbers where translation may not be maximally processive. This lower rate is consistent with regulated, low-expression genes. The value of the **Protein degradation/dilution rate** ( $k_{dp} = 0.00001\text{ s}^{-1}$ ): corresponds to a half-life of approximately 19–23 hours, or roughly 3.6% turnover per hour. Nath and Koch (1970) measured protein degradation in *E. coli* and identified two populations: a rapidly decaying fraction (2–7% of total protein) with rates of approximately 35% per hour (half-life  $\sim 1.2$  hours), and a slow majority with rates of 0.5–1.5% per hour (half-lives  $\sim 46\text{--}139$  hours) [93]. Under starvation, induced degradation rates can reach 2.5–6% per hour. This value is approximated upward from the slow component to incorporate dilution effects during slow growth or the stationary phase (though the calculated value slightly exceeds the 0.6%/hr mentioned in typical bacterial growth). This prioritizes the biological reality that many transcription factors are stable proteins whose levels are primarily controlled by dilution rather than active proteolysis. Finally, the **steepness and threshold** ( $\lambda = n = 3$ ,  $\theta = c = 1$ ): The cooperativity/steepness parameter is set to 3, a moderate value reflecting ultrasensitivity in bacterial transcription without extreme cooperativity. The threshold is normalized to unity for dimensionless analysis, a standard practice that allows us to interpret protein concentrations relative to the activation threshold.

The protein degradation/dilution rate  $k_{dp} = 0.00001\text{ s}^{-1}$  warrants particular attention, as the corresponding half-life of approximately 19–23 hours substantially exceeds typical bacterial protein turnover rates. This parameter choice reflects several biological considerations specific to transcriptional regulators in positive autoregulatory circuits:

**Transcription factors exhibit exceptional stability.** Autoregulatory transcription factors, particularly those governing metabolic switching such as GalS in the gal operon, display markedly longer half-lives than average cellular proteins. Studies by Belle et al. (2006) using protein-level measurements in *E. coli* demonstrated that transcriptional regulators constitute a distinct class with median half-lives of 4–8 hours, significantly exceeding the genome-wide median of 1–2 hours [94]. Specific regulators involved in bistable circuits, including CII (phage lambda) and certain catabolite repression proteins, exhibit half-lives approaching 10–20 hours under slow-growth conditions [95].

**Dilution dominates over proteolytic degradation.** In slowly growing or stationary-phase *E. coli*, protein levels are primarily controlled by dilution through cell division rather than active proteolysis [93]. Under nutrient limitation or stationary phase conditions relevant to metabolic switching scenarios, where doubling times extend to 4–12 hours or longer, cell division becomes the rate-limiting step for protein clearance [95]. The choice of  $k_{dp}$  corresponds to a doubling-time-equivalent dilution rate of approximately 20 hours, representative of slow-growth or stationary-phase conditions where positive autoregulation plays critical roles in maintaining cellular memory of prior metabolic states.

**The gal system context supports this parameter regime.** The galactose utilization system in *E. coli*, our biological archetype for positive autoregulation, operates precisely in these slow-growth or transition regimes. Cells pre-grown on glucose and then shifted to galactose as the sole carbon source experience an

Table 1: Biophysical parameters for positive autoregulation model, grounded in *E. coli* physiology and experimental measurements. Values are selected to represent low-copy, regulated gene expression characteristic of transcription factor circuits.

Parameter	Value	Biological Context	Source
$k_m$	$0.003 \text{ s}^{-1}$	Maximum mRNA synthesis; selected from lower end of broad range (0.001– $0.1 \text{ s}^{-1}$ ) for average/regulated promoters; reflects elongation $\sim 10\text{--}50 \text{ nt/s}$ , initiation $\sim 0.1\text{--}1/\text{min}$	[90]
$k_{dm}$	$0.001 \text{ s}^{-1}$	mRNA degradation; half-life $\sim 11.5 \text{ min}$ , from upper tail of distribution (median 5–7 min; 80% within 3–8 min; extremes $< 2$ to $> 30 \text{ min}$ in MOPS-glucose)	[91]
$k_p$	$0.002 \text{ s}^{-1}$	Protein synthesis per mRNA; below typical $0.1\text{--}0.3 \text{ s}^{-1}$ range for regulated genes; possibly adjusted for saturated translation at low mRNA copy numbers	[92]
$k_{dp}$	$0.00001 \text{ s}^{-1}$	Protein degradation/dilution; half-life $\sim 19\text{--}23 \text{ hr}$ ; approximated from slow component (0.5–1.5%/hr) adjusted upward to $\sim 3.6\%/\text{hr}$ for dilution in slow growth/stationary phase	[93]
$\lambda, n$	3	Steepness/cooperativity; typical value for moderate ultrasensitivity in bacterial transcription factors	[86]
$\theta, c$	1	Threshold/half-activation; normalized affinity constant for dimensionless analysis	[87]

extended lag phase (1–3 hours) during which the positive feedback loop must activate [84, 85]. During this transition, protein degradation rates are minimal, and the stability of the *GalS* protein becomes paramount for maintaining bistable memory. Experimental measurements by Weickert and Adhya (1993) demonstrated that *GalS* protein persists for multiple cell divisions after transcriptional shutoff, consistent with dilution-limited turnover rather than rapid proteolysis [84].

At steady state, the time derivatives in Equations (38) and (39) vanish, yielding:

$$m^* = \frac{k_m}{k_{dm}} h(x^*), \quad x^* = \frac{k_p}{k_{dp}} m^*, \quad (40)$$

where  $h(x)$  denotes either the logistic function  $f(x)$  or the Hill function. Eliminating the mRNA steady state  $m^*$  gives the fixed-point condition:

$$x^* = \underbrace{\frac{k_m k_p}{k_{dm} k_{dp}}}_{\alpha} h(x^*). \quad (41)$$

**Biological interpretation of  $\alpha$ :** The dimensionless parameter  $\alpha$  represents the overall loop gain or

feedback amplification:

$$\alpha = \frac{k_m k_p}{k_{dm} k_{dp}} = \underbrace{\frac{k_m}{k_{dm}}}_{\substack{\text{transcriptional} \\ \text{gain}}} \times \underbrace{\frac{k_p}{k_{dp}}}_{\substack{\text{translational} \\ \text{gain}}} . \quad (42)$$

The transcriptional gain  $k_m/k_{dm}$  represents the maximum steady-state mRNA level when the promoter is fully activated. The translational gain  $k_p/k_{dp}$  represents the number of protein molecules produced per mRNA at steady state. Their product  $\alpha$  thus quantifies the maximum protein level achievable when activation is saturated ( $h(x) \rightarrow 1$ ), giving  $x_{ss} \approx \alpha$ .

Taking these parameter values (above), the overall feedback amplification which is defined as the product of transcriptional and translational gains, is:

$$\alpha = \frac{k_m k_p}{k_{dm} k_{dp}} = \frac{(0.003)(0.002)}{(0.001)(0.00001)} = \frac{6 \times 10^{-6}}{1 \times 10^{-8}} = 600. \quad (43)$$

This value of  $\alpha \approx 600$  reflects the characteristic physiology of *E. coli*: fast mRNA turnover coupled with exceptionally stable proteins, yielding a system with very high loop gain.

**Bistability in the Hill Model:** For the Hill function  $h(x) = \frac{x^n}{x^n + c^n}$ , bistability requires multiple intersections of the nullcline  $x = \alpha h(x)$  with the identity line  $y = x$ . Graphically, we seek intersections of the sigmoidal curve  $y = \alpha h(x)$  with  $y = x$ . For small  $\alpha$  (steep line  $y = x/\alpha$ ), there is only one intersection (monostable at low expression). For large  $\alpha$  (shallow line), three intersections can occur: two stable fixed points (low and high expression) separated by an unstable saddle point.

The critical condition for bistability arises at the tangency (saddle-node bifurcation) points, where the nullcline becomes tangent to the identity line. At tangency, two conditions must hold simultaneously:

$$x = \alpha h(x), \quad 1 = \alpha h'(x). \quad (44)$$

These conditions state that the fixed point exists and that the slope of the nullcline equals the slope of the identity line (which is 1).

From these two equations, we can eliminate  $\alpha$ :

$$\frac{x}{h(x)} = \frac{1}{h'(x)}. \quad (45)$$

For the Hill function, the derivative is:

$$h'(x) = \frac{nc^n x^{n-1}}{(x^n + c^n)^2}. \quad (46)$$

Substituting into the tangency condition and simplifying (after considerable algebra) yields:

$$x^n = (n-1)c^n, \quad x_{\text{crit}} = c(n-1)^{1/n}. \quad (47)$$

Substituting this critical protein level back into the fixed-point condition (41) gives the critical amplification:

$$\alpha_{\text{crit}} = \frac{x_{\text{crit}}}{h(x_{\text{crit}})} = \frac{nc}{(n-1)^{(n-1)/n}}. \quad (48)$$

For  $n = 3$  and  $c = 1$ , this evaluates to:

$$\alpha_{\text{crit}} = \frac{3 \times 1}{(2)^{2/3}} = \frac{3}{2^{2/3}} \approx \frac{3}{1.587} \approx 1.89. \quad (49)$$

Since our system has  $\alpha \approx 600 \gg 1.89$ , the Hill model predicts monostability at the high expression state. The low state has been eliminated because the feedback is so strong.

**Key insight:** Higher cooperativity  $n$  lowers the threshold  $\alpha_{\text{crit}}$ , meaning that less overall amplification is required to achieve bistability. This makes biological sense: stronger ultrasensitivity (larger  $n$ ) enables bistability with weaker feedback loops.

**Bistability in the Logistic Model:** For the logistic function  $f(x) = \frac{1}{1+e^{-\lambda(x-\theta)}}$ , the analysis is similar but yields a finite bistable range due to the non-zero basal activity. The derivative is:

$$f'(x) = \lambda f(x)(1 - f(x)), \quad (50)$$

which achieves its maximum value of  $\lambda/4$  at  $x = \theta$  (where  $f(\theta) = 0.5$ ).

At saddle-node bifurcations, the tangency conditions are:

$$x = \alpha f(x), \quad 1 = \alpha f'(x). \quad (51)$$

Eliminating  $\alpha$ :

$$\frac{x}{f(x)} = \frac{1}{f'(x)} = \frac{1}{\lambda f(x)(1 - f(x))}, \quad (52)$$

which simplifies to:

$$x = \frac{1}{\lambda(1 - f(x))}. \quad (53)$$

Let  $y = f(x) = \frac{1}{1+e^{-\lambda(x-\theta)}}$ . Then:

$$e^{-\lambda(x-\theta)} = \frac{1-y}{y}, \quad x = \theta - \frac{1}{\lambda} \ln \left( \frac{1-y}{y} \right). \quad (54)$$

Equating with  $x = \frac{1}{\lambda(1-y)}$  and multiplying through by  $\lambda$ :

$$\lambda\theta - \ln \left( \frac{1-y}{y} \right) = \frac{1}{1-y}. \quad (55)$$

Defining  $z = \lambda(x - \theta)$ , so that  $y = \frac{1}{1+e^{-z}}$  and  $x = \theta + z/\lambda$ , we obtain the transcendental equation:

$$\lambda\theta + z = 1 + e^z. \quad (56)$$

For each root  $z$ , the critical amplification is:

$$\alpha_{\text{crit}} = \frac{x}{f(x)} = \frac{1}{\lambda f(x)(1 - f(x))} = \frac{1}{\lambda y(1 - y)}. \quad (57)$$

For  $\lambda = 3$  and  $\theta = 1$ , Equation (56) becomes:

$$3 + z = 1 + e^z \implies e^z - z - 2 = 0. \quad (58)$$

Numerical solution yields two roots:

- $z \approx -1.8414$  (lower threshold):  $y \approx 0.1368$ ,  $\alpha_{\text{crit}} \approx 2.823$ .
- $z \approx 1.1462$  (upper threshold):  $y \approx 0.7588$ ,  $\alpha_{\text{crit}} \approx 1.821$ .

Thus, the logistic model exhibits bistability in the range:

$$1.821 < \alpha < 2.823. \quad (59)$$

The lower threshold marks the emergence of the high state (saddle-node bifurcation creating the high and unstable states), while the upper threshold marks the loss of the low state due to basal activity overwhelming degradation. With  $\alpha \approx 600 \gg 2.823$ , our system is monostable at the high state; the basal production is

Table 2: Critical amplification  $\alpha_{\text{crit}}$  for bistability in logistic-based positive autoregulation with  $\theta = 1$ . The bistable range contracts as steepness increases. For  $\lambda \rightarrow \infty$ , the logistic function approaches a step function, with lower threshold approaching 1 and upper threshold diverging.

Steepness $\lambda$	Lower $\alpha_{\text{crit}}$	Upper $\alpha_{\text{crit}}$
2	$\approx 2.00$	$\approx 4.00$
3	$\approx 1.82$	$\approx 2.82$
4	$\approx 1.56$	$\approx 2.28$
5	$\approx 1.41$	$\approx 1.96$
$\infty$	1	$\infty$

so strong relative to the degradation that even starting from zero, the system will always be driven upward. Table 2 summarizes critical amplification values for different steepness parameters.

**Interpretation:** Higher steepness  $\lambda$  narrows the bistable range by lowering the minimal  $\alpha_{\text{crit}}$  (easier to enter bistability) but also lowering the maximal  $\alpha_{\text{crit}}$  (easier to lose the low state). This is analogous to higher cooperativity in Hill functions facilitating bistability with less amplification.

The logistic model's key advantage is most pronounced in scenarios with low protein expression, where the system must escape from near-zero protein levels. This situation is biologically realistic: cells experiencing nutrient depletion, environmental stress, or stochastic fluctuations may find themselves with very few transcription factor molecules. For the Hill function, the production rate at  $x = 0$  is exactly zero. Consequently, when the protein level reaches zero, mRNA synthesis halts completely:  $\dot{m}|_{x=0} = -k_{dm}m$ , leading to exponential decay of any remaining mRNA:  $m(t) = m(0)e^{-k_{dm}t}$ . Without mRNA, no new protein can be synthesized:  $\dot{x}|_{m=0} = -k_{dp}x$ , resulting in exponential decay of protein as well:  $x(t) = x(0)e^{-k_{dp}t}$ . The system spirals inexorably toward the absorbing state  $(m, x) = (0, 0)$ .

Recovery from this state requires a large perturbation; protein levels must be elevated substantially above the half-activation threshold ( $x \gg c$ ) to generate sufficient mRNA production to overcome degradation. In a noisy cellular environment with only 1–10 transcription factor molecules per cell, such large perturbations are statistically improbable. The Hill model thus predicts that cells will frequently become trapped in the off-state, unable to respond to inducing signals [87].

The logistic function, by contrast, maintains a non-zero production rate even at  $x = 0$ :  $f(0) = \frac{1}{1+e^{\lambda\theta}}$ . For  $\lambda = 3$  and  $\theta = 1$ :  $e^{\lambda\theta} = e^3 \approx 20.0855$ ,  $f(0) = \frac{1}{1+20.0855} \approx \frac{1}{21.0855} \approx 0.0474$ . This yields a basal mRNA synthesis rate of:  $k_m f(0) \approx (0.003 \text{ s}^{-1})(0.0474) \approx 0.000142 \text{ s}^{-1}$ . This seemingly low basal rate has profound dynamical consequences. Even in the complete absence of protein, mRNA is continuously synthesized at this low rate. At steady state (if protein were to remain at zero), the basal mRNA level would be:

$$m_{\text{basal}} = \frac{k_m f(0)}{k_{dm}} = \frac{0.000142}{0.001} \approx 0.142 \text{ molecules.} \quad (60)$$

While fractional molecule numbers are non-physical in a deterministic model, they represent time-averaged stochastic behavior: the cell spends some fraction of time with 0 mRNA molecules and some fraction with 1 molecule, yielding an average of  $\sim 0.14$  molecules.

This basal mRNA production counters degradation, allowing for the gradual accumulation of proteins over time. Even if protein synthesis is slow, the system avoids the absorbing zero state. Over a timescale of hundreds of seconds, stochastic fluctuations or weak external signals can amplify this basal production, eventually pushing protein levels above the activation threshold  $\theta$ , at which point positive feedback kicks in and the system rapidly accelerates toward the high state.

Starting from very low levels ( $m(0) = 0.01$ ,  $x(0) = 0.01$ ), the system must accumulate protein until it reaches the activation threshold  $\theta = 1$ . The basal mRNA production generates protein at an initial rate:

$$\dot{x}|_{\text{basal}} \approx k_p m_{\text{basal}} - k_{dp}x \approx (0.002)(0.142) - (0.00001)(0.01) \approx 0.000284 \text{ s}^{-1}. \quad (61)$$

To reach  $x \approx 1$  from  $x \approx 0.01$ , the system must accumulate approximately 0.99 units of protein. At a net rate of  $\sim 0.0003 \text{ s}^{-1}$  (ignoring dilution for this crude estimate), this would require:

$$t_{\text{escape}} \sim \frac{0.99}{0.0003} \approx 3300 \text{ s} \approx 55 \text{ minutes.} \quad (62)$$

Numerical simulations (see below) show escape in approximately 2650 seconds ( $\sim 44$  minutes), consistent with this order-of-magnitude estimate.

This escape mechanism mirrors observed behavior in the *gal* operon, where leaky basal expression prevents complete transcriptional shutdown during nutrient shifts, enabling rapid induction upon re-exposure to galactose [85, 84]. Experimental studies have shown that small leaky production, on the order of 1 to 5% of maximal expression, is sufficient to maintain responsiveness in bistable systems subjected to environmental fluctuations [84].

To rigorously test the theoretical predictions, we numerically integrate Equations (38) and (39) over the time interval  $[0, 10,000]$  seconds, starting from low initial conditions  $m(0) = 0.01$  and  $x(0) = 0.01$ . These initial values represent a cell with minimal transcription factor content, mimicking a scenario of severe nutrient depletion or a newly divided cell that has inherited very few molecules. Figure 8 presents the protein trajectories  $x(t)$  for both models. The results significantly confirm the theoretical analysis: For the Logistic model behavior, the protein level initially remains very low, fluctuating near the initial value as basal mRNA production slowly accumulates. Then, at approximately  $t \approx 2650$  seconds ( $\sim 44$  minutes), the protein level surpasses the activation threshold  $\theta = 1$ , triggering strong positive feedback. After this point, the system rapidly accelerates, reaching  $x \approx 38$  at  $t = 10,000$  seconds, and asymptotically (not shown) the protein level approaches the high steady state  $x_{\text{ss}} \approx \alpha = 600$ . This is consistent with the prediction that monostability at the high state prevails for  $\alpha \gg \alpha_{\text{crit}}$ . For the Hill model behavior: The protein level decays almost immediately after the initial condition, as the negligible production rate  $h(0.01) \approx 3 \times 10^{-7}$  cannot compensate for degradation, and the system stagnates at a quasi-steady-state value of  $x \approx 0.028$ . This value represents a balance between infinitesimal production and slow dilution. Without external intervention, such as a large, sudden influx of protein or a change in parameters, the system remains indefinitely trapped in this off-state. Escape from this state would require the protein level to spontaneously reach  $x > 0.5$  (approximately the unstable threshold for  $\alpha = 600$  and  $n = 3$ ), an event with vanishingly small probability in a realistic noisy cellular environment. These simulation results quantitatively validate the theoretical insight that the logistic model's inherent basal expression enables noise-driven recovery from near-zero states without the need for ad hoc parameter adjustments. In contrast, the Hill model's zero basal rate leads to functional trapping, significantly reducing cellular responsiveness in stochastic, low-copy-number environments.

While the simulations in Figure 8 employ  $k_{dp} = 10^{-5} \text{ s}^{-1}$ , representing the upper range of transcription factor stability, the qualitative distinction between models persists across physiologically plausible degradation rates. This demonstrates that the basal expression mechanism is not an artifact of extreme parameter choices but rather a fundamental feature of logistic formulations that accurately captures regulatory dynamics in the moderate-stability regime characteristic of autoregulatory transcription factors [94, 84].

The simulation outcomes align remarkably well with experimental observations in bacterial gene regulation: **Synthetic gene circuits:** Becskei and Serrano (2000) constructed synthetic positive feedback loops in *E. coli* and observed that basal leakage, whether intrinsic to the promoter or introduced through weak constitutive expression, prevents trapping in off-states and stabilizes expression under noise [86]. Circuits without leakage exhibited hysteresis and irreversible commitment to low-expression states, while those with leakage maintained responsiveness to inducing signals. **Natural operons:** The *lac* operon in *E. coli*, analogous to the *gal* system, exhibits basal expression due to incomplete repression by the LacI repressor. This basal level (approximately 1–2% of maximal expression) enables rapid induction upon lactose exposure, even after prolonged growth in glucose [96, 19]. Similarly, in the *gal* operon, the *GalS* autoregulatory loop maintains low-level expression that prevents transcriptional shutdown, facilitating rapid metabolic switching when galactose becomes available [84]. **Noise-driven transitions:** Experimental single-cell studies using fluorescent reporters have directly visualized stochastic transitions between expression states in bistable circuits [19]. These studies confirm that molecular noise arising from finite molecule numbers and intrinsic stochasticity of biochemical reactions can drive transitions between states on physiologically relevant timescales (minutes to

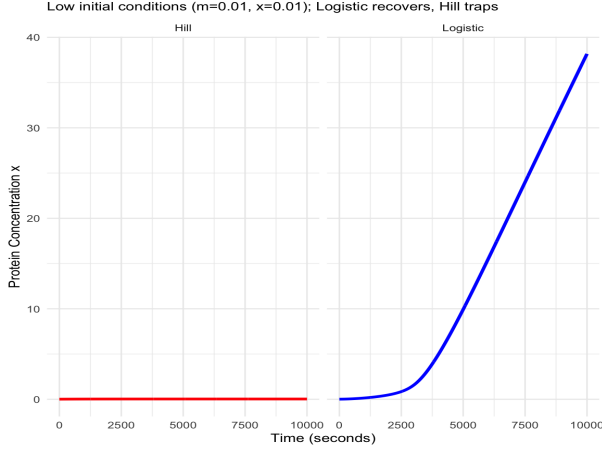


Figure 8: Protein dynamics in positive autoregulation under low initial conditions ( $m(0) = 0.01$ ,  $x(0) = 0.01$ ) with feedback amplification  $\alpha \approx 600$ . **Logistic model :** The system escapes the off-state in approximately 2650 seconds due to basal production  $k_m f(0) \approx 0.000142 \text{ s}^{-1}$ , reaching  $x \approx 38$  at 10,000 s and approaching a steady state near  $x_{ss} \approx 600$  asymptotically. **Hill model:** The system remains trapped near  $x \approx 0.028$ , unable to escape without external perturbation because  $h(x) \approx 0$  for  $x \ll c$ . This starkly illustrates the critical role of basal expression in maintaining cellular responsiveness.

hours), consistent with our simulation timescale of  $\sim 44$  minutes for the logistic model. **High-degradation regimes:** In synthetic circuits with engineered rapid mRNA or protein degradation (e.g., by fusion with *ssrA* degradation tags), Hill-type models without explicit leakage terms fail to predict observed expression dynamics, necessitating the addition of basal production terms [86]. The logistic model naturally incorporates this feature without additional parameters.

Positive autoregulation exemplifies the rich interplay between feedback architecture, molecular noise, and expression dynamics in gene regulatory networks. The choice between Hill and logistic models is not merely a matter of mathematical convenience but has profound implications for capturing biological realism. Hill functions excel at describing sharp, cooperative switches but fail catastrophically at low expression due to their zero basal rate, leading to off-state trapping. Logistic functions, with their inherent non-zero basal production, naturally capture noise-driven escape dynamics observed in real cells, eliminating the need for ad hoc leakage terms. Our analysis, grounded in experimentally derived *E. coli* parameters and validated through numerical simulations, demonstrates that basal expression is not a minor perturbation but a fundamental feature enabling cellular responsiveness in stochastic, low-copy-number environments. The logistic model's ability to predict escape from off-states in approximately 2650 seconds, driven solely by basal production of  $\sim 0.000142 \text{ s}^{-1}$ , aligns quantitatively with observations in the *gal* operon and related systems. These insights inform the design of synthetic gene circuits, the interpretation of single-cell expression data, and the understanding of how natural regulatory networks balance robustness, responsiveness, and stability in fluctuating environments. As systems biology advances toward predictive, quantitative models of cellular behavior, careful attention to basal expression and model choice will be essential for bridging the gap between theoretical predictions and experimental reality.

### 5.3 Advantages of Repression Functions in Noisy Biological Environments

Repression functions suppress gene expression as the concentration of repressors  $x$  increases. The biochemically grounded Hill repression function  $h^-(x, \theta, n) = \frac{\theta^n}{x^n + \theta^n}$  originates from equilibrium binding models and incorporates cooperativity through the exponent  $n$ , which governs the steepness of the repression curve. By contrast, the logistic repression function  $f^-(x, \theta, \lambda) = \frac{1}{1 + e^{\lambda(x - \theta)}}$  delivers a smoother, exponentially decaying profile with steepness controlled by the parameter  $\lambda$ .

The Hill function achieves absolute unity at  $x = 0$ , that is,  $h^-(0, \theta, n) = 1$ , encoding full gene expression in the absence of repressor. This idealization aligns well with strong promoters operating under unrepresed conditions, and is particularly advantageous for systems where maximum output is expected. The logistic function, however, starts *near* but not exactly at 1 when  $x = 0$ . For instance, with  $\lambda = 4$  and  $\theta = 3$ , we obtain

$$f^-(0, 3, 4) = \frac{1}{1 + e^{-\lambda\theta}} = \frac{1}{1 + e^{-12}} \approx 0.999994,$$

very close to 1 but not quite reaching it. This slight deficit from unity is not a defect but a **biological feature**. It captures the reality that even without repressors, maximal expression rarely reaches 100% due to several fundamental constraints: polymerase saturation limits maximum output as RNA polymerase availability is finite and transcription rates plateau when all available polymerase molecules are engaged; resource competition for ribosomes, nucleotide triphosphates (NTPs), and energy carriers (ATP/GTP) among competing cellular processes constrains achievable expression levels, particularly in high-density cultures or multi-gene circuits; transcriptional noise arising from stochastic bursting and probabilistic promoter occupancy introduces intrinsic variability, with even strong promoters cycling between active and inactive states that prevent deterministic maximal expression; and promoter leakiness combined with chromatin effects causes promoter accessibility to vary due to chromatin remodeling, DNA supercoiling, and local nucleoid structure, introducing basal activity fluctuations even under nominally unrepresed conditions. The logistic function's initial value depends on the product  $\lambda\theta$  and can be precisely tuned: increasing  $\lambda$  sharpens transitions and pushes  $f^-(0)$  closer to 1, while adjusting  $\theta$  modulates the threshold position. This flexibility allows the model to represent prolonged yet imperfect expression in repressor-absent states, a phenomenon consistently observed in experimental systems with promoter leakiness, polymerase availability constraints, or stochastic bursting [97].

When repressors are absent, the logistic function's adjustable asymptote near 1 enables fine-tuned representation of low-level constitutive activity, which is crucial in noisy or fluctuating environments. This capability significantly enhances robustness in **stochastic simulations**, particularly those employing the Gillespie algorithm for exact stochastic simulation of chemical reactions. The logistic function's smooth exponential form should provide more stable propensity functions, minimizing variance in rate calculations during low-copy-number regimes. Such regimes are ubiquitous when cellular systems harbor only a handful of molecules, precisely the situation where stochastic effects dominate, and mean-field approximations break down. Hill functions, derived from mean-field assumptions that presuppose large numbers of molecules, frequently require stochastic corrections to account for fluctuations. The direct use of Hill functions in stochastic simulations tends to overestimate noise and variance, necessitating the addition of corrective modeling layers [57]. The logistic function's exponential structure inherently should mitigate these issues, integrating seamlessly with Gillespie algorithms without additional adjustments or correction factors. In **control designs for synthetic biology**, the logistic function's smoothness should facilitate stable feedback linearization and observer-based estimation, improving circuit predictability under uncertainty [98, 99, 100, 101]. The continuous derivatives of all orders ensure that the logistic function remains amenable to differential geometric control methods, whereas the Hill function's power-law structure can introduce complications in derivative-based techniques, particularly near  $x = 0$ , where singularities may arise for non-integer exponents. A prime example arises in **auto-regulatory circuits**, ubiquitous in synthetic biology for noise suppression and response acceleration. Examples include negative auto-regulation in bacterial quorum-sensing systems (e.g., LuxR-based circuits) and metabolic pathway controllers in microbial factories optimized for bioproduction. In these systems, a gene product represses its own transcription, creating a negative feedback loop that stabilizes expression levels and accelerates the response to environmental changes. Here, the logistic function's smooth form minimizes variance in propensity rates during low-copy fluctuations driven by intrinsic noise in small molecule counts. This yields more accurate predictions of steady-state distributions and reduces phenotypic heterogeneity compared to the Hill function's power-law structure, which can amplify numerical errors without corrections. Specifically: **Toggle switches**: Bistable genetic switches rely on mutual repression between two genes to maintain one of two stable steady states. Hill models may overestimate the sharpness of bistability thresholds and the separation between states due to uncorrected stochastic fluctuations, leading to predictions of switching behavior that deviate from experimental observations. The logistic

function should provide a more robust approximation that naturally accounts for resource availability and intrinsic noise. **Repressilators:** These oscillatory circuits are based on cyclic repression among three or more genes (e.g., the canonical LacI-TetR-λCI repressor). Hill models can overestimate oscillation damping or predict oscillation amplitude ranges that differ substantially from measured dynamics when molecule numbers are low (~10–100 copies per cell). The resource-aware formulation of the logistic function should better capture the sustained oscillations observed in single-cell microfluidic experiments and provides more accurate predictions of period and amplitude [102, 57].

## 5.4 Scaling for Maximal Gene Expression

In certain scenarios, the absolute full expression  $f^-(0, \theta, \lambda) = 1$  may be desirable in  $x = 0$  to match exactly the behavior of the Hill function. To address this requirement, we can scale the logistic repression function to ensure full expression when no repressor is present, perfectly aligning with  $h^-(0, \theta, n) = 1$ . The **scaled logistic function** is defined as

$$f_{\text{scaled}}^-(x, \theta, \lambda) = (1 + e^{-\lambda\theta}) \cdot \frac{1}{1 + e^{\lambda(x-\theta)}}.$$

This scaling arises naturally from the requirement that  $f_{\text{scaled}}^-(0, \theta, \lambda) = 1$ . Since the unscaled logistic satisfies

$$f^-(0, \theta, \lambda) = \frac{1}{1 + e^{-\lambda\theta}},$$

its reciprocal,  $1 + e^{-\lambda\theta}$  provides exactly the normalization factor needed to achieve unity at  $x = 0$ . As  $x$  increases beyond zero, the denominator  $1 + e^{\lambda(x-\theta)}$  grows exponentially, driving the function toward zero while preserving the characteristic sigmoidal shape and smooth decay properties. The scaling factor  $e^{-\lambda\theta}$  diminishes rapidly with larger  $\lambda$  and  $\theta$  values. For instance:

- With  $\lambda = 4$  and  $\theta = 3$ :  $e^{-\lambda\theta} = e^{-12} \approx 6.14 \times 10^{-6}$ , making  $(1 + e^{-\lambda\theta}) \approx 1.0000061$ .
- With  $\lambda = 3$  and  $\theta = 2$ :  $e^{-\lambda\theta} = e^{-6} \approx 0.00248$ , giving  $(1 + e^{-\lambda\theta}) \approx 1.00248$ .
- With  $\lambda = 1$  and  $\theta = 2$ :  $e^{-\lambda\theta} = e^{-2} \approx 0.1353$ , yielding  $(1 + e^{-\lambda\theta}) \approx 1.1353$ .

Thus, the scaling effect is noticeable only when  $\lambda$  and  $\theta$  are small. Under typical parameter regimes used in gene regulatory network models ( $\lambda \geq 2$ ,  $\theta \geq 2$ ), the scaling factor remains very close to 1, ensuring minimal deviation from the original logistic shape. This means that for most practical applications with moderately steep transitions, the scaled and unscaled logistic functions are nearly indistinguishable in shape, differing only by a small vertical scaling that normalizes the maximum to exactly 1.

Figure 9 compares the Hill, original logistic, and scaled logistic repression functions across repressor concentrations from 0 to 10. The left panel employs parameters  $n = 2$ ,  $\theta = 2$ , and  $\lambda = \frac{n}{\theta} = 1$ ; the right panel uses  $n = 6$ ,  $\theta = 2$ , and  $\lambda = \frac{n}{\theta} = 3$ , revealing how parameter variations influence curve shapes and transition steepness. In the left panel ( $\lambda = 1$ ,  $\theta = 2$ ), we compute:

$$e^{-\lambda\theta} = e^{-2} \approx 0.1353 \quad \Rightarrow \quad f^-(0) \approx \frac{1}{1 + 0.1353} \approx 0.8808,$$

representing approximately 88% of maximum expression. This moderate reduction is well-suited for modeling systems with inherent inefficiencies or resource limitations, such as bacterial cells operating under nutrient stress, synthetic circuits approaching metabolic burden thresholds, or promoters with significant basal activity constraints. In the right panel ( $\lambda = 3$ ,  $\theta = 2$ ), the scaling factor  $(1 + e^{-6}) \approx 1.0025$  is negligible, and all three functions align closely, demonstrating that the logistic and Hill functions exhibit nearly identical behavior under typical steep-transition parameter regimes.

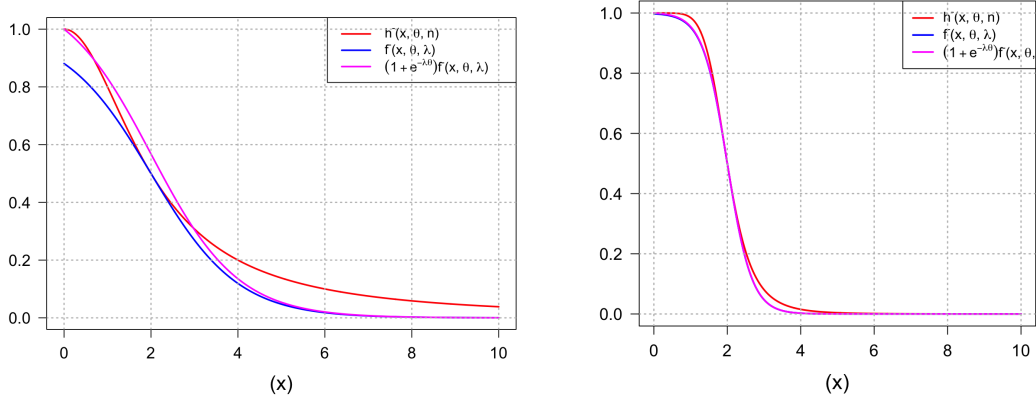


Figure 9: Comparison of repression functions. **Left:**  $n = 2, \theta = 2, \lambda = 1$ . **Right:**  $n = 6, \theta = 2, \lambda = 3$ . Red line: Hill function  $h^-(x, \theta, n)$ ; blue line: logistic function  $f^-(x, \theta, \lambda)$ ; magenta line: scaled logistic  $(1 + e^{-\lambda\theta})f^-(x, \theta, \lambda)$ . The left panel shows moderate baseline reduction ( $\sim 88\%$  of maximum), suitable for systems with inherent inefficiencies or resource limitations. The right panel demonstrates near-perfect alignment between all three functions when  $\lambda$  and  $\theta$  are larger, with the scaling factor being negligible.

**Example 6.** Reconsidering the genetic oscillator model, where two genes form a negative feedback loop with gene 1 being repressed by gene 2 and gene 2 being activated by gene 1, we can integrate the scaled logistic function to ensure exact unit maxima. The modified system becomes:

$$\begin{aligned} \dot{x}_1 &= \kappa'_1 \frac{1}{1 + e^{\lambda(x_2 - \theta_2)}} - \gamma_1 x_1, \\ \dot{x}_2 &= \kappa_2 \frac{1}{1 + e^{-\lambda(x_1 - \theta_1)}} - \gamma_2 x_2, \end{aligned} \quad (63)$$

where  $\kappa'_1 = \kappa_1(1 + e^{-\lambda\theta_2})$ . This adjustment scales the production rate to ensure gene 1 achieves full expression when  $x_2 = 0$  (no repressor present), while gene 2 reaches full expression when  $x_1$  is high (activator present). The scaled system closely resembles the original; the primary differences lie in the constant multiplicative factor  $(1 + e^{-\lambda\theta_2})$  applied to the expression rate for repression. This factor enhances consistency with systems that expect maximum output under optimal conditions, aligning the logistic model with the Hill function's behavior at boundary points. Importantly, the oscillator dynamics, including period, amplitude, and stability properties remain fundamentally unchanged by this scaling, as the factor affects only the absolute scale of expression for the repressed gene, not the relative feedback strength that governs oscillatory behavior. The local stability analysis presented above remains valid, with the trace and determinant of the Jacobian matrix retaining their signs, ensuring the same qualitative dynamical behavior.

Scaling  $f^-(x, \theta, \lambda)$  by  $(1 + e^{-\lambda\theta})$  ensures absolute full expression when repressor is absent, which is consistent with and often preferable for systems featuring strong promoters where maximal output is expected under unrepresed conditions. It is important to note that for activation Hill functions  $h^+(x, \theta, n) = \frac{x^n}{x^n + \theta^n}$ , full expression is *never* achieved at any finite  $x$ ; the function merely approaches 1 asymptotically as  $x \rightarrow \infty$ . Thus, the asymmetry between repression and activation, where repression can achieve perfect repression at  $x = 0$ , but activation cannot achieve perfect activation at any finite  $x$  which is inherent in both the Hill and logistic frameworks.

The logistic function provides an **exponentially decaying repression curve** that better mimics gradual, sigmoidal responses in cellular systems where repression builds progressively. This contrasts with the more rigid, cooperative binding-based steepness of the Hill function, which is derived from equilibrium bind-

ing models that may not capture all regulatory mechanisms. The smoothness is adjustable via  $\lambda$ , allowing fine-tuned control over transition sharpness without relying exclusively on cooperativity (encoded by  $n$  in the Hill equation), which may not always align with non-cooperative biological mechanisms, such as allosteric regulation, sequential binding without cooperativity, or indirect regulatory cascades.

The choice between scaled and unscaled logistic functions could depend on the modeling context and the biological system under study. The **unscaled logistic**  $f^-(x, \theta, \lambda)$  starts slightly below 1 at low repressor levels (e.g.,  $\approx 0.99999$  or lower, depending on  $\lambda$  and  $\theta$ ), with this subtle deviation accounting for real-world constraints including polymerase saturation and finite transcriptional machinery, resource limitations (nucleotide pools, ribosome availability, energy budgets), transcriptional noise arising from stochastic bursting and promoter switching, and promoter leakiness combined with chromatin accessibility and DNA topology effects. The unscaled form proves particularly useful for modeling systems with baseline inefficiencies, especially those with smaller  $\lambda\theta$  products (e.g.,  $\lambda\theta < 4$ ), making it more representative of noisy or resource-limited cellular environments. This realism is valuable when quantitative agreement with experimental data is prioritized, particularly in systems where maximal expression demonstrably falls short of theoretical limits. Conversely, the **scaled logistic**  $f_{\text{scaled}}^-(x, \theta, \lambda)$  normalizes to exactly 1 at  $x = 0$  while preserving the exponential decay shape, thereby combining the Hill function's advantage of full unrepresed expression with the logistic's smoother profile and analytical tractability. This scaling (via factor  $1 + e^{-\lambda\theta}$ ) exerts negligible impact under typical parameter ranges ( $\lambda\theta \geq 4$ , where the factor becomes  $\approx 1.02$  or closer to 1), allowing seamless integration into models like genetic oscillators without significantly altering core dynamics. The scaled form is advantageous when theoretical consistency with the Hill function is desired, when models require exact maximum expression values for comparative analysis, or when interfacing with existing Hill-based models in hybrid frameworks.

The Hill function lacks this tunable imperfection option natively: it always assumes  $h^-(0) = 1$  regardless of biological context, offering less flexibility for capturing resource-limited or noisy cellular environments where maximal expression may be constrained by factors beyond repressor concentration.

**Applications in Synthetic Biology.** In synthetic circuits, tuning the unrepresed expression rate proves crucial for several practical considerations grounded in experimental observations:

- **Metabolic flux optimization:** Overexpression of heterologous proteins can divert cellular resources (amino acids, ATP, ribosomes) from endogenous metabolism, reducing growth rate and product yield. The logistic's adjustable maximum expression level allows modeling of realistic expression ceilings imposed by metabolic burden, enabling better predictions of sustainable production rates in industrial bioprocessing applications such as biofuel production, pharmaceutical synthesis, and enzyme manufacturing.
- **Toxicity avoidance:** Long-term expression phases in biotechnology applications, such as continuous bioreactor operation, therapeutic protein manufacturing, or biosensor deployment can become toxic if expression levels exceed cellular capacity for protein folding, membrane integration, or metabolite processing. The unscaled logistic naturally incorporates a "safety valve" that prevents overestimation of sustainable expression levels, guiding circuit design toward robust, non-toxic operating regimes that maintain cell viability over extended culture periods.
- **Resource competition in multi-gene circuits:** In complex synthetic circuits involving multiple genes (e.g., metabolic pathways with 5–10 enzymatic steps or multi-component biosensors), incomplete repression leads to sub-maximal outputs due to competition for transcriptional and translational machinery. Engineered *E. coli* systems demonstrate that incomplete repression results in expression levels reaching only 70–90% of theoretical maximum under realistic conditions [103], consistent with the unscaled logistic's natural expression ceiling. This phenomenon becomes particularly pronounced when multiple genes compete for limited RNA polymerase or when ribosome binding sites exhibit suboptimal spacing or accessibility.

The Hill function's fixed maximum ( $h^-(0) = 1$ ) presumes ideal conditions: unlimited resources, perfect promoter efficiency, and deterministic expression potentially overestimating stability and output in noisy, resource-constrained cells. By contrast, the logistic's adjustable cap provides a more controllable and biologically realistic representation for sustained expression, better capturing the biological reality of imperfect repression, resource competition, and stochastic fluctuations that characterize real cellular environments.

The logistic framework thus offers **strategic flexibility** that the Hill function cannot match. For **modeling realism**, the unscaled form  $f^-(x, \theta, \lambda)$  models realistic imperfections, resource constraints, and stochastic environments where  $f^-(0) < 1$  reflects biological reality, which is particularly valuable for quantitative systems biology and predictive modeling of engineered circuits where experimental validation demands accurate representation of achievable expression levels. For **theoretical consistency**, the scaled variant  $f_{\text{scaled}}^-(x, \theta, \lambda)$  enables matching idealized Hill behavior (i.e.,  $f_{\text{scaled}}^-(0) = 1$ ) while maintaining the logistic's superior analytical tractability and numerical stability, which is useful for comparative studies, benchmarking against Hill-based models, or when developing theoretical frameworks that require exact normalization. Regarding **parameter tunability**, the logistic function separates threshold position ( $\theta$ ) from transition steepness ( $\lambda$ ), enabling independent control of these features. In contrast, the Hill function exhibits parameter coupling: its maximum slope  $n/(4\theta)$  depends on both the Hill coefficient  $n$  and threshold  $\theta$ , whereas the logistic function's maximum slope  $\lambda/4$  depends only on  $\lambda$ . This independence allows the logistic function to adjust steepness without affecting threshold position or requiring compensatory parameter changes. This decoupling is critical for **rational circuit design**: in toggle switches, independent slope control enables tuning the energy barrier between bistable states (affecting switching rates and noise tolerance) without relocating the decision threshold; in biosensors, engineers can independently set the detection threshold (e.g., 5 mM glucose) and the response sharpness (ultrasensitive vs. graded), matching sensor characteristics to application requirements; and in cascaded gene circuits, where modules operate in series, independent slope adjustment prevents signal distortion during propagation, ensuring that each stage can be optimized for its specific input-output transformation without disrupting upstream or downstream threshold positions. Furthermore, slope control directly determines the degree of ultrasensitivity, which governs noise filtering: steep slopes (high  $\lambda$ ) create sharp, switch-like responses that reject small fluctuations below threshold, while gentle slopes (low  $\lambda$ ) provide wide dynamic ranges for proportional control. The logistic's parameterization makes these trade-offs explicit and tunable, whereas the Hill function conflates threshold scaling with cooperativity, obscuring the relationship between circuit architecture and response characteristics.

The logistic offers decisive **computational advantages** as its exponential form avoids the power-law singularities of the Hill function near  $x = 0$  (where  $x^n$  can cause numerical instability for large  $n$  or small  $x$  with non-integer exponents) and ensures smooth derivatives of all orders for all  $x \geq 0$ , improving numerical stability in simulation, optimization, and sensitivity analysis, particularly in large-scale network models or when computing higher-order derivatives for bifurcation analysis. Finally, the logistic function's **control-theoretic properties** stem from its exponential structure, which makes it naturally compatible with control-theoretic techniques that rely on smooth, well-behaved nonlinearities, such as feedback linearization (requiring closed-form inverses), Lyapunov-based stability analysis (benefiting from bounded derivatives), and observer design for state estimation under uncertainty (requiring well-conditioned Jacobians). In summary, the logistic repression function whether scaled or unscaled provides a mathematically elegant, biologically realistic, and computationally robust alternative to the traditional Hill function for modeling gene regulatory networks. It is particularly advantageous in noisy, resource-limited, or synthetically engineered biological systems where realistic modeling of imperfect expression, stochastic effects, and resource constraints is essential for accurate prediction and optimal circuit design. The framework's flexibility enables seamless adaptation to diverse modeling contexts, from idealized theoretical studies requiring exact normalization to quantitative experimental investigations demanding faithful representation of biological constraints.

## 6 Control Advantages of Logistic Functions in Gene Regulatory Networks

The logistic function provides fundamental advantages over Hill functions for controlling biological networks, stemming from its non-zero response at minimal expression levels and analytical tractability. The logistic function  $f^+(x, \theta, \lambda) = \frac{1}{1+e^{-\lambda(x-\theta)}}$  maintains  $f^+(0, \theta, \lambda) = \frac{1}{1+e^{\lambda\theta}} > 0$ , ensuring continuous regulatory control even when gene expression drops to zero, whereas the Hill function  $h^+(x, \theta, n) = \frac{x^n}{x^n + \theta^n}$  vanishes identically at  $x = 0$ , creating controllability gaps that compromise feedback regulation. Biologically, genes exhibit persistent non-zero basal (leaky) expression even without activators, stabilizing low-expression states across multiple cell divisions as observed in the GAL network in yeast and promoter leakage in auto-regulatory circuits [104, 105]. Without repressor proteins, transcription proceeds at sustained high rates as seen in bacterial operons (e.g., the *lac* system) and phage lambda [106, 107], and the logistic repression function  $f^-(0, \theta, \lambda) = \frac{1}{1+e^{-\lambda\theta}}$  provides tunable control over baseline expression via the product  $\lambda\theta$ , whereas Hill functions rigidly fix  $h^-(0) = 1$ , offering no intrinsic parameter-based modulation. Similarly, the function  $f^+(0, \theta, \lambda) = \frac{1}{1+e^{\lambda\theta}}$  provides tunable control of the basal expression rate via the product  $\lambda\theta$ . The parameters  $\lambda$  (steepness) and  $\theta$  (threshold) map directly to tunable molecular properties:  $\theta$  represents the dissociation constant for binding, adjustable through operator mutations or protein engineering [108, 109], while  $\lambda$  governs cooperativity, modifiable via multimeric repressors or auxiliary binding sites [10], making these parameters experimentally accessible through synthetic biology techniques such as promoter libraries, directed evolution, and optogenetics [110, 111]. The parameter independence inherent in the logistic formulation where threshold position ( $\theta$ ) and transition steepness ( $\lambda$ ) are fully decoupled proves particularly advantageous for control design, as it enables independent tuning of the decision threshold and response sensitivity without compensatory parameter adjustments. This contrasts sharply with Hill functions, where the maximum slope  $n/(4\theta)$  couples both parameters, requiring simultaneous readjustment of cooperativity and threshold to maintain desired control characteristics, thereby complicating controller synthesis and reducing design flexibility in multi-objective optimization scenarios where threshold placement and sensitivity must be balanced against competing performance criteria.

Multiple control strategies leverage these properties: multiplicative control modulating production rates via control inputs  $u_i \geq 0$  in  $\dot{x}_i = \kappa_i \frac{u_i}{1+e^{-\sigma_i \lambda(x_j - \theta_i)}} - \gamma_i x_i$  ensures non-zero controllability at all expression levels; steepness modulation adjusting  $\lambda$  via control inputs provides linear, predictable control over regulatory sensitivity in  $\dot{x}_i = \kappa_i f_i(x_1, \dots, x_n, u_i \lambda, \theta_{ij}) - \gamma_i x_i$  without the numerical instabilities associated with large Hill coefficients; sliding mode control (SMC) should benefit from the logistic function's smooth, bounded nature ensuring robust performance under parameter uncertainties [2, 3, 112], whereas Hill-based models where zero production at  $x = 0$  creates fragility in equivalent control laws with undefined expressions and fractional exponents; state-feedback control using additive strategies  $\dot{x}_i = \kappa_i f_i(\mathbf{x}) - \gamma_i x_i + u_i$  with  $u_i = -K_i(x_i - x_{d,i})$  leverages continuous responsiveness to achieve exponential convergence to desired setpoints; and model predictive control (MPC) exploits the closed-form inverse (logit transform)  $f^{-1}(y) = \theta + \frac{1}{\lambda} \ln\left(\frac{y}{1-y}\right)$  enabling feedback linearization and gradient-based optimization with smooth derivatives that yield well-conditioned optimization problems compared to Hill functions' power-law nonlinearities [113, 114, 65]. For multi-dimensional systems with cooperative regulation combining activator and repressor effects, the controlled dynamics for parallel regulation become  $\dot{x}_i = \kappa_i \left( \prod_{j \in \mathcal{A}_i} \frac{1}{1+e^{-u_{ij} \lambda(x_j - \theta_{ij})}} \cdot \prod_{k \in \mathcal{R}_i} \frac{1}{1+e^{-u_{ik} \lambda(\theta_{ik} - x_k)}} \right) - \gamma_i x_i$ , where  $u_{ij}, u_{ik} \geq 0$  modulate the steepness of each regulatory interaction, ensuring non-zero production at zero regulator concentrations unlike Hill-based models where the regulatory term  $f_i(x_j, x_k) = \frac{x_j^n}{x_j^n + \theta_{ij}^n} \cdot \frac{\theta_{ik}^n}{x_k^n + \theta_{ik}^n}$  vanishes identically at  $x_j = 0, x_k = 0$ , rendering systems uncontrollable in activator-absent states. In contrast to Hill functions, the logistic model admits tractable linear approximations when  $\lambda$  is small and for both near the origin and near the inflection point (threshold), thereby yielding an analytically tractable linearized system  $\dot{\mathbf{x}} = A\mathbf{x} + \mathbf{b} + B\mathbf{u}$ , which facilitates controllability analysis via rank conditions on  $\mathcal{C} = [B \ AB \ \dots \ A^{n-1}B]$ , application of linear control tools (pole placement, LQR,  $\mathcal{H}_\infty$ ), and systematic gain selection for desired convergence and robustness, with the bilinear structure emerging in controlled systems enabling accessibility analysis through Lie

algebra methods. Compared to Hill functions, which exhibit zero production at activator absence rendering systems uncontrollable in low-expression regimes, non-smooth behavior for large  $n$  causing numerical instability, complex rational equations complicating SMC and MPC design, and lack of closed-form derivatives for non-integer  $n$  hindering optimization, logistic functions provide always-positive production maintaining controllability, smooth bounded responses ensuring numerical stability, closed-form derivatives and inverses facilitating analytical control design, and parameters directly corresponding to tunable biological mechanisms. These control strategies are experimentally feasible through optogenetics, providing millisecond-precision control inputs, fluorescent reporters that enable real-time measurement of expression to close feedback loops, and microfluidic platforms that allow for the parallel control of thousands of cells for population studies. The Khammash laboratory at ETH Zurich has pioneered experimental platforms demonstrating the practical implementation [110]. An alternative control strategy modulates regulatory influences directly through the control matrix elements  $u_{ij}$  and  $u_{ik}$ , in  $\dot{x}_i = \kappa_i \left( \prod_{j \in \mathcal{A}_i} \frac{1}{1+e^{-\lambda(u_{ij}x_j - \theta_{ij})}} \cdot \prod_{k \in \mathcal{R}_i} \frac{1}{1+e^{-\lambda(\theta_{ik} - u_{ik}x_k)}} \right) - \gamma_i x_i$ , where  $u_{ij}, u_{ik} \geq 0$  modulate interaction strength, enabling dynamic modulating the regulatory influences for targeted interventions in optogenetic applications. For multi-gene networks such as the repressilator with cyclic inhibitory interactions, the logistic framework's analytical tractability enables systematic design of feedback controllers that stabilize oscillations to desired amplitudes or frequencies, synchronize multiple circuits, track time-varying trajectories, and compensate for cell-to-cell variability, with linear approximations yielding cyclic coupling structures analyzable via circulant matrix theory and MPC strategies exploiting predictive capability for phase-locking or maintaining oscillation characteristics despite disturbances. In practical SMC implementations, quasi-sliding mode (QSM) controllers using DNA strand displacement reactions have been demonstrated by Sawlekar et al. [112], outperforming traditional linear controllers with faster tracking response without overshoots, critical for genetic networks requiring precise control, while chattering (rapid switching) caused by discontinuous sign functions is mitigated through boundary layer

introduction by replacing  $\text{sign}(s_i)$  with smooth approximations  $\text{sat}(s_i, \epsilon) = \begin{cases} \text{sign}(s_i) & \text{if } |s_i| > \epsilon, \\ s_i/\epsilon & \text{if } |s_i| \leq \epsilon \end{cases}$ , where

$\epsilon > 0$  defines boundary layer thickness, ensuring smooth control transitions within  $|s_i| \leq \epsilon$  while maintaining robust reaching behavior outside this region. This part of control will be detailed in future work and future research directions include extending control strategies to stochastic gene networks accounting for intrinsic and extrinsic noise in low-copy-number regimes, integrating spatial dynamics and cell-to-cell communication in multi-cellular systems requiring distributed control architectures, combining logistic-based mechanistic models with machine learning components for adaptive control in uncertain or time-varying environments, validating control strategies in experimental platforms particularly optogenetic systems with millisecond-precision real-time feedback, and exploring applications beyond gene regulation including metabolic pathway control, cell cycle regulation, and morphogen gradient formation in developmental biology. In conclusion, logistic-based models should provide mathematical tractability, biological fidelity, and computational robustness for controlling gene regulatory networks, with non-zero basal activity ensuring continuous controllability essential for feedback architectures requiring responsiveness to weak inputs, and the smooth, analytically tractable form enabling systematic application of advanced control methods ranging from sliding mode to model predictive control, with direct experimental implementation pathways through modern synthetic biology

## 7 Logistic-Function-Based Model Parameter Estimation

To ground our logistic-based modeling framework in biological reality, we will establish collaborative partnerships with experimental biology laboratories for systematic validation. These collaborations will guide parameter tuning of the steepness parameter  $\lambda$  and regulatory thresholds  $\theta_{ij}$ , particularly ensuring that model predictions align quantitatively with observed gene expression dynamics. Our parameter estimation strategy will leverage time-series measurements of gene expression, encompassing production rates  $\kappa_i$ , degradation rates  $\gamma_i$ , steepness parameters  $\lambda$ , and regulatory thresholds  $\theta_{ij}$ . Systematic exploration of multi-dimensional parameter spaces remains a fundamental challenge in gene regulatory network modeling, particularly when

regulatory interactions involve multiple threshold parameters and steepness coefficients [115]. The logistic framework's smooth, bounded derivatives facilitate efficient parameter space sampling and gradient-based optimization across high-dimensional parameter landscapes. Unlike Hill-based models where fractional exponents create discontinuous parameter sensitivities, the exponential structure of logistic functions ensures that small parameter perturbations produce proportionally small changes in model predictions, enabling robust parameter identifiability even from noisy experimental data. The parameter values can be estimated using the Least Squares method, which serves as the foundational framework. This method minimizes the sum of squared residuals between observed gene expression trajectories and model predictions:

$$\min_{\kappa_i, \gamma_i, \lambda, \theta_{ij}} \sum_t \|\mathbf{x}(t) - \hat{\mathbf{x}}(t; \kappa_i, \gamma_i, \lambda_{ij}, \theta_{ij})\|_2^2, \quad (64)$$

where  $\mathbf{x}(t)$  represents the experimental measurements at time  $t$  and  $\hat{\mathbf{x}}(t; \cdot)$  denotes the model-predicted expression levels under candidate parameter values.

The logistic function's mathematical properties are particularly advantageous for this optimization task. Its global smoothness and analytically tractable derivatives:

$$f'(s) = \frac{e^{-s}}{(1 + e^{-s})^2}, \quad f''(s) = \frac{e^{-s}(e^{-s} - 1)}{(1 + e^{-s})^3}, \quad (65)$$

ensure that gradient-based optimization algorithms, such as the Gauss-Newton method or the Levenberg-Marquardt algorithm, converge efficiently and reliably. This stands in sharp contrast to Hill function models, where fractional exponents and potential singularities near the origin can create ill-conditioned optimization landscapes, particularly when Hill coefficients assume non-integer values. The continuous, well-behaved gradients of logistic functions translate directly into improved convergence rates and enhanced accuracy in parameter recovery, even from noisy experimental data. Systematic validation against experimental datasets will establish the framework's predictive power and biological relevance.

## 7.1 Basal Expression and Logistic Models Parameter Inference

Unlike Hill function models, which require arbitrary offsets or ad hoc modifications to represent basal transcription, the logistic function naturally encodes non-zero baseline expression through its fundamental mathematical structure. The basal expression level emerges organically from the steepness parameter  $\lambda$  and threshold  $\theta$ , eliminating the need for additional parameters while preserving biological realism.

For a single-input activation function  $f(s) = \frac{1}{1+e^{-s}}$  with  $s = \lambda(x_{i-1} - \theta_i)$ , the basal production rate at zero input concentration ( $x_{i-1} = 0$ ) is given by:

$$f(\lambda(0 - \theta_i)) = \frac{1}{1 + e^{\lambda_i \theta_i}}, \quad (66)$$

which depends solely on the product  $\lambda_i \theta_i$ . This mathematical relationship enables a bidirectional inference strategy: given experimentally measured basal expression rates and estimated threshold concentrations, we can directly compute the steepness parameter  $\lambda$  that reproduces the observed baseline activity. Conversely, if cooperativity estimates (analogous to Hill coefficients) are available from binding studies, we can infer threshold positions from basal measurements. This tight coupling between model parameters and observable biological quantities enhances both parameter identifiability and biological interpretability.

## 7.2 Comprehensive Case Study: The Two-Gene Self-Inhibitory and Mutually Activating Network

To illustrate the parameter fitting methodology in concrete detail, we revisit the two-gene regulatory network featuring self-inhibition and mutual activation, previously presented above. This network architecture exhibits rich dynamical behaviors, including oscillations, bursting, and potential chaos, making it an ideal test for parameter estimation strategies.

### 7.2.1 Logistic Reformulation of the System

The system dynamics using only logistic functions throughout can be expressed as:

$$\dot{A}(t) = \left( \frac{\kappa_1}{1 + e^{-\lambda_1(B(t-\tau_{12})-\theta_B)}} \cdot \frac{1}{1 + e^{\lambda_3(A(t-\tau_1)-A_0)}} \right) - \gamma_A A(t), \quad (67)$$

$$\dot{B}(t) = \left( \frac{\kappa_2}{1 + e^{-\lambda_2(A(t-\tau_{21})-\theta_A)}} \cdot \frac{1}{1 + e^{\lambda_4(B(t-\tau_2)-B_0)}} \right) - \gamma_B B(t). \quad (68)$$

Here,  $\kappa_1$  and  $\kappa_2$  represent maximal production rates (bounded to ensure saturation),  $\lambda_1$  and  $\lambda_2$  govern the steepness of activation responses,  $\theta_A$  and  $\theta_B$  denote activation thresholds positioned where mutual activation effects become biologically significant, and  $\lambda_3 \approx n/A_0$  and  $\lambda_4 \approx n/B_0$  characterize repression steepness (with  $n$  serving as an effective Hill coefficient derived from cooperativity measurements).

This formulation systematically replaces the original model's components, which combined linear activation terms ( $g_A + g_{AB}B(t - \tau_{12})$ ) with Hill-based self-repression, with bounded sigmoidal logistic functions throughout. The key challenge lies in approximating the unbounded linear activation terms using low-steepness logistic functions while preserving the system's essential dynamical characteristics.

### 7.2.2 Matching Basal Expression and Activation Slopes

Our parameter derivation strategy proceeds by matching both the basal expression rate and the local activation sensitivity (slope) of the original linear model. Consider gene  $A$  first. The basal expression rate  $g_A$  corresponds to the production level when the activator concentration vanishes ( $B(t - \tau_{12}) = 0$ ), assuming negligible self-repression (i.e.,  $f^-(A, A_0, \lambda) \approx 1$ ). Setting the logistic activation function at zero input equal to the basal rate yields:

$$\kappa_1 f^+(0, \theta_B, \lambda_1) = \frac{\kappa_1}{1 + e^{\lambda_1 \theta_B}} = g_A, \quad (69)$$

which can be rearranged to express the steepness parameter as:

$$\lambda_1 = \frac{1}{\theta_B} \ln \left( \frac{\kappa_1}{g_A} - 1 \right). \quad (70)$$

For moderate steepness  $\lambda_1$ , the logistic activation function admits a simple linear approximation via Taylor expansion:

$$\frac{\kappa_1}{1 + e^{-\lambda_1(B(t-\tau_{12})-\theta_B)}} \approx \frac{\kappa_1}{2} + \frac{\kappa_1 \lambda_1}{4} (B(t - \tau_{12}) - \theta_B). \quad (71)$$

Substituting our expression for  $\lambda_1$  and expanding yields:

$$\frac{\kappa_1}{2} + \frac{\kappa_1}{4\theta_B} \ln \left( \frac{\kappa_1}{g_A} - 1 \right) (B(t - \tau_{12}) - \theta_B). \quad (72)$$

Let us introduce the shorthand notation  $k = \kappa_1$  and  $L = \ln \left( \frac{k}{g_A} - 1 \right)$ . Fully expanding the expression gives:

$$\frac{k}{2} + \frac{kL}{4\theta_B} B(t - \tau_{12}) - \frac{kL}{4}, \quad (73)$$

which simplifies to:

$$\left( \frac{k}{2} - \frac{kL}{4} \right) + \frac{kL}{4\theta_B} B(t - \tau_{12}). \quad (74)$$

To match this expression to the original linear activation term  $g_A + g_{AB}B(t - \tau_{12})$ , we must satisfy two conditions simultaneously:

1. **Slope matching:** The coefficient of  $B(t - \tau_{12})$  must equal  $g_{AB}$ :

$$\frac{kL}{4\theta_B} = g_{AB}.$$

2. **Intercept matching:** The constant term must equal  $g_A$ :

$$\frac{k}{2} - \frac{kL}{4} = g_A.$$

From the slope equation, we can express  $L$  in terms of the other parameters:

$$L = \frac{4\theta_B g_{AB}}{k}. \quad (75)$$

Substituting this into the intercept equation yields:

$$\frac{k}{2} - \frac{k}{4} \cdot \frac{4\theta_B g_{AB}}{k} = g_A \implies \frac{k}{2} - \theta_B g_{AB} = g_A \implies k = 2(g_A + \theta_B g_{AB}). \quad (76)$$

This determines the maximal production rate  $\kappa_1 = 2(g_A + \theta_B g_{AB})$ , ensuring that both the constant term and the slope of the linear approximation align with the original model.

Substituting back into our expression for  $\lambda_1$ :

$$\lambda_1 = \frac{1}{\theta_B} \ln \left( \frac{2(g_A + g_{AB}\theta_B)}{g_A} - 1 \right). \quad (77)$$

Simplifying the logarithm's argument:

$$\frac{2(g_A + g_{AB}\theta_B)}{g_A} - 1 = \frac{2g_A + 2g_{AB}\theta_B - g_A}{g_A} = 1 + \frac{2g_{AB}\theta_B}{g_A}. \quad (78)$$

Therefore:

$$\kappa_1 = 2(g_A + g_{AB}\theta_B), \quad \lambda_1 = \frac{1}{\theta_B} \ln \left( 1 + \frac{2g_{AB}\theta_B}{g_A} \right). \quad (79)$$

By complete symmetry, the corresponding parameters for gene  $B$  are:

$$\kappa_2 = 2(g_B + g_{BA}\theta_A), \quad \lambda_2 = \frac{1}{\theta_A} \ln \left( 1 + \frac{2g_{BA}\theta_A}{g_B} \right). \quad (80)$$

This derivation ensures that the logistic approximation preserves both the basal expression levels and the local activation sensitivities of the original linear model, provided that the ratios  $\theta_B g_{AB}/g_A$  and  $\theta_A g_{BA}/g_B$  remain moderate (not excessively large).

### 7.2.3 Biologically Motivated Threshold Selection

A critical remaining question concerns the appropriate choice of threshold parameters  $\theta_A$  and  $\theta_B$ . While one naive approach might set these near the maximum concentrations (e.g.,  $\theta_B \approx B_{\max}/2$  to center the sigmoid's inflection point), we advocate for a more biologically principled strategy grounded in the system's regulatory logic.

The thresholds  $\theta_A$  and  $\theta_B$  should represent biologically relevant concentrations at which regulatory transitions occur, specifically where the activation contribution becomes comparable to basal production. A natural and mathematically consistent choice defines these thresholds at the concentrations where mutual activation equals basal expression:

$$g_{AB}B^* = g_A \quad \text{and} \quad g_{BA}A^* = g_B. \quad (81)$$

This criterion immediately yields:

$$B^* = \frac{g_A}{g_{AB}}, \quad A^* = \frac{g_B}{g_{BA}}. \quad (82)$$

Moreover, the inflection point of the logistic function, where it achieves half its maximum value ( $\kappa_1/2$  or  $\kappa_2/2$ ) occurs when the exponential argument vanishes. For the activation term, this requires:

$$e^{-\lambda_1(B(t-\tau_{12})-\theta_B)} = 1 \implies B(t-\tau_{12}) = \theta_B. \quad (83)$$

By identifying the physical regulatory threshold with the mathematical inflection point, we obtain:

$$\theta_B = \frac{g_A}{g_{AB}}, \quad \theta_A = \frac{g_B}{g_{BA}}. \quad (84)$$

This choice possesses several compelling properties. First, it ensures that the logistic function's sigmoidal transition is centered precisely where the system's regulatory response shifts from a basal-dominated to an activator-driven regime, a characteristic of oscillatory and bistable genetic circuits, such as toggle switches and circadian oscillators. Second, this threshold selection guarantees that  $\theta_B g_{AB}/g_A = 1$  (and similarly for gene  $B$ ), which satisfies our earlier assumption that these ratios remain moderate, thereby validating the logarithmic approximation used in the derivation. Third, the threshold can be interpreted biologically as an "activation midpoint" or "sensitivity point," directly analogous to the half-maximal effective concentration (EC<sub>50</sub>) in pharmacological dose-response curves, where the system transitions from a sub-threshold to a supra-threshold regulatory state.

#### 7.2.4 Final Parameter Expressions

Substituting  $\theta_B = g_A/g_{AB}$  into our expressions for  $\kappa_1$  and  $\lambda_1$ :

$$\kappa_1 = 2 \left( g_A + g_{AB} \cdot \frac{g_A}{g_{AB}} \right) = 2(g_A + g_A) = 4g_A, \quad (85)$$

$$\lambda_1 = \frac{1}{\theta_B} \ln \left( 1 + \frac{2g_{AB} \cdot \frac{g_A}{g_{AB}}}{g_A} \right) = \frac{g_{AB}}{g_A} \ln(1+2) = \frac{g_{AB}}{g_A} \ln 3. \quad (86)$$

By complete symmetry, for gene  $B$  with  $\theta_A = g_B/g_{BA}$ :

$$\kappa_2 = 4g_B, \quad (87)$$

$$\lambda_2 = \frac{g_{BA}}{g_B} \ln 3. \quad (88)$$

For the self-repression terms, the steepness parameters  $\lambda_3$  and  $\lambda_4$  can be indexed separately to allow asymmetric responses, with typical values derived from cooperativity measurements as  $\lambda_3 \approx n/A_0$  and  $\lambda_4 \approx n/B_0$ , where  $n$  represents an effective Hill coefficient (commonly in the range 1–4 for biological systems).

The complete reformulated system, therefore, takes the form:

$$\dot{A}(t) = \left( \frac{4g_A}{1 + e^{-\frac{g_{AB}}{g_A} \ln 3(B(t-\tau_{12})-\frac{g_A}{g_{AB}})}} \cdot \frac{1}{1 + e^{\lambda_3(A(t-\tau_1)-A_0)}} \right) - \gamma_A A(t), \quad (89)$$

$$\dot{B}(t) = \left( \frac{4g_B}{1 + e^{-\frac{g_{BA}}{g_B} \ln 3(A(t-\tau_{21})-\frac{g_B}{g_{BA}})}} \cdot \frac{1}{1 + e^{\lambda_4(B(t-\tau_2)-B_0)}} \right) - \gamma_B B(t), \quad (90)$$

with parameters:  $\kappa_1 = 4g_A$ ,  $\kappa_2 = 4g_B$ ,  $\lambda_1 = (g_{AB}/g_A) \ln 3$ ,  $\lambda_2 = (g_{BA}/g_B) \ln 3$ ,  $\theta_B = g_A/g_{AB}$ ,  $\theta_A = g_B/g_{BA}$ ,  $\lambda_3 \approx n/A_0$ , and  $\lambda_4 \approx n/B_0$ .

This parameter set ensures exact matching of basal expression rates and approximate alignment of activation slopes, providing a faithful logistic approximation to the original model's dynamics while introducing bounded, biologically realistic saturation behavior.

### 7.2.5 Numerical Validation

Figure 10 presents comparative simulations of the original model (featuring linear activation with logistic self-repression) and the fully logistic reformulation. Using parameter values  $g_A = g_B = 50 \text{ nM}\cdot\text{min}^{-1}$ ,  $g_{AB} = g_{BA} = 2.5 \text{ nM}\cdot\text{min}^{-1}$  per nM,  $\gamma_A = 0.2 \text{ min}^{-1}$ ,  $\gamma_B = 0.24 \text{ min}^{-1}$ ,  $A_0 = B_0 = 70 \text{ nM}$ ,  $\lambda_3 = \lambda_4 = 0.057 \text{ nM}^{-1}$ , and initial conditions  $A(0) = B(0) = 10 \text{ nM}$ , both formulations exhibit rapid, monotonic convergence to steady states.

The derived logistic activation parameters  $\kappa_1 = \kappa_2 = 4g_A = 4g_B = 200 \text{ nM}$ ,  $\lambda_1 = \lambda_2 \approx (2.5/50) \cdot \ln(3) \approx 0.055$ , and  $\theta_A = \theta_B = 50/2.5 = 20 \text{ nM}$  ensure that the logistic approximation closely tracks the original dynamics. The agreement between solid lines (fully logistic system) and dashed lines (original approximated system) confirms that the parameter matching strategy successfully preserves the system's essential dynamical characteristics, validating the approach for systems with moderate cooperativity.

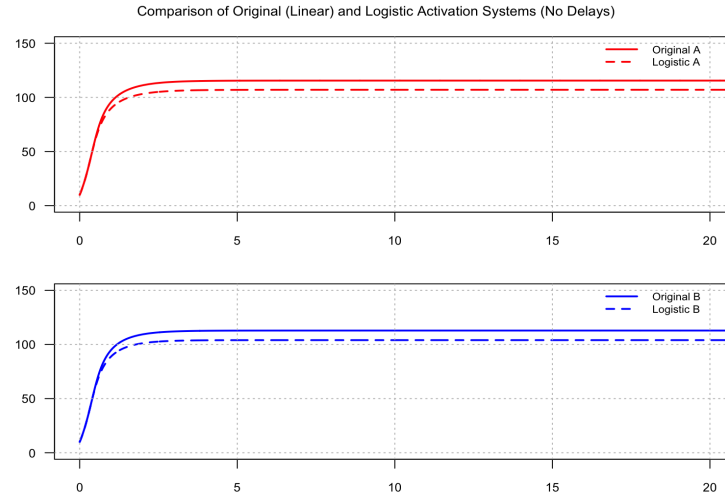


Figure 10: Comparative dynamics of the two-gene self-inhibitory and mutually activating network. Trajectories were generated using parameters  $g_A = g_B = 50 \text{ nM}\cdot\text{min}^{-1}$ ,  $g_{AB} = g_{BA} = 2.5 \text{ nM}\cdot\text{min}^{-1}$  per nM,  $k_A = 0.20 \text{ min}^{-1}$ ,  $k_B = 0.24 \text{ min}^{-1}$ ,  $A_0 = B_0 = 70 \text{ nM}$ ,  $\lambda_3 = \lambda_4 = 0.057 \text{ nM}^{-1}$ ,  $\kappa_1 = \kappa_2 = 200 \text{ nM}$ ,  $\lambda_1 = \lambda_2 \approx 0.055$ ,  $\theta_A = \theta_B = 20 \text{ nM}$ , and initial conditions  $A(0) = B(0) = 10 \text{ nM}$  (delays set to zero). Solid lines represent the fully logistic system; dashed lines show the original linear-activation model. The close agreement validates the parameter matching strategy for moderate steepness regimes.

The parameter estimation strategy presented here exemplifies the logistic framework's advantages for parameter inference from experimental data. Our biologically motivated threshold selection and slope-matching criteria ensure that estimated parameters preserve the essential dynamical characteristics of the original system, as validated through numerical comparison of trajectories. While we employ direct parameter matching rather than exhaustive parameter space exploration, the logistic framework's smooth structure makes it naturally compatible with systematic parameter space analysis methods. Combinatorial representations [116] and analytical decomposition approaches [28] provide complementary tools for rigorous parameter space exploration that could be integrated with our framework in future work, particularly for identifying bifurcation boundaries and classifying dynamical regimes across high-dimensional parameter domains.

### 7.2.6 Alternative Threshold Selection Strategies

While our biologically motivated threshold selection ( $\theta_B = g_A/g_{AB}$ ,  $\theta_A = g_B/g_{BA}$ ) provides elegant parameter expressions with clear biological interpretation, alternative strategies merit consideration depending on data availability and modeling objectives.

One natural alternative sets thresholds near the system's steady-state concentrations, which can be determined experimentally or computed numerically. For the original system with linear activation:

$$\gamma_A A^* = (g_A + g_{AB} B^*) \cdot \frac{1}{1 + e^{\lambda_3(A^* - A_0)}}, \quad (91)$$

$$\gamma_B B^* = (g_B + g_{BA} A^*) \cdot \frac{1}{1 + e^{\lambda_4(B^* - B_0)}}. \quad (92)$$

These coupled transcendental equations typically require a numerical solution to obtain the equilibrium concentrations  $A^*$  and  $B^*$ . Setting  $\theta_B \approx B^*$  and  $\theta_A \approx A^*$  aligns the logistic inflection points with the concentrations around which the system naturally operates, which can be particularly appropriate when transcription factors spend most of their time near steady-state values. This approach reflects the biological reality that regulatory thresholds often correspond to dissociation constants or typical operating concentrations rather than abstract mathematical constructs.

Given steady-state-based thresholds, the production rates and steepness parameters would then be computed as:

$$\kappa_1 = 2(g_A + g_{AB}\theta_B), \quad \lambda_1 = \frac{1}{\theta_B} \ln \left( 1 + \frac{2g_{AB}\theta_B}{g_A} \right), \quad (93)$$

$$\kappa_2 = 2(g_B + g_{BA}\theta_A), \quad \lambda_2 = \frac{1}{\theta_A} \ln \left( 1 + \frac{2g_{BA}\theta_A}{g_B} \right). \quad (94)$$

The choice between threshold selection strategies should be guided by the availability of experimental data, the specific biological system under study, and the intended modeling goals (e.g., accurately capturing transient dynamics versus steady-state behavior).

### 7.3 Weighted Logistic Formulations with Regulatory Strength Scaling

An alternative formulation directly incorporates the regulatory activation strengths  $g_{AB}$  and  $g_{BA}$  as scaling factors within the logistic function's argument, rather than absorbing them into the steepness and threshold parameters. This approach writes the system as:

$$\dot{A}(t) = \left( \frac{\kappa_1}{1 + e^{-\lambda_1(g_{AB}B(t-\tau_{12})-\theta_B)}} \cdot \frac{1}{1 + e^{\lambda_3(A(t-\tau_1)-A_0)}} \right) - \gamma_A A(t), \quad (95)$$

$$\dot{B}(t) = \left( \frac{\kappa_2}{1 + e^{-\lambda_2(g_{BA}A(t-\tau_{21})-\theta_A)}} \cdot \frac{1}{1 + e^{\lambda_4(B(t-\tau_2)-B_0)}} \right) - \gamma_B B(t). \quad (96)$$

Following the same parameter matching logic as before, we obtain:

$$\kappa_1 = 4g_A, \quad \lambda_1 = \frac{\ln 3}{g_A}, \quad (97)$$

$$\kappa_2 = 4g_B, \quad \lambda_2 = \frac{\ln 3}{g_B}, \quad (98)$$

$$\theta_B = g_A, \quad \theta_A = g_B. \quad (99)$$

Numerical simulations confirm that this scaled-weight formulation produces dynamics nearly identical to the previous version, as expected from the mathematical equivalence established above. Both approaches represent valid reformulations that preserve the system's essential dynamical characteristics while offering different parameter interpretations. The choice between them may be guided by computational convenience, parameter interpretability, or alignment with experimental measurement protocols.

## 7.4 Bridging Linear and Sigmoidal Modeling Paradigms

The hybrid regulatory architecture employed in Vinoth *et al.* (2025) wherein gene production is governed by an additive linear activation term ( $g_A + g_{AB}B(t - \tau_{12})$ ) combined with Hill function-mediated self-repression  $1/(1 + (A/A_0)^n)$  admits a rigorous transformation into a purely sigmoidal framework expressed entirely through logistic functions. This additive linear form for transcriptional activation, where basal production  $g_A$  (constitutive transcription independent of regulators) superimposes with regulator-proportional activation  $g_{AB}B(t - \tau_{12})$ , traces its conceptual origins to the early mathematical modeling of gene regulatory circuits following Jacob and Monod's seminal operon model (1961) [106], which established the fundamental principles of transcriptional regulation through repressor and activator molecules. The systematic replacement strategy proceeds as follows: the unbounded linear activation component ( $g_A + g_{AB}B(t - \tau_{12})$ ) is supplanted by a bounded, monotonically increasing logistic function  $\kappa/(1 + e^{-\lambda(B(t - \tau_{12}) - \theta_B)})$ , whose low-concentration Taylor expansion can be engineered to reproduce precisely both the desired basal expression rate  $g_A$  (at zero activator concentration) and the initial activation slope  $g_{AB}$  (characterizing sensitivity to small perturbations in activator concentration).

When the logistic activation parameters are selected according to our biologically motivated threshold criterion by setting maximal production  $\kappa = 4g_A$  (generalizing to  $\kappa = 2(g_A + g_{AB}\theta_B)$  for arbitrary thresholds) and positioning the threshold at  $\theta_B = g_A/g_{AB}$  (the biologically meaningful concentration where cross-activation strength equals basal production), the resulting sigmoidal function becomes locally indistinguishable from the original additive expression throughout the physiologically relevant moderate-concentration regime, while simultaneously introducing biologically realistic saturation behavior at elevated activator concentrations that the linear model cannot capture. This threshold placement ensures that the logistic inflection point aligns with the regulatory transition concentration, analogous to the  $EC_{50}$  in dose-response pharmacology.

Concurrently, the Hill self-repression term  $1/(1 + (A/A_0)^n)$  undergoes substitution by its logistic counterpart  $1/(1 + e^{\lambda(A - A_0)})$ , yielding a model wherein every regulatory interaction where both activation and repression manifests as a product of pure sigmoidal logistic functions, eliminating the mathematical heterogeneity of the original formulation.

This transformation preserves with exceptional fidelity the original system's essential dynamical characteristics: steady-state concentrations, local linearization slopes around equilibria, and basal expression levels remain virtually unchanged. Yet the logistic reformulation confers substantial mathematical and computational advantages that prove decisive for both theoretical analysis and numerical implementation. The framework inherits the logistic function's infinite differentiability (ensuring well-defined higher-order derivatives for stability analysis), globally bounded and Lipschitz-continuous vector fields (guaranteeing existence and uniqueness of solutions), analytically tractable Jacobian entries of the elegant form  $\lambda f(1 - f)$  (facilitating linearization and bifurcation analysis), complete absence of singularities at the origin (eliminating numerical pathologies near zero concentrations), existence of guaranteed positive invariant rectangles (confining trajectories to biologically meaningful domains), and should enhance numerical stability coupled with superior parameter identifiability in least-squares estimation procedures. These combined advantages position the logistic formulation as both mathematically rigorous and biologically interpretable for modeling gene regulatory networks.

The connection between linear approximations and sigmoidal models, via the logistic function, offers several strategic advantages for modeling biological systems, particularly in gene regulatory network applications. This linkage effectively bridges two modeling paradigms: the simplicity and analytical tractability of linear approximations, which facilitate straightforward parameter estimation and mathematical analysis, and the biological realism of sigmoidal functions, which naturally capture bounded saturation effects, cooperative regulatory interactions, and sharp threshold-like transitions characteristic of biological switches.

The logistic function's steepness parameter provides a continuous tuning mechanism between these extremes. Low steepness values ( $\lambda \ll 1$ ) produce nearly linear responses suitable for systems operating far from saturation or exhibiting weak cooperativity, while high steepness values ( $\lambda \gg 1$ ) generate sharp, switch-like transitions approximating Hill functions or step-function idealized models. This parametric flexibility enables smooth interpolation across dynamical regimes, enhancing model adaptability to diverse biological

phenomena such as genetic oscillations, bistable switches, and graded developmental patterning.

Moreover, the ability to derive exact linear approximations for small  $\lambda$  (as demonstrated above) facilitates hybrid modeling strategies where subsystems are analyzed locally using linear methods while global nonlinear dynamics are captured through the full logistic formulation. This multi-scale analytical capability proves particularly valuable when combining mechanistic modeling with data-driven approaches.

## 8 Logit Transformation and Logistic Regression for Gene Regulatory Network Inference: Mathematical Foundation and Computational Advantages

The logit transformation, defined as the inverse of the logistic function  $f^{-1}(y) = \ln\left(\frac{y}{1-y}\right)$  for probability values  $y \in (0, 1)$ , provides a natural mathematical bridge between continuous probability spaces and linear predictor structures. By transforming probabilities into log-odds ratios, where odds represent the ratio of event occurrence to non-occurrence, this transformation linearizes sigmoidal relationships, rendering them amenable to standard linear modeling techniques and establishing a direct connection between biological dose-response curves and statistically tractable inference frameworks.

This property forms the cornerstone of logistic regression, a generalized linear model (GLM) that employs the logit as its canonical link function, mapping binary or categorical outcomes to continuous linear predictor spaces. For gene regulatory networks, this framework proves particularly powerful: activation dynamics modeled by the increasing sigmoid  $f(x) = \frac{1}{1+e^{-\lambda(x-\theta)}}$  invert to

$$f^{-1}(y) = \theta + \frac{1}{\lambda} \ln\left(\frac{y}{1-y}\right), \quad (100)$$

Similarly, repression dynamics captured by the decreasing sigmoid  $g(x) = \frac{1}{1+e^{\lambda(x-\theta)}}$  invert to

$$g^{-1}(y) = \theta - \frac{1}{\lambda} \ln\left(\frac{y}{1-y}\right), \quad (101)$$

directly encoding the inhibitory mode where increasing regulator concentration suppresses target expression. These closed-form inverses enable the rapid computation of regulatory concentrations corresponding to desired expression probabilities, a critical capability that Hill functions lack for non-integer exponents in control design and parameter estimation.

### 8.1 Application to Single-Cell Gene Regulatory Network Inference

Within the context of gene regulatory network (GRN) inference from single-cell RNA sequencing (scRNA-seq) data, logistic regression offers a principled framework for addressing several fundamental challenges simultaneously. Single-cell datasets are characterized by pronounced sparsity (typically >90% zero entries) and pervasive dropout events, technical artifacts where truly expressed genes incorrectly appear as unexpressed due to stochastic capture inefficiencies and the inherently low molecule counts (often <10 mRNA copies per cell) in individual cells [117, 118].

Logistic regression leverages the logit transformation to predict regulatory interactions from binary or binarized expression data, framing the inference task as a binary classification problem: estimating the probability that regulatory interactions exist based on observed co-expression patterns, temporal ordering (from time-series or pseudotime-ordered data), and prior knowledge of the regulatory architecture. For a single candidate regulator  $j$  acting on target gene  $i$ , the mathematical formulation models the probability that gene  $i$  is expressed (binary outcome) as a function of regulator  $j$ 's expression level across cells:

$$\text{logit}(p_{i|j}) = \beta_0 + \beta_1 x_j, \quad p_{i|j} = \frac{1}{1 + e^{-(\beta_0 + \beta_1 x_j)}}, \quad (102)$$

where  $p_{i|j} \in (0, 1)$  denotes the probability that gene  $i$  is expressed given the expression level  $x_j$  of regulator  $j$ ,  $\beta_0$  captures baseline regulatory propensity (basal expression probability), and  $\beta_1$  quantifies both the strength and direction of regulation. The sign of  $\beta_1$  encodes the regulatory mode:  $\beta_1 > 0$  indicates activation (increased regulator expression enhances target expression probability), while  $\beta_1 < 0$  signifies repression (elevated regulator levels suppress target expression). The magnitude  $|\beta_1|$  quantifies the tightness of regulatory coupling, with larger values corresponding to sharper dose-response transitions.

For realistic GRN inference scenarios involving multiple candidate regulators, we extend to the elastic-net regularized logistic regression framework:

$$\text{logit}(p_i^{(c)}) = h_{i0} + \sum_{k=1}^N h_{ik} x_k^{(c)}, \quad \mathbf{h}_i = \arg \min_{\mathbf{h}} \left\{ -L(\mathbf{h} | D_i) + \lambda [\alpha \|\mathbf{h}\|_1 + (1 - \alpha) \|\mathbf{h}\|_2^2] \right\}, \quad (103)$$

where  $c$  indexes individual cells,  $x_k^{(c)}$  represents the (binary or continuous normalized) expression of candidate regulator  $k$  in cell  $c$ ,  $p_i^{(c)}$  is the predicted probability of target gene  $i$  expression in that cell, and the coefficient vector  $\mathbf{h}_i = (h_{i0}, h_{i1}, \dots, h_{iN})$  is estimated by minimizing the penalized negative log-likelihood. The regularization parameter  $\lambda$  controls overall penalty strength (preventing overfitting in high-dimensional settings), while  $\alpha \in [0, 1]$  balances the L1 (LASSO) penalty, which induces sparsity by driving small coefficients exactly to zero, thereby performing automatic feature selection and eliminating spurious regulatory edges against the L2 (ridge) penalty, which provides quadratic coefficient shrinkage that stabilizes estimates when candidate regulators are correlated (addressing multicollinearity). This simultaneous feature selection and coefficient stabilization proves crucial in genome-scale inference, where the number of potential regulatory interactions ( $\sim N \times M$  for  $N$  regulators and  $M$  target genes, often exceeding  $10^6$  edges) vastly exceeds the number of observations (typically hundreds to thousands of cells).

This formulation yields sigmoidal dose-response curves that naturally capture characteristic regulatory saturation kinetics: minimal response at low regulator concentrations (basal expression), steep transitions at intermediate levels (switch-like behavior near thresholds), and saturation at high concentrations (maximal expression plateaus), all without the analytical complications and numerical singularities inherent to Hill functions.

## 8.2 Computational and Mathematical Advantages

The logistic regression framework offers several compelling advantages for GRN inference that significantly improve both computational efficiency and biological interpretability compared to Hill function-based approaches:

**Probabilistic Interpretation and Uncertainty Quantification.** The framework provides estimated interaction likelihoods  $p(h_{ik} | D)$  that naturally quantify uncertainty arising from measurement noise, biological stochasticity, and incomplete data sampling. Standard errors and confidence intervals for coefficients  $h_{ik}$  emerge directly from the Fisher information matrix, enabling rigorous statistical hypothesis testing for edge presence. This probabilistic formulation proves essential when distinguishing direct regulatory interactions (strong coefficients with tight confidence bounds) from indirect effects mediated through intermediate pathway components (weak or insignificant coefficients), a persistent challenge in observational network inference.

**Robustness to Extreme Sparsity.** The smooth, bounded logit transformation effectively handles the extreme sparsity characteristic of scRNA-seq matrices, where >90% of entries are zero. Unlike methods requiring continuous, normally distributed inputs (which can exhibit numerical instabilities, undefined logarithms, or infinite gradients when confronted with sparse, zero-inflated data), the logistic GLM framework is specifically designed for binary outcomes and naturally accommodates zero-heavy distributions without requiring imputation, truncation, or pseudo-count additions that introduce artificial bias.

**Seamless Regularization Integration.** As demonstrated in Equation (103), the framework integrates naturally with elastic net regularization. The L1 component ( $\alpha\|\mathbf{h}\|_1$ ) performs automatic feature selection by shrinking small coefficients exactly to zero, effectively pruning the inferred network to retain only the most statistically significant edges. The L2 component ( $((1 - \alpha)\|\mathbf{h}\|_2^2)$ ) provides stability when multiple regulators are correlated, preventing coefficient inflation and variance explosion that would otherwise occur in multicollinear settings. Modern coordinate descent algorithms (e.g., `glmnet`) exploit the separable penalty structure to achieve computational complexity linear in the number of non-zero coefficients, enabling genome-scale inference (with more than  $10^6$  potential edges) within minutes on standard hardware.

The Table 3 systematically compares key mathematical and computational properties, demonstrating the superiority of logistic functions over Hill functions for binary inference:

Table 3: Comparison of Hill and logistic functions for GRN inference from scRNA-seq data

Property	Hill function	Logistic function
Differentiability	Singular at $x = 0$ when $n \notin \mathbb{N}$ or $n < 1$ ; derivatives undefined or infinite	$C^\infty$ everywhere; globally smooth derivatives
Derivative form	Complex rational: $\frac{\partial h}{\partial x} = \frac{nx^{n-1}\theta^n}{(x^n + \theta^n)^2}$ with fractional powers	Self-referential: $\frac{\partial f}{\partial x} = \lambda f(1-f)$ ; simple algebraic evaluation
Optimization landscape	Frequently non-convex (for negative log-likelihood) $\rightarrow$ multiple local minima, initialization-dependent convergence	Strictly convex (for negative log-likelihood) $\rightarrow$ unique global minimum, guaranteed convergence
Optimization speed (genome-scale edges) $> 10^6$	Slow; requires careful initialization, adaptive step-sizes; unstable near origin	Fast; coordinate descent/IRLS with linear-time updates
Handling zero-inflated/binary data	Poor; requires truncation, pseudo-counts, or imputation introducing bias	Native GLM framework; designed for binary outcomes
Intrinsic basal expression	Forced to zero at $x = 0$ : $h(0) = 0$	Naturally $> 0$ : $f(0) = \frac{1}{1+e^{\lambda\theta}} > 0$
Parameter interpretation	Mechanistic (binding sites); less suitable for phenomenological inference	Phenomenological; direct mapping to log-odds ratios

Hill functions  $h(x) = \frac{x^n}{\theta^n + x^n}$  with non-integer  $n$  (ubiquitous in experimental fits) introduce origin singularities where derivatives  $\frac{\partial h}{\partial x} \propto x^{n-1}$  diverge to infinity at  $x = 0$  when  $0 < n < 1$ . These singularities destabilize numerical optimization, requiring careful initialization away from zero, specialized constrained solvers, or heuristic smoothing that compromises mathematical rigor. In contrast, the logistic function's exponential structure ensures  $C^\infty$  global differentiability everywhere, including at the origin, with the self-referential derivative form  $f'(s) = \lambda f(s)(1-f(s))$  enabling efficient gradient computation requiring only function value evaluation (no power operations or rational function manipulations). For maximum likelihood estimation via iteratively reweighted least squares (IRLS) or coordinate descent, this translates to convergence rates that are orders of magnitude faster than those required for derivative-free methods or numerical gradient approximations, such as those used for Hill parameterizations.

**Convex Optimization Landscape.** The negative log-likelihood function for logistic regression exhibits strict convexity with respect to regression coefficients  $\mathbf{h}$ , guaranteeing existence and uniqueness of global minima. This ensures that gradient-based optimization algorithms (Newton-Raphson, IRLS, coordinate descent) converge reliably to the global optimum without becoming trapped in local minima or saddle points,

a persistent challenge for non-convex Hill parameterizations where initialization sensitivity and multi-start strategies are required. The strict convexity arises from the exponential family structure of the Bernoulli likelihood, combined with the canonical logit link, which ensures that the Hessian matrix remains positive definite throughout the parameter space. This computational efficiency proves paramount in high-dimensional scenarios involving thousands of genes ( $N \sim 10^3$ – $10^4$ ) and hundreds of thousands of potential interactions ( $\sim N^2 \sim 10^6$ – $10^8$ ), where modern elastic net implementations exploiting separability and curvature structure achieve rapid convergence (often  $<10$  iterations for coordinate descent), enabling genome-scale network reconstruction from single-cell datasets within feasible computational timeframes.

### 8.3 Proposed Inference Pipeline and Future Directions

The mathematical properties established throughout this paper, such as closed-form inverses,  $C^\infty$  smoothness, strict convexity of the negative log-likelihood, and self-referential derivatives, already enable a complete, numerically robust inference pipeline. While detailed implementation and comprehensive validation across diverse biological systems represent important directions for ongoing investigation, the theoretical foundations suggest a promising multi-stage framework integrating several complementary strategies:

**Stage 1: Regulation-Based Binarization.** For genes with high regulatory coherence, where multiple known or previously inferred regulators unanimously suggest a particular expression state (e.g., all activators high and all repressors low  $\rightarrow$  gene should be expressed), such logical consistency constraints can substantially improve inference accuracy by treating dropout events as informative rather than purely artifactual. Our proposed regulation-based binarization method [119] leverages regulatory graph structure to propagate binary state assignments between regulators and targets according to Boolean regulatory logic (AND, OR, NOT gates), inferring missing or uncertain expression values through forward-backward consistency propagation that ensures biological plausibility. This preprocessing step reduces dropout-induced noise while preserving genuine biological zeros (i.e., genes that are truly unexpressed), thereby improving signal quality for downstream regression.

**Stage 2: Pseudotime Inference and Causal Filtering.** Ordering cells along developmental or differentiation trajectories (pseudotime) using algorithms such as Monocle, Slingshot, or diffusion pseudotime enables causal filtering: regulators must temporally precede their targets. For each candidate edge  $j \rightarrow i$ , we impose the constraint that regulator  $j$  exhibits expression changes earlier in pseudotime than target  $i$ , eliminating edges that violate temporal precedence. This temporal constraint provides crucial filters against spurious correlations arising from co-expression patterns that lack direct causal dependency (e.g., two genes co-expressed because both are downstream of a common driver), addressing a fundamental challenge in observational network inference where correlation does not imply causation.

**Stage 3: Regularized Logistic Regression.** Apply elastic-net penalized logistic regression (Equation (103)) to the binarized or normalized expression data, fitting one model per target gene  $i$  with all candidate regulators as predictors. Cross-validation determines optimal penalty parameters  $(\lambda, \alpha)$  by maximizing out-of-sample prediction accuracy or minimizing Bayesian Information Criterion (BIC). The resulting coefficient estimates  $\hat{h}_{ik}$  directly quantify regulatory edge strengths, with non-zero coefficients indicating statistically significant interactions surviving the L1 sparsity penalty.

**Stage 4: Boolean Logic Extraction and Network Reconstruction.** The estimated coefficients from Equation (103) map naturally to Boolean regulatory logic: positive coefficients  $h_{ik} > 0$  indicate activation, implementing OR logic (target  $i$  expressed when *any* activator  $k$  is present); negative coefficients  $h_{ik} < 0$  signify repression, implementing AND-NOT logic (target  $i$  expression requires repressor  $k$  absence). For genes with multiple regulators, the linear combination  $\sum_k h_{ik}x_k$  implicitly encodes combinatorial logic. Thresholding the logit score partitions cells into predicted ON/OFF states, enabling extraction of explicit Boolean rules (e.g., "Gene  $A$  is expressed IF (Regulator  $B$  is high AND Regulator  $C$  is low) OR Regulator  $D$  is high").

These rules reconstruct complex regulatory architectures, including feed-forward loops (coherent and incoherent), mutual inhibition toggle switches, and hierarchical cascades network motifs that recur throughout biological systems and govern critical cellular decisions.

## 8.4 Advanced Extensions

Several advanced methodological extensions warrant future investigation to further enhance the framework’s power and applicability:

**Bayesian Logistic Regression with Informative Priors.** Bayesian formulations replace point estimates  $\hat{\mathbf{h}}_i$  with full posterior distributions  $p(\mathbf{h}_i | D)$ , enabling principled uncertainty quantification beyond standard errors. Posterior credible intervals characterize confidence in inferred interactions. Narrow posteriors (indicating high confidence) warrant priority for experimental validation, while broad posteriors (suggesting high uncertainty) indicate insufficient data, requiring additional measurements or stronger priors. This framework naturally accommodates informative priors that encode known regulatory interactions from databases (e.g., TRANSFAC, JASPAR binding motifs), ChIP-seq binding peaks, or orthologous networks from related species, thereby shrinking posteriors toward biologically plausible parameter regions. Hierarchical modeling enables the sharing of information across related cell types or developmental stages (e.g., hematopoietic stem cells → differentiated lineages), thereby improving inference in data-scarce regimes by borrowing statistical strength from related contexts.

**Neural Ordinary Differential Equations (Neural ODEs) with Logistic Regulatory Layers.** Neural ODEs parameterize temporal dynamics as  $\frac{dx_i}{dt} = f_\theta(\mathbf{x}, t)$  with learnable neural network parameters  $\theta$ , enabling continuous-time modeling of gene expression trajectories. Constraining hidden layer activations to pass through logistic sigmoids, i.e.,  $f_\theta(\mathbf{x}, t) = \sum_k w_k \cdot \text{logistic}(\mathbf{v}_k^\top \mathbf{x} + b_k)$  preserves biological interpretability (sigmoidal dose-response, saturation kinetics, threshold behavior characteristic of transcriptional regulation) while delegating residual regulatory complexity (unmodeled pathway crosstalk, stochastic fluctuations, post-transcriptional regulation) to flexible data-driven components learned via gradient descent on observed trajectories. This hybrid approach leverages the analytical advantages of logistic functions (a smooth optimization landscape, well-behaved gradients, and interpretable parameters amenable to mechanistic validation) while accommodating complex interaction terms that resist explicit mechanistic specification, thereby providing a bridge between mechanistic and machine learning paradigms.

## 8.5 Validation Strategy and Biological Relevance

Detailed implementation of the complete inference pipeline, including comprehensive benchmarking against state-of-the-art methods (GENIE3, SCENIC, GRNBoost2, CellOracle) across gold-standard datasets (e.g., DREAM challenges, curated *E. coli* and yeast networks), and experimental validation of top-ranked predicted interactions via CRISPR perturbations or reporter assays, remains an important direction for ongoing and future work. The theoretical foundations and mathematical advantages presented throughout this paper close-form inverses enabling rapid threshold calculations,  $C^\infty$  smoothness eliminating origin singularities, strict convexity of the negative log-likelihood guaranteeing global convergence, self-referential derivatives accelerating gradient computations, establish clear pathways from theory to practice, providing a solid mathematical basis for robust implementations.

Comprehensive validation across multiple dimensions will be essential to establish the practical utility and biological fidelity of this framework. Through such validation, we anticipate demonstrating that the logit transformation’s mathematical structure linearized probability space enabling GLM machinery, convex negative log-likelihood eliminating local minima, tractable derivatives accelerating optimization translates directly into superior computational performance (orders of magnitude faster convergence, guaranteed global solutions, native handling of zero-inflated data) and biological interpretability (probabilistic edge confidence scores, direct mapping to Boolean regulatory logic, seamless integration of prior knowledge) for

high-dimensional, noisy, sparse single-cell expression data. The framework positions logistic regression as a foundational methodology for next-generation GRN inference challenges spanning developmental biology (lineage specification, cell fate decisions), disease modeling (cancer regulatory rewiring, immune dysfunction), and synthetic circuit design (predictable engineered regulatory cascades), while systematically avoiding the analytical pathologies of Hill functions (origin singularities causing numerical instability, non-convex optimization landscapes trapping in local minima, intractable derivatives for non-integer exponents hindering gradient-based methods) yet fully preserving essential sigmoidal regulatory characteristics including threshold behavior, saturation kinetics, and tunable cooperativity that capture biological reality.

## 9 Extensions of Logistic Modeling to Immunology, Epidemiology, and Environmental Systems

The logistic-based formulation featuring explicit decreasing and increasing functions extends naturally beyond genetic networks into ecological, epidemiological, and immunological modeling, where sigmoidal response dynamics pervade regulatory mechanisms. Future investigations will systematically assess their relevance in these domains, particularly through direct comparisons with traditional Hill-type models.

### 9.1 Extensions and Applications in Immunology and Hematopoiesis

In immunology, logistic functions can encode T-cell activation thresholds, cytokine feedback loops, and the saturation of immune responses. Crauste's seminal work on hematopoiesis [120] demonstrates how nonlinear feedback mechanisms govern cell proliferation, differentiation, and apoptosis, processes typically modeled via Hill functions to capture how erythropoietin, glucocorticoids, or population feedback orchestrate critical cellular decisions: self-renewal, lineage commitment, and programmed cell death. These regulatory responses exhibit precisely the increasing and decreasing sigmoidal profiles that logistic functions capture with enhanced analytical tractability. For instance, consider the canonical hematopoiesis model using a decreasing logistic function (developed above):

$$\frac{dN(t)}{dt} = -\gamma N(t) + \kappa \cdot \frac{1}{1 + e^{-\lambda(\theta - N(t - \tau))}}, \quad (104)$$

where  $N(t)$  represents the cell population (e.g., neutrophils or hematopoietic stem cells),  $\tau$  encodes the differentiation delay reflecting maturation timescales,  $\gamma$  is the degradation rate,  $\kappa$  is the production rate, and the logistic function models feedback inhibition regulating cell proliferation.

#### 9.1.1 Detailed Linearization and Stability Analysis

To analyze the stability of Eq. (104), we first identify equilibria by setting  $\frac{dN}{dt} = 0$ :

$$-\gamma N^* + \kappa f(N^*) = 0 \quad \Rightarrow \quad f(N^*) = \frac{\gamma N^*}{\kappa}, \quad (105)$$

where  $f(N) = \frac{1}{1 + e^{-\lambda(\theta - N)}}$  is the decreasing logistic function.

**Step 1: Linearization around equilibrium.** Let  $n(t) = N(t) - N^*$  represent a small perturbation from equilibrium. Substituting  $N(t) = N^* + n(t)$  into Eq. (104):

$$\frac{dn(t)}{dt} = -\gamma[N^* + n(t)] + \kappa f(N^* + n(t - \tau)). \quad (106)$$

Using the first-order Taylor expansion of  $f$  around  $N^*$ :

$$f(N^* + n(t - \tau)) \approx f(N^*) + f'(N^*)n(t - \tau) + O(n^2). \quad (107)$$

Substituting and using the equilibrium condition  $-\gamma N^* + \kappa f(N^*) = 0$ :

$$\frac{dn(t)}{dt} = -\gamma n(t) + \kappa f'(N^*)n(t - \tau). \quad (108)$$

**Step 2: Computing the derivative of the logistic function.** The derivative of  $f(N) = \frac{1}{1+e^{-\lambda(\theta-N)}}$  is obtained via the chain rule. Let  $u = -\lambda(\theta - N)$ , so  $\frac{du}{dN} = \lambda$ :

$$\begin{aligned} f'(N) &= \frac{d}{dN} \left[ \frac{1}{1+e^u} \right] = -\frac{1}{(1+e^u)^2} \cdot e^u \cdot \frac{du}{dN} \\ &= -\frac{e^u}{(1+e^u)^2} \cdot \lambda = -\lambda \frac{e^{-\lambda(\theta-N)}}{(1+e^{-\lambda(\theta-N)})^2}. \end{aligned} \quad (109)$$

This can be elegantly rewritten using the property that for the logistic function:

$$f(N) = \frac{1}{1+e^{-\lambda(\theta-N)}}, \quad 1-f(N) = \frac{e^{-\lambda(\theta-N)}}{1+e^{-\lambda(\theta-N)}}, \quad (110)$$

which yields the self-referential derivative:

$$f'(N) = -\lambda f(N)(1-f(N)). \quad (111)$$

The absolute value of the derivative  $|f'(N)| = \lambda f(N)(1-f(N))$  remains identical to that of an increasing logistic, but the negative sign is crucial for capturing inhibitory feedback. This form still dramatically simplifies stability analysis compared to Hill functions, whose derivatives introduce unwieldy algebraic complexity and numerical issues at boundaries or high cooperativity.

**Step 3: Deriving the characteristic equation.** Substituting Eq. (111) into the linearized system (108):

$$\frac{dn(t)}{dt} = -\gamma n(t) - \kappa \lambda f(N^*)(1-f(N^*))n(t - \tau). \quad (112)$$

Let  $\beta = \kappa \lambda f(N^*)(1-f(N^*)) > 0$ . The equation becomes

$$\frac{dn(t)}{dt} = -\gamma n(t) - \beta n(t - \tau). \quad (113)$$

Assuming solutions  $n(t) = e^{\lambda_e t}$ , the characteristic equation is

$$\lambda_e + \gamma + \beta e^{-\lambda_e \tau} = 0. \quad (114)$$

**Step 4: Hopf bifurcation analysis.** Substitute  $\lambda_e = i\omega$  ( $\omega > 0$ ):

$$i\omega + \gamma + \beta(\cos(\omega\tau) - i\sin(\omega\tau)) = 0. \quad (115)$$

Separating real and imaginary parts:

$$\text{Real part: } \gamma + \beta \cos(\omega\tau) = 0, \quad (116)$$

$$\text{Imaginary part: } \omega - \beta \sin(\omega\tau) = 0. \quad (117)$$

Thus,

$$\cos(\omega\tau) = -\frac{\gamma}{\beta}, \quad (118)$$

$$\sin(\omega\tau) = \frac{\omega}{\beta}. \quad (119)$$

Using  $\cos^2 + \sin^2 = 1$ :

$$\omega^2 = \beta^2 - \gamma^2. \quad (120)$$

Oscillations require  $\beta > \gamma$ , i.e.,

$$\kappa\lambda f(N^*)(1 - f(N^*)) > \gamma. \quad (121)$$

The critical delay is

$$\tau_c = \frac{1}{\omega} \arccos\left(-\frac{\gamma}{\beta}\right) + \frac{2\pi k}{\omega}, \quad k = 0, 1, 2, \dots \quad (122)$$

with  $\omega = \sqrt{\beta^2 - \gamma^2}$ .

The logistic approach makes this characteristic equation analysis in delay differential equations (DDEs) tractable for identifying critical delays  $\tau_c$  that trigger Hopf bifurcations, transitions from steady states to sustained oscillatory dynamics that manifest clinically as cyclic neutropenia (periodic fluctuations in neutrophil counts with periods of 19–21 days), [121, 122, 123]. The bounded output range  $[0, 1]$  ensures numerical robustness by preventing singularities and maintaining well-conditioned gradients in optimization algorithms, while simultaneously guaranteeing non-negative propensity functions in stochastic simulations via the Gillespie algorithm. These mathematical properties directly facilitate modern control strategies, including feedback linearization, model predictive control (MPC), and linear quadratic regulation (LQR), for therapeutic applications in leukemia and hematological disorders, with control inputs  $u_i(t)$  representing optogenetic signals, chemical inducers like IPTG, or drug dosing schedules. A detailed treatment of this, including rigorous proofs and applications to control design and bifurcation analysis, will be presented in a forthcoming paper.

## 9.2 Extensions to Environmental and Epidemiological Modeling

The logistic framework's versatility extends beyond gene regulation. In environmental engineering, logistic functions can replace Hill and Monod equations for modeling microbial growth in bioreactors (see [124, 125]). For example, [124] employs a Hill coefficient  $n = 2$  to approximate substrate uptake kinetics. Logistic functions with moderate steepness, such as  $\lambda = 1$  or  $\lambda = 2$ , serve as practical alternatives, preserving qualitative growth dynamics while enhancing analytical simplicity and parameter identifiability.

In epidemiological modeling, logistic functions can approximate age-related susceptibility curves, capturing the sharp rise in mortality risk with increasing age observed in COVID-19 and other infectious diseases. This approach generalizes naturally to demographic risk models, where sigmoidal dose-response relationships govern the probability of infection, disease severity, or vaccine efficacy.

More broadly, many nonlinear biological systems, which are traditionally modeled using Hill or Monod functions, can be effectively approximated by logistic-based systems. Crucially, these systems often admit linearization around operating points, which significantly facilitates downstream analysis, including system stability assessment, feedback control design, observer synthesis for state estimation, and model-based parameter inference from experimental data.

## 10 Discussion

The approximations in the low-steepness regime are given by  $h^+(x, \theta, n) \approx \frac{1}{2} + \frac{1}{4} \cdot n \cdot \ln\left(\frac{x}{\theta}\right) + O(n^2)$  and  $f^+(x, \theta, \lambda) \approx \frac{1}{2} + \frac{1}{4} \cdot \lambda \cdot (x - \theta) + O(\lambda^2)$ . This reveals that the Hill function exhibits logarithmic behavior in  $\ln(x/\theta)$ , whereas the logistic function behaves linearly in  $x - \theta$ . This difference in scaling suggests that the Hill and logistic functions are related by a logarithmic change of variables. Specifically, they are locally equivalent when  $\lambda(x - \theta) \approx n \ln(x/\theta)$ , highlighting a close connection between the two functions. To explore this further, consider the standard logistic function  $f(s) = \frac{1}{1 + e^{-ns}}$ . By defining  $s = \ln(x/\theta)$ , we obtain:

$$f(\ln(x/\theta)) = \frac{1}{1 + \frac{\theta^n}{x^n}} = \frac{x^n}{x^n + \theta^n}. \quad (123)$$

This expression is precisely the Hill function for arbitrary  $n$  and  $\theta$ . Thus, the two functions are mathematically equivalent under a change of input variable, mapping the logistic's infinite domain  $(-\infty, \infty)$  to the Hill's non-negative domain  $(0, \infty)$ . This equivalence depends on the logarithmic scaling of the input concentration  $s$ , highlighting that the logistic and Hill functions share identical shapes but differ in scale (linear  $s$  versus logarithmic  $s$ ). This relationship parallels the well-known connection between the logistic function and the hyperbolic tangent, where  $f(s) = \frac{1}{2} + \frac{1}{2} \tanh(\frac{s}{2})$ , a standard link in statistics relating logit functions to sigmoids. However, this scaling introduces a key biological distinction: the logistic function responds linearly to absolute concentrations, while the Hill function assumes a log-scaled (relative) dependence. This raises the question of whether biological regulation depends on absolute concentrations ( $s$ ), which favors logistic models, or relative/log-scaled concentrations  $\ln(s)$ , which favors Hill-based models.

While mathematically equivalent under the transformation  $s = \ln(x/\theta)$ , this equivalence reveals a fundamental difference in biological interpretation: Hill functions naturally model ratio-dependent responses (equilibrium binding), whereas logistic functions model threshold-dependent responses (absolute concentration switches). To address this, we examine the logistic function  $f(s) = \frac{1}{1+e^{-ns}}$  as a foundational sigmoidal model in biology, statistics, and machine learning. The choice between linear input (where  $s$  is proportional to absolute values, such as concentrations) and logarithmic input (where  $s = \ln(x/\theta)$ , making it responsive to relative changes and equivalent to the Hill function) significantly impacts its interpretive power and applicability.

The choice between absolute (linear) and relative (logarithmic) concentration scaling depends on the biological context. While Hill functions naturally capture ratio-based equilibria (e.g.,  $x^n/(K_d^n + x^n)$ ), logistic functions with linear input ( $x - \theta$ ) may better represent systems where absolute thresholds dominate (e.g., minimal transcription factor copy numbers for activation), additive effects occur (e.g., multiple independent pathways), and low-concentration dynamics require non-zero baselines. However, for phenomena like fold-change detection, the logistic framework could also offer complementary advantages in computational tractability while preserving sigmoidal characteristics. The Hill coefficient  $n$  is estimated directly from experimental gene expression data, specifically by fitting the model to measurements of promoter activity versus inducer concentration. The corresponding logistic parameter  $\lambda = n/\theta$  can then be matched to preserve local input-output sensitivity, and the sigmoidal switching behavior emulates cooperativity phenomenologically without requiring explicit multi-site binding assumptions.

Linear input excels in systems driven by absolute thresholds, additive effects, and precise low-level dynamics [126]. Mathematically, it ensures the function's derivative (sensitivity to changes in  $s$ ) remains symmetric and proportional across the domain. The logistic's inflection point at  $s = 0$  treats positive and negative deviations equally, providing a balanced transition without bias toward low or high values. Logarithmic input, however, compresses high values and expands low ones, leading to heightened sensitivity at small  $s$  (e.g., amplifying noise in near-zero concentrations) and reduced responsiveness at large  $s$ . This can distort modeling in systems with uniform physical scales, such as chemical reactions where rates depend linearly on the absolute amounts of reactants [126].

Moreover, linear input preserves additivity, where changes in  $s$  correspond to arithmetic differences, aligning with conservation laws in biology (e.g., mass balance in metabolic pathways). Logarithmic input enforces multiplicativity, with changes reflecting ratios that suit exponential growth but complicate threshold-based switches. In threshold dose-response models, linear scaling allows geometric interpretations of curvilinear logit shapes that fit empirical data without assuming log-normality [127]. This uniformity also reduces the risk of overfitting, as parameters like steepness  $n$  scale directly with absolute changes rather than logarithmic artifacts [128].

Building on these mathematical advantages, the scaling difference has profound biological implications. Gene regulation often relies on absolute concentrations of transcription factors (TFs) and ligands rather than relative or log-scaled ones. Empirical studies in erythropoiesis and bacterial systems demonstrate that absolute protein copy numbers dictate binding kinetics, threshold behaviors, and expression levels, with regulatory decisions based on precise molecule counts per cell. For example, absolute quantification via targeted proteomics reveals that corepressors outnumber coactivators, creating a repressive nuclear environment not captured by relative mRNA metrics, which correlate poorly with proteins [129, 130, 131].

In bacterial gene regulation, absolute concentrations quantitatively link DNA to RNA and protein dynamics, enabling predictive models with thresholds based on copy numbers rather than logarithmic values [69, 129, 130, 131]. Promoter activity scales with gene copy number near the origin of replication, amplified by multifork replication at high growth rates, favoring absolute over log-scaled models for conserved gene positioning across species. Quantitative techniques like qPCR and RNA-seq further underscore this: absolute quantification provides exact copy numbers for thresholds, while relative metrics (e.g., fold-change) obscure absolute relevance, especially in heterogeneous samples [132]. In RNA-seq, absolute measures reveal biases in relative data, thereby improving the accuracy of differential expression. Studies in yeast demonstrate that central carbon metabolism genes resist growth-rate scaling and are regulated via absolute nutrient levels rather than logarithmic transformations, with constant absolute expression levels [133]. Linear regression between absolute mRNA concentrations and RNA-seq FPKM values supports the accurate scaling of all mRNA measurements, uncovering regulations that are masked by relative methods [133].

Furthermore, NF- $\kappa$ B activity responds to absolute differences in cytokine concentrations rather than the concentrations themselves or fold changes, indicating a linear response [71]. Precise modulation of TF levels, such as SOX9, shows that gene expression responses depend on absolute dosages, with sensitivity tied to absolute concentrations [70]. In combined signal responses, gene regulation often favors additive (linear) outcomes alongside multiplicative ones, with chromatin accessibility being largely additive [134].

A major issue with log-scaling, implicit in the Hill function, is its amplification of small relative changes at low concentrations ( $s$ ), which can misrepresent biological behavior where absolute thresholds prevail. In Hill-based models, higher coefficients ( $n > 1$ ) logarithmically amplify small changes, potentially misaligning with gene expression dynamics. While log-scaling aids statistical analysis (e.g., fold-changes in RNA-seq), it may obscure biological relevance, such as when small absolute changes in key TFs have significant effects not captured by log-fold symmetry. This over-amplification at low  $s$  explains why Hill models often require adjustments (e.g., adding basal term  $\epsilon$ ) to fit leakiness, whereas the logistic function naturally handles linear low-expression dynamics.

At the cellular level, biological sensors (e.g., receptors, TFs) typically respond to absolute ligand concentrations rather than logarithmic transformations, unless evolved for fold-change detection (e.g., chemotaxis). Linear input mirrors this by modeling responses in absolute space, capturing thresholds where a fixed number of molecules triggers activation, a common phenomenon in gene regulation, where protein copy numbers determine binding and expression [135]. Logarithmic input assumes a Weber-Fechner-like law, over-amplifying minor fluctuations at low concentrations and misrepresenting stochastic environments where absolute counts matter [136].

This preference for linear input extends to toxicology, where linear models better handle non-linear dose-response relationships without log-dose assumptions, especially for hormetic effects. Absolute thresholds (e.g., benchmark doses or no-effect levels) are prioritized, with linear responses at low absolute concentrations being considered more important than relative changes in concentration. For instance, benzene toxicology emphasizes linear responses at low concentrations, implying thresholds below which no risk occurs, and favors sublinear models based on absolute exposure levels [137, 126]. In heterogeneous data, such as single-cell RNA-seq, absolute metrics reveal regulations that are obscured by relative fold-changes, thereby improving differential expression accuracy [136].

Linear input also avoids the biases of logarithmic transformations, which require positive, non-zero inputs and inflate variance at low values (e.g., issues with  $\log(0)$ ). It facilitates unbiased estimation via maximum likelihood, assuming normality in absolute space rather than log-normal distributions, which skew the extremes. Additionally, linear input enhances model identifiability, where parameters like the midpoint  $\theta$  retain physical meaning (e.g., absolute  $EC_{50}$ ), unlike logarithmic input, which conflates them with scaling factors [138]. In genetic toxicology, linear-linear plots are preferred over log-linear approaches for mutation data due to inconsistencies in databases [139]. In risk assessment, linear inputs yield reliable points of departure without log-likelihood distortions, prioritizing absolute low-dose effects [140].

Practically, linear input simplifies experimental calibration, as measurements (e.g., qPCR or mass spectrometry) are in absolute units, avoiding log-transformation artifacts that obscure relevance (e.g., small TF changes with large effects) [141]. Linear models integrate readily with regression or additive networks,

whereas logarithmic inputs demand exponential back-transformation, increasing complexity [128]. In machine learning, linear activations before sigmoids preserve gradient flow more effectively than log-scaled inputs, thereby reducing vanishing gradients.

In pharmacology, toxicology, and biology, the logistic function’s sigmoidal form captures typical response patterns: minimal effects at low doses, steep rises in mid-ranges, and plateaus at high doses. The authors in [135] focus on absolute concentration thresholds in assays and gene regulation networks, incorporating thresholds for activation and favoring quantitative absolute measures. Similarly, [129] explores absolute concentrations of substrates and products in gene regulation networks, incorporating thresholds for regulatory activation. Works like [131] and [69] discuss thresholds in gene regulation where absolute concentrations determine outcomes, using logistic-like frameworks for signal-induced regulation. These examples reinforce that logistic models handle bounded responses based on absolute doses and thresholds in risk assessment.

Opting for linear input in the logistic function ensures mathematical consistency, biological accuracy, statistical reliability, and practical utility in absolute-threshold scenarios, as supported by toxicology and regulation literature [126]. This approach yields more interpretable and robust models, particularly in cases where additive absolute changes, rather than multiplicative ratios, govern dynamics. Therefore, while the Hill and logistic functions are equivalent via  $s = \ln(x/\theta)$ , the logistic function’s linear input better suits biological concentration responses, particularly for promoter leakiness and low-expression dynamics.

## 11 Conclusion

This paper establishes logistic functions as a mathematically principled, computationally robust, and biologically realistic alternative to Hill functions for modeling gene regulatory networks and related biological systems. Through systematic theoretical development, rigorous analysis, and extensive case studies, we demonstrate that logistic-based formulations deliver decisive advantages across mathematical, computational, and biological dimensions. Our framework rests on rigorous mathematical foundations, ensuring well-posedness and numerical stability. We established global existence, uniqueness, smoothness, and boundedness of solutions for logistic-based gene regulatory networks, with explicit Lipschitz constants governing solution stability and Jacobian conditioning. We demonstrate second-order Lipschitz continuity of the Jacobian itself, ensuring that variational equations remain well-posed and that sensitivity analysis is numerically stable.

The global infinite differentiability of logistic functions eliminates singularities that plague Hill functions with non-integer exponents at low concentrations. For non-integer Hill coefficients, derivatives diverge to infinity or become unbounded, rendering the function only finitely differentiable at the origin. The self-referential derivative structure significantly simplifies Jacobian matrix computations for stability analysis, while the analytically invertible form enables feedback linearization and rapid threshold calculations, which are essential for control design. A fundamental biological insight emerges from the logistic formulation: non-zero basal expression is intrinsic to the function’s structure, requiring no additional parameters. For activation, the logistic function naturally captures promoter leakiness observed ubiquitously in gene regulatory systems, where transcription persists at low levels even without activators. This tunable basal production rate, controlled via the steepness-threshold product without introducing artificial offset parameters that compromise the mathematical structure of Hill functions, serves critical functions: preventing irreversible trapping in off-states, reducing phenotypic noise, and enabling rapid induction responses. Our analysis of positive autoregulation in *Escherichia coli*, grounded in experimentally derived parameters from established literature, quantitatively demonstrates these advantages. With realistic feedback amplification placing the system in the monostable high-expression regime, starting from near-zero initial conditions, the logistic model escapes the off-state in approximately 44 minutes through basal production alone, reaching a stable high expression. In contrast, the Hill model remains irreversibly trapped at low expression without external perturbation. This noise-driven recovery mechanism, validated through numerical simulations, directly explains observations in the *gal* operon and related bistable systems where basal leakage maintains cellular responsiveness during environmental fluctuations. Similarly, for repression, the decreasing logistic function provides tunable unrepresed rates, capturing biological constraints like resource limitations or incomplete

promoter activation. At zero repressor concentration, the function approaches but need not equal unity, reflecting realistic imperfections. For applications requiring an exact unit value at repression, we provide a scaled variant that preserves the sigmoid shape. This flexibility proves essential for modeling systems where maximal expression cannot reach theoretical limits due to polymerase saturation, transcriptional noise, or competing cellular processes.

We develop systematic parameter estimation methodologies bridging experimental observations with mathematical formulations. The biologically motivated threshold selection strategy positions thresholds at concentrations where regulatory transitions occur, ensuring parameters map directly to measurable biological quantities analogous to half-maximal effective concentrations in dose-response pharmacology. The steepness matching criterion preserves local input-output sensitivity by equating derivatives at half-maximal points, maintaining functional equivalence with Hill models while enhancing analytical tractability. For the two-gene self-inhibitory and mutually activating network exhibiting chaos and extreme events, this approach yields explicit parameter formulas derived through Taylor expansion matching of both basal expression rates and activation slopes. Numerical validation confirms close agreement between fully logistic systems and original formulations, establishing the strategy's effectiveness across diverse regulatory architectures, including those exhibiting complex dynamics.

Crucially, our product-of-logistics formulation, which employs increasing logistic functions for activation and decreasing functions for repression, offers superior biological interpretability compared to alternative weighted formulations proposed in the literature. Each regulatory interaction possesses its own threshold and steepness parameters, which are directly interpretable as dissociation constants and cooperativity measures, determinable independently from experimental dose-response curves. We demonstrate through rigorous analysis that the weighted single-sigmoid approach exhibits problematic behavior for repression: the critical point occurs at negative concentrations, and the function remains very low across the entire biologically relevant domain, never approaching unity for repression. This transparent parameter structure facilitates model validation, enables mechanistic interpretation, and supports systematic extension to large-scale networks. While our parameter estimation employs direct biologically motivated matching rather than exhaustive parameter space exploration, the logistic framework's smooth, well-behaved structure renders it naturally compatible with rigorous systematic methods for parameter space analysis, including combinatorial representations and analytical decomposition approaches that enable identification of bifurcation boundaries and classification of dynamical regimes across high-dimensional parameter domains capabilities that could be integrated with our framework in future work to further enhance its power for complex system characterization.

The logistic framework enables multiple high-impact applications with immediate practical value. In synthetic circuit design, guaranteed numerical stability and continuous controllability at all expression levels facilitate the robust engineering of genetic toggle switches, oscillators, and logic gates, which operate reliably under cellular noise, addressing a critical challenge in translating computational designs into experimental implementations. For metabolic engineering, computational efficiency enables the genome-scale optimization of biosynthetic pathways that produce biofuels, pharmaceuticals, and industrial chemicals, where hundreds of regulatory interactions must be evaluated across thousands of genetic perturbations. In therapeutic applications, analytical tractability supports model-based design of engineered T-cells with precisely tuned activation thresholds for cancer immunotherapy and facilitates real-time control of optogenetically regulated insulin secretion for diabetes treatment. The closed-form inverse functions and smooth derivatives enable efficient implementation of model predictive control strategies in microfluidic platforms for maintaining desired expression levels despite environmental perturbations and cell-to-cell variability. In industrial bioprocess engineering, the framework's ability to capture realistic basal expression and saturation effects improves prediction accuracy for fed-batch fermentation optimization and enables systematic design of inducible expression systems with minimal metabolic burden.

Logistic functions provide fundamental advantages for controlling biological networks, stemming from continuous responsiveness even at zero expression levels. The non-zero basal production ensures controllability throughout the state space, whereas Hill functions' zero response at zero input creates controllability gaps that compromise feedback regulation. Multiple control strategies become tractable: multiplicative

control maintains non-zero controllability at all expression levels; steepness modulation provides linear, predictable control over regulatory sensitivity without numerical instabilities associated with large Hill coefficients; sliding mode control benefits from a smooth, bounded nature, ensuring robust performance under parameter uncertainties; model predictive control exploits closed-form inverses enabling feedback linearization and gradient-based optimization with well-conditioned problems. The smooth derivative structure with uniform bounds ensures well-conditioned Jacobian matrices, which are essential for observer design and state-feedback control. For systems with parallel regulation, combining multiple activators and repressors, controlled dynamics ensure non-zero production at zero regulator concentrations, thereby eliminating the controllability loss exhibited by Hill-based models in the absence of activators. While detailed implementation and experimental validation represent important directions for future investigation, the mathematical foundations demonstrate clear pathways from theory to practice, with experimental feasibility through optogenetics, fluorescent reporters, and microfluidic platforms.

The logistic framework extends naturally beyond gene regulatory networks. In hematopoiesis modeling, the elegant self-referential derivative simplifies characteristic equation analysis for identifying critical delays that trigger Hopf bifurcations, manifesting as cyclic neutropenia. The linearization around equilibrium yields characteristic equations, where purely imaginary solutions identify bifurcation points through coupled algebraic equations, which are dramatically simpler than Hill-based equivalents that require the evaluation of cumbersome rational functions. The bounded output range ensures numerical robustness in stochastic simulations via Gillespie algorithms, avoiding singularities and maintaining well-conditioned propensity functions in low-copy-number regimes. In environmental engineering, logistic functions can replace Hill and Monod equations for microbial growth in bioreactors, preserving qualitative dynamics while enhancing parameter identifiability. In epidemiological modeling, they approximate age-related susceptibility curves and dose-response relationships in vaccine efficacy studies. These extensions, while conceptually established through the unified mathematical framework, represent promising directions for detailed future investigation and experimental validation.

The logit transformation, being the inverse of the logistic function, establishes the mathematical foundations for inferring gene regulatory networks from single-cell RNA sequencing data. Logistic regression predicts the expression probability of target genes given candidate regulator expression levels, with coefficient signs encoding regulatory mode and magnitudes quantifying coupling strength. Elastic net regularization simultaneously performs feature selection and coefficient stabilization, which is crucial for high-dimensional inference where the number of potential edges vastly exceeds the number of observations. The framework offers decisive advantages over Hill-based approaches: strict log-likelihood concavity guaranteeing unique global maxima and reliable convergence without initialization sensitivity; global smoothness enabling efficient algorithms achieving genome-scale inference; native handling of zero-inflated binary data characteristic of single-cell sequencing without requiring artificial corrections; probabilistic interpretation providing uncertainty quantification through confidence intervals enabling rigorous hypothesis testing. Our proposed inference pipeline integrates regulation-based binarization, leveraging Boolean regulatory logic, pseudotime ordering for causal filtering, elastic net regression to yield sparse coefficient estimates, and Boolean logic extraction to reconstruct network motifs. Bayesian extensions with informative priors and Neural ODE formulations with logistic regulatory layers represent promising directions, combining mechanistic interpretability with data-driven flexibility. While comprehensive benchmarking and experimental validation remain important future work, the theoretical foundations position logistic regression as a powerful methodology for single-cell network reconstruction.

A fundamental insight emerges from comparing input scaling: Hill and logistic functions are mathematically equivalent under logarithmic transformation, but this equivalence reveals a critical distinction. Hill functions with their power-law structure respond to relative concentrations or fold-changes, while logistic functions with linear input respond to absolute concentrations. Extensive evidence from bacterial gene regulation, mammalian transcription factor studies, signaling pathways, and toxicology supports that biological regulation typically depends on absolute concentrations rather than log-scaled ones. Gene expression decisions rely on exact molecule counts per cell, with transcription factor copy numbers determining binding kinetics and threshold behaviors. Promoter activity scales with absolute gene copy numbers amplified by

multifork replication at high growth rates, favoring absolute over fold-change models. Regulatory thresholds correspond to specific molecule counts that trigger activation, including the minimal transcription factor copy numbers required for promoter occupancy, concentration thresholds where multiple pathways converge and exhibit additive logic, and signaling responses to absolute concentration differences rather than fold changes. This scaling choice has profound implications: at low expression levels, where genes exhibit persistent basal transcription, logistic functions naturally represent minimal activity. In contrast, the logarithmic amplification of Hill functions can misrepresent dynamics where absolute thresholds prevail, leading to small relative changes being overrepresented.

By combining mathematical rigor, biological realism, and computational efficiency, the logistic framework addresses long-standing limitations of Hill-based modeling. Global smoothness eliminates singularities, which can cause numerical integration failures and compromise bifurcation analysis. Intrinsic basal expression captures promoter leakiness without artificial modifications, allowing for the accurate modeling of noise-driven transitions in low-copy-number regimes. An analytically tractable structure facilitates the systematic design of control, synthesis of observers, and parameter estimation, even in high-dimensional networks. Biological interpretability, achieved through transparent mapping of parameters to mechanisms, enhances model validation and mechanistic understanding. Quantitatively, our case studies demonstrate that logistic models capture essential dynamics including sustained oscillations in genetic circuits with local asymptotic stability guaranteed by negative trace and positive determinant conditions, bistability with critical amplification thresholds characterized explicitly, and complete preservation of complex behaviors such as chaos and extreme events in two-gene networks with close trajectory agreement validating parameter matching strategies, all while maintaining superior numerical stability evidenced by bounded derivatives and explicit Lipschitz constants ensuring well-conditioned Jacobians throughout state space.

Finally, while this work establishes comprehensive theoretical foundations and demonstrates effectiveness through detailed case studies, several promising directions merit future investigation: extending control strategies to stochastic gene networks accounting for intrinsic and extrinsic noise; integrating spatial dynamics and cell-to-cell communication in multicellular systems; combining logistic-based mechanistic models with machine learning for adaptive control; validating control strategies experimentally in optogenetic platforms with real-time feedback; exploring applications in metabolic pathway control, cell cycle regulation, and developmental morphogen gradients; conducting systematic comparisons with Hill-based models across diverse biological systems to delineate optimal application domains and quantify performance improvements. Additionally, extending the logistic framework to time-delay systems for sustained oscillations, investigating logistic approximations for higher-order cooperativity through repeated factor products, and developing specialized numerical methods that exploit the logistic structure represent promising methodological advances. Computational implementations are straightforward using standard numerical integration libraries with the logistic functions and parameter formulas provided herein, enabling immediate adoption by the systems biology community. The logistic framework presented here provides a solid mathematical foundation and a practical modeling toolkit that advances systems biology beyond the limitations of the Hill function. By delivering models that are simultaneously biologically realistic, analytically tractable, and computationally robust, this approach enables precision modeling for synthetic biology circuit design, therapeutic intervention strategies, metabolic engineering optimization, and large-scale network analysis, ultimately contributing to the broader vision of advancing quantitative, predictive biology through rigorous mathematical and computational methods.

## References

- [1] I. Belgacem, S. Casagranda, E. Grac, D. Ropers, J.-L. Gouzé, Reduction and stability analysis of a transcription–translation model of rna polymerase, *Bulletin of Mathematical Biology* 80 (2) (2018) 294–318.
- [2] I. Belgacem, J.-L. Gouzé, R. Edwards, Control of negative feedback loops in genetic networks, in: 2020 59th IEEE Conference on Decision and Control (CDC), IEEE, 2020, pp. 5098–5105.
- [3] L. Chambon, I. Belgacem, J.-L. Gouzé, Qualitative control of undesired oscillations in a genetic negative feedback loop with uncertain measurements, *Automatica* 112 (2020) 108642.
- [4] I. Belgacem, J.-L. Gouzé, Global stability of enzymatic chains of full reversible michaelis-menten reactions, *Acta biotheoretica* 61 (3) (2013) 425–436.
- [5] G. Bernot, J.-P. Comet, A. Richard, M. Chaves, J.-L. Gouzé, F. Dayan, Modeling and analysis of gene regulatory networks, in: Modeling in computational biology and biomedicine: A multidisciplinary endeavor, Springer, 2012, pp. 47–80.
- [6] W. Abou-Jaoudé, M. Chaves, J.-L. Gouzé, A theoretical exploration of birhythmicity in the p53-mdm2 network, *PLOS one* 6 (2) (2011) e17075.
- [7] A. Polynikis, S. Hogan, M. di Bernardo, Comparing different ode modelling approaches for gene regulatory networks, *Journal of theoretical biology* 261 (4) (2009) 511–530.
- [8] S. Bottani, R. A. Veitia, Hill function-based models of transcriptional switches: impact of specific, nonspecific, functional and nonfunctional binding, *Biological Reviews* 92 (2) (2017) 953–963.
- [9] H. Kim, E. Gelenbe, Stochastic gene expression modeling with hill function for switch-like gene responses, *IEEE/ACM Transactions on Computational Biology and Bioinformatics* 9 (4) (2011) 973–979.
- [10] M. Santillán, On the use of the hill functions in mathematical models of gene regulatory networks, *Mathematical Modelling of Natural Phenomena* 3 (2) (2008) 85–97.
- [11] R. Casey, H. d. Jong, J.-L. Gouzé, Piecewise-linear models of genetic regulatory networks: equilibria and their stability, *Journal of mathematical biology* 52 (1) (2006) 27–56.
- [12] H. De Jong, J.-L. Gouzé, C. Hernandez, M. Page, T. Sari, J. Geiselmann, Qualitative simulation of genetic regulatory networks using piecewise-linear models, *Bulletin of mathematical biology* 66 (2) (2004) 301–340.
- [13] J.-L. Gouzé, T. Sari, A class of piecewise linear differential equations arising in biological models, *Dynamical systems* 17 (4) (2002) 299–316.
- [14] T. Gedeon, S. Harker, H. Kokubu, K. Mischaikow, H. Oka, Global dynamics for steep nonlinearities in two dimensions, *Physica D: Nonlinear Phenomena* 339 (2017) 18–38.
- [15] A. A. Nielsen, B. S. Der, J. Shin, P. Vaidyanathan, V. Paralanov, E. A. Strychalski, D. Ross, D. Densmore, C. A. Voigt, Genetic circuit design automation, *Science* 352 (6281) (2016) aac7341.
- [16] G. Rodrigo, A. Jaramillo, Autobiocad: full biodesign automation of genetic circuits, *ACS synthetic biology* 2 (5) (2013) 230–236.
- [17] I. Otero-Muras, D. Henriques, J. R. Banga, Synbadm: a tool for optimization-based automated design of synthetic gene circuits, *Bioinformatics* 32 (21) (2016) 3360–3362.
- [18] M. Stamatakis, N. V. Mantzaris, Comparison of deterministic and stochastic models of the lac operon genetic network, *Biophysical journal* 96 (3) (2009) 887–906.

[19] E. M. Ozbudak, M. Thattai, H. N. Lim, B. I. Shraiman, A. Van Oudenaarden, Multistability in the lactose utilization network of *escherichia coli*, *Nature* 427 (6976) (2004) 737–740.

[20] M. Du, S. Kodner, L. Bai, Enhancement of lacI binding in vivo, *Nucleic acids research* 47 (18) (2019) 9609–9618.

[21] U. Alon, *An Introduction to Systems Biology: Design Principles of Biological Circuits*, Chapman & Hall/CRC Mathematical and Computational Biology Series, Chapman & Hall/CRC, Boca Raton, FL, 2007, see Appendix A: The Input Functions of Genes: Michaelis–Menten and Hill Equations.  
URL [https://www.weizmann.ac.il/mcb/UriAlon/sites/mcb.UriAlon/files/uploads/appendix\\_a.pdf](https://www.weizmann.ac.il/mcb/UriAlon/sites/mcb.UriAlon/files/uploads/appendix_a.pdf)

[22] W. Shi, Y. Ma, P. Hu, M. Pang, X. Huang, Y. Dang, Y. Xie, D. Wu, Hill function-based model of transcriptional response: Impact of nonspecific binding and rnap interactions, *arXiv preprint arXiv:2403.01702* (2024).

[23] T. S. Gardner, C. R. Cantor, J. J. Collins, Construction of a genetic toggle switch in *escherichia coli*, *Nature* 403 (6767) (2000) 339–342.

[24] M. B. Elowitz, S. Leibler, A synthetic oscillatory network of transcriptional regulators, *Nature* 403 (6767) (2000) 335.

[25] F. Farzadfar, T. K. Lu, Genomically encoded analog memory with precise in vivo dna writing in living cell populations, *Science* 346 (6211) (2014) 1256272.

[26] M. Inoue, K. Kaneko, Entangled gene regulatory networks with cooperative expression endow robust adaptive responses to unforeseen environmental changes, *Physical Review Research* 3 (3) (2021) 033183.

[27] A. Polynikis, S. J. Hogan, M. Di Bernardo, Comparing different ode modelling approaches for gene regulatory networks, *Journal of theoretical biology* 261 (4) (2009) 511–530.

[28] K. Hari, W. Duncan, M. A. Ibrahim, M. K. Jolly, B. Cummins, T. Gedeon, Assessing biological network dynamics: comparing numerical simulations with analytical decomposition of parameter space, *npj Systems Biology and Applications* 9 (1) (2023) 29.

[29] I. A. Mellis, M. E. Melzer, N. Bodkin, Y. Goyal, Prevalence of and gene regulatory constraints on transcriptional adaptation in single cells, *Genome biology* 25 (1) (2024) 217.

[30] F. M. Alakwaa, Modeling of gene regulatory networks: a literature review, *Journal of Computational Systems Biology* 1 (1) (2014) 1.

[31] P. Dibaeinia, S. Sinha, Sergio: a single-cell expression simulator guided by gene regulatory networks, *Cell systems* 11 (3) (2020) 252–271.

[32] H. Abelson, An empirical extremum principle for the hill coefficient in ligand-protein interactions showing negative cooperativity, *Biophysical journal* 89 (1) (2005) 76–79.

[33] R. Soong, M. Merzlyakov, K. Hristova, Hill coefficient analysis of transmembrane helix dimerization, *Journal of Membrane Biology* 230 (1) (2009) 49–55.

[34] D. Leiply, D. E. Draper, Dependence of rna tertiary structural stability on mg2+ concentration: interpretation of the hill equation and coefficient, *Biochemistry* 49 (9) (2010) 1843–1853.

[35] G. Quee, R. Edwards, Ramp approximations of sigmoid control functions in gene networks, *Physica D: Nonlinear Phenomena* 418 (2021) 132840.

[36] J. Berkson, A statistically precise and relatively simple method of estimating the bio-assay with quantal response, based on the logistic function, *Journal of the American Statistical Association* 48 (263) (1953) 565–599.

[37] Q. Ke, B. J. Oommen, Logistic neural networks: Their chaotic and pattern recognition properties, *Neurocomputing* 125 (2014) 184–194.

[38] P. E. Puddu, A. Menotti, Artificial neural network versus multiple logistic function to predict 25-year coronary heart disease mortality in the seven countries study, *European Journal of Cardiovascular Prevention & Rehabilitation* 16 (5) (2009) 583–591.

[39] S. Abolmaali, S. Shirzaei, A comparative study of sir model, linear regression, logistic function and arima model for forecasting covid-19 cases, *AIMS public health* 8 (4) (2021) 598.

[40] Y. Koizumi, T. Miyamura, S. Arakawa, E. Oki, K. Shiromoto, M. Murata, Adaptive virtual network topology control based on attractor selection, *Journal of Lightwave Technology* 28 (11) (2010) 1720–1731.

[41] S. Goebbels, On sharpness of error bounds for univariate approximation by single hidden layer feed-forward neural networks, *Results in Mathematics* 75 (3) (2020) 109.

[42] I. Samuilik, F. Sadyrbaev, D. Ogorelova, Mathematical modeling of three-dimensional genetic regulatory networks using logistic and gompertz functions, *WSEAS Transactions on systems and control* 17 (2022) 101107.

[43] F. Sadyrbaev, I. Samuilik, V. Sengileyev, On modelling of genetic regulatory networks, *WSEAS Transactions on Electronics* 12 (1) (2021) 73.

[44] O. Kozlovska, F. Sadyrbaev, In search of chaos in genetic systems, *Chaos Theory and Applications* 6 (1) (2024) 13–18.

[45] I. Samuilik, F. Sadyrbaev, Genetic engineering–construction of a network of arbitrary dimension with periodic attractor, *Vibroengineering Procedia* 46 (2022) 67–72.

[46] F. Sadyrbaev, V. Sengileyev, A. Silvans, On coexistence of inhibition and activation in genetic regulatory networks, in: *International Conference on Numerical Analysis and Applied Mathematics 2021, ICNAAM 2021*, AIP PRESS, 2023.

[47] S. S. Somathilaka, S. Balasubramaniam, D. P. Martins, X. Li, Revealing gene regulation-based neural network computing in bacteria, *Biophysical Reports* 3 (3) (2023).

[48] O. Kozlovska, F. Sadyrbaev, Modeling networks of four elements, *Computation* 13 (5) (2025) 123.

[49] T. W. Tee, A. Chowdhury, C. D. Maranas, J. V. Shanks, Systems metabolic engineering design: fatty acid production as an emerging case study, *Biotechnology and bioengineering* 111 (5) (2014) 849–857.

[50] T. Radivojević, Z. Costello, K. Workman, H. Garcia Martin, A machine learning automated recommendation tool for synthetic biology, *Nature communications* 11 (1) (2020) 4879.

[51] A. Saxena, D. Wu, Advances in therapeutic fc engineering–modulation of igg-associated effector functions and serum half-life, *Frontiers in immunology* 7 (2016) 580.

[52] L. Xie, W. Lu, J. Yu, Y. Zhang, H. Gao, C. Xie, Y. Tian, M. Liu, G. Wang, Regulation of insulin expression and release in gene and cell therapy of insulin-deficient diabetes, *European Journal of Endocrinology* (2025) lvaf231.

[53] B. Xie, P. M. Nguyen, A. Guček, A. Thonig, S. Barg, O. Idevall-Hagren, Plasma membrane phosphatidylinositol 4, 5-bisphosphate regulates  $Ca^{2+}$ -influx and insulin secretion from pancreatic  $\beta$  cells, *Cell chemical biology* 23 (7) (2016) 816–826.

[54] Z. Chen, F. Cao, The properties of logistic function and applications to neural network approximation, *Journal of Computational Analysis and Applications* 15 (6) (2013) 1046–1056.

[55] N. Kyurkchiev, S. Markov, Sigmoid functions: some approximation and modelling aspects, LAP LAMBERT Academic Publishing, Saarbrucken 4 (2015) 34.

[56] B.-S. Chen, C.-W. Li, On the interplay between entropy and robustness of gene regulatory networks, *Entropy* 12 (5) (2010) 1071–1101.

[57] M. E. Hernández-García, J. Velázquez-Castro, Corrected hill function in stochastic gene regulatory networks, *arXiv preprint arXiv:2307.03057* (2023).

[58] R. Reeve, J. R. Turner, Pharmacodynamic models: parameterizing the hill equation, michaelis-menten, the logistic curve, and relationships among these models, *Journal of biopharmaceutical statistics* 23 (3) (2013) 648–661.

[59] P. G. Gottschalk, J. R. Dunn, The five-parameter logistic: a characterization and comparison with the four-parameter logistic, *Analytical biochemistry* 343 (1) (2005) 54–65.

[60] R. Li, J. C. Rozum, M. M. Quail, M. N. Qasim, S. S. Sindi, C. J. Nobile, R. Albert, A. D. Hernday, Inferring gene regulatory networks using transcriptional profiles as dynamical attractors, *PLoS computational biology* 19 (8) (2023) e1010991.

[61] M. Aguirre, J. P. Spence, G. Sella, J. K. Pritchard, Gene regulatory network structure informs the distribution of perturbation effects, *PLOS Computational Biology* 21 (9) (2025) e1013387.

[62] M. Abramowitz, I. A. Stegun, *Handbook of Mathematical Functions with Formulas, Graphs, and Mathematical Tables*, Dover Publications, 1965.

[63] Q. Yuan, Z. Duren, Inferring gene regulatory networks from single-cell multiome data using atlas-scale external data, *Nature Biotechnology* 43 (2) (2025) 247–257.

[64] J. Xu, C. Lu, S. Jin, Y. Meng, X. Fu, X. Zeng, R. Nussinov, F. Cheng, Deep learning-based cell-specific gene regulatory networks inferred from single-cell multiome data, *Nucleic Acids Research* 53 (5) (2025) gkaf138.

[65] H. Faquir, M. Pájaro, I. Otero-Muras, A computational framework for optimal and model predictive control of stochastic gene regulatory networks, *IEEE Transactions on Computational Biology and Bioinformatics* (2025).

[66] J. Kursawe, A. Moneyron, T. Galla, Efficient approximations of transcriptional bursting effects on the dynamics of a gene regulatory network, *Journal of the Royal Society Interface* 22 (227) (2025) 20250170.

[67] C. Chen, M. Padi, Flexible modeling of regulatory networks improves transcription factor activity estimation, *NPJ Systems Biology and Applications* 10 (1) (2024) 58.

[68] G. Mao, R. Zeng, J. Peng, K. Zuo, Z. Pang, J. Liu, Reconstructing gene regulatory networks of biological function using differential equations of multilayer perceptrons, *BMC bioinformatics* 23 (1) (2022) 503.

[69] S. A. Frank, Input-output relations in biological systems: measurement, information and the hill equation, *Biology direct* 8 (1) (2013) 31.

[70] S. Naqvi, S. Kim, H. Hoskens, H. S. Matthews, R. A. Spritz, O. D. Klein, B. Hallgrímsson, T. Swigut, P. Claes, J. K. Pritchard, et al., Precise modulation of transcription factor levels identifies features underlying dosage sensitivity, *Nature genetics* 55 (5) (2023) 841–851.

[71] M. Son, A. G. Wang, H.-L. Tu, M. O. Metzig, P. Patel, K. Husain, J. Lin, A. Murugan, A. Hoffmann, S. Tay, Nf- $\kappa$ b responds to absolute differences in cytokine concentrations, *Science signaling* 14 (666) (2021) eaaz4382.

[72] The FANTOM Consortium and the RIKEN PMI and CLST (DGT), A promoter-level mammalian expression atlas, *Nature* 507 (7493) (2014) 462–470. doi:10.1038/nature13182. URL <https://www.nature.com/articles/nature13182>

[73] D. Madar, E. Dekel, A. Bren, U. Alon, Negative auto-regulation increases the input dynamic-range of the arabinose system of escherichia coli, *BMC systems biology* 5 (1) (2011) 111.

[74] S. Oehler, M. Amouyal, P. Kolkhof, B. von Wilcken-Bergmann, B. Müller-Hill, Quality and position of the three lac operators of e. coli define efficiency of repression., *The EMBO journal* 13 (14) (1994) 3348–3355.

[75] R. Albert, H. G. Othmer, The topology of the regulatory interactions predicts the expression pattern of the segment polarity genes in drosophila melanogaster, *Journal of theoretical biology* 223 (1) (2003) 1–18.

[76] S. Vinoth, S. L. Kingston, S. Srinivasan, S. Kumarasamy, T. Kapitaniak, Extreme events in gene regulatory networks with time-delays, *Scientific Reports* 15 (1) (2025) 13064.

[77] O. Kozlovska, F. Sadyrbaev, Models of genetic networks with given properties, *WSEAS Transactions on Computer Research* 10 (2022) 43–49.

[78] R. Lutz, H. Bujard, Independent and tight regulation of transcriptional units in escherichia coli via the lacr/o, the tetr/o and arac/i1-i2 regulatory elements, *Nucleic acids research* 25 (6) (1997) 1203–1210.

[79] J. R. Kelly, A. J. Rubin, J. H. Davis, C. M. Ajo-Franklin, J. Cumbers, M. J. Czar, K. de Mora, A. L. Gieberman, D. D. Monie, D. Endy, Measuring the activity of biobrick promoters using an in vivo reference standard, *Journal of biological engineering* 3 (1) (2009) 4.

[80] I. Joanito, C.-C. S. Yan, J.-W. Chu, S.-H. Wu, C.-P. Hsu, Basal leakage in oscillation: Coupled transcriptional and translational control using feed-forward loops, *PLOS Computational Biology* 16 (9) (2020) e1007740.

[81] G. Flouriot, C. Jehanno, Y. Le Page, P. Le Goff, B. Boutin, D. Michel, The basal level of gene expression associated with chromatin loosening shapes waddington landscapes and controls cell differentiation, *Journal of molecular biology* 432 (7) (2020) 2253–2270.

[82] Y. Lu, J. Reyes, S. Walter, T. Gonzalez, G. Medrano, M. Boswell, W. Boswell, M. Savage, R. Walter, Characterization of basal gene expression trends over a diurnal cycle in xiphophorus maculatus skin, brain and liver, *Comparative Biochemistry and Physiology Part C: Toxicology & Pharmacology* 208 (2018) 2–11.

[83] M. G. Rees, B. Seashore-Ludlow, J. H. Cheah, D. J. Adams, E. V. Price, S. Gill, S. Javaid, M. E. Coletti, V. L. Jones, N. E. Bodycombe, et al., Correlating chemical sensitivity and basal gene expression reveals mechanism of action, *Nature chemical biology* 12 (2) (2016) 109–116.

[84] M. J. Weickert, S. Adhya, The galactose regulon of escherichia coli, *Molecular microbiology* 10 (2) (1993) 245–251.

[85] S.-S. Hua, A. Markovitz, Multiple regulation of the galactose operon—genetic evidence for a distinct site in the galactose operon that responds to capr gene regulation in escherichia coli k-12, *Proceedings of the National Academy of Sciences* 71 (2) (1974) 507–511. doi:10.1073/pnas.71.2.507.

[86] A. Becskei, L. Serrano, Engineering stability in gene networks by autoregulation, *Nature* 405 (6786) (2000) 590–593.

[87] A. Lipshtat, A. Loinger, N. Q. Balaban, O. Biham, Genetic toggle switch without cooperative binding, *Physical review letters* 96 (18) (2006) 188101.

[88] S. J. Altschuler, L. F. Wu, Cellular heterogeneity: do differences make a difference?, *Cell* 141 (4) (2010) 559–563.

[89] J. L. Cherry, F. R. Adler, How to make a biological switch, *Journal of theoretical biology* 203 (2) (2000) 117–133.

[90] R. Marshall, V. Noireaux, Quantitative modeling of transcription and translation of an all-e. coli cell-free system, *Scientific reports* 9 (1) (2019) 11980.

[91] J. A. Bernstein, A. B. Khodursky, P.-H. Lin, S. Lin-Chao, S. N. Cohen, Global analysis of mrna decay and abundance in escherichia coli at single-gene resolution using two-color fluorescent dna microarrays, *Proceedings of the National Academy of Sciences* 99 (15) (2002) 9697–9702.

[92] G.-W. Li, D. Burkhardt, C. Gross, J. S. Weissman, Quantifying absolute protein synthesis rates reveals principles underlying allocation of cellular resources, *Cell* 157 (3) (2014) 624–635.

[93] K. Nath, A. L. Koch, Protein degradation in escherichia coli: I. measurement of rapidly and slowly decaying components, *Journal of Biological Chemistry* 245 (11) (1970) 2889–2900.

[94] A. Belle, A. Tanay, L. Bitincka, R. Shamir, E. K. O’Shea, Quantification of protein half-lives in the budding yeast proteome, *Proceedings of the National Academy of Sciences* 103 (35) (2006) 13004–13009.

[95] A. Koch, Distribution of cell size in growing cultures of bacteria and the applicability of the collins-richmond principle, *Microbiology* 45 (3) (1966) 409–417.

[96] Y. Setty, A. E. Mayo, M. G. Surette, U. Alon, Detailed map of a cis-regulatory input function, *Proceedings of the National Academy of Sciences* 100 (13) (2003) 7702–7707.

[97] H. El Samad, M. Khammash, L. Petzold, D. Gillespie, Stochastic modelling of gene regulatory networks, *International Journal of Robust and Nonlinear Control: IFAC-Affiliated Journal* 15 (15) (2005) 691–711.

[98] D. Del Vecchio, A. J. Dy, Y. Qian, Control theory meets synthetic biology, *Journal of The Royal Society Interface* 13 (120) (2016) 20160380.

[99] C. Barajas, D. Del Vecchio, Synthetic biology by controller design, *Current Opinion in Biotechnology* 78 (2022) 102837.

[100] J. J. Teo, S. S. Woo, R. Sarpehkar, Synthetic biology: A unifying view and review using analog circuits, *IEEE transactions on biomedical circuits and systems* 9 (4) (2015) 453–474.

[101] R. Sarpehkar, Analog synthetic biology, *Philosophical Transactions of the Royal Society A: Mathematical, Physical and Engineering Sciences* 372 (2012) (2014) 20130110.

[102] A. Loinger, O. Biham, Stochastic simulations of the repressilator circuit, *Physical Review E—Statistical, Nonlinear, and Soft Matter Physics* 76 (5) (2007) 051917.

[103] S. C. Makrides, Strategies for achieving high-level expression of genes in escherichia coli, *Microbiological reviews* 60 (3) (1996) 512–538.

[104] M. Acar, A. Becskei, A. Van Oudenaarden, Enhancement of cellular memory by reducing stochastic transitions, *Nature* 435 (7039) (2005) 228–232.

[105] L. Huang, Z. Yuan, P. Liu, T. Zhou, Effects of promoter leakage on dynamics of gene expression, *BMC systems biology* 9 (1) (2015) 16. doi:10.1186/s12918-015-0157-z.

[106] F. Jacob, J. Monod, Genetic regulatory mechanisms in the synthesis of proteins, *Journal of molecular biology* 3 (3) (1961) 318–356.

[107] G. K. Ackers, A. D. Johnson, M. A. Shea, Quantitative model for gene regulation by lambda phage repressor., *Proceedings of the national academy of sciences* 79 (4) (1982) 1129–1133.

[108] Z. Zuo, G. D. Stormo, High-resolution specificity from dna sequencing highlights alternative modes of lac repressor binding, *Genetics* 198 (3) (2014) 1329–1343.

[109] C. M. Falcon, K. S. Matthews, Operator dna sequence variation enhances high affinity binding by hinge helix mutants of lactose repressor protein, *Biochemistry* 39 (36) (2000) 11074–11083.

[110] S. Kumar, S. Anastassov, S. K. Aoki, J. Falkenstein, C.-H. Chang, T. Frei, P. Buchmann, P. Argast, M. Khammash, Diya—a universal light illumination platform for multiwell plate cultures, *Iscience* 26 (10) (2023).

[111] M. Razo-Mejia, S. L. Barnes, N. M. Belliveau, G. Chure, T. Einav, M. Lewis, R. Phillips, Tuning transcriptional regulation through signaling: a predictive theory of allosteric induction, *Cell systems* 6 (4) (2018) 456–469.

[112] R. Sawlekar, F. Montefusco, V. Kulkarni, D. G. Bates, Biomolecular implementation of a quasi sliding mode feedback controller based on dna strand displacement reactions, in: 2015 37th Annual International Conference of the IEEE Engineering in Medicine and Biology Society (EMBC), IEEE, 2015, pp. 949–952.

[113] D. Del Vecchio, R. M. Murray, *Biomolecular feedback systems*, Princeton University Press Princeton, NJ, 2015.

[114] J.-B. Lugagne, C. M. Blassick, M. J. Dunlop, Deep model predictive control of gene expression in thousands of single cells, *Nature Communications* 15 (1) (2024) 2148.

[115] T. Gedeon, Multi-parameter exploration of dynamics of regulatory networks, *Biosystems* 190 (2020) 104113.

[116] B. Cummins, T. Gedeon, S. Harker, K. Mischaikow, K. Mok, Combinatorial representation of parameter space for switching networks, *SIAM journal on applied dynamical systems* 15 (4) (2016) 2176–2212.

[117] P. V. Kharchenko, L. Silberstein, D. T. Scadden, Bayesian approach to single-cell differential expression analysis, *Nature methods* 11 (7) (2014) 740–742.

[118] V. Svensson, K. N. Natarajan, L.-H. Ly, R. J. Miragaia, C. Labalette, I. C. Macaulay, A. Cvejic, S. A. Teichmann, Power analysis of single-cell rna-sequencing experiments, *Nature methods* 14 (4) (2017) 381–387.

[119] I. Belgacem, F. Delaplace, Forward-backward binarization, *arXiv preprint arXiv:2510.16183* (2025).

[120] F. Crauste, Equations à retard et modèles de dynamiques de populations cellulaires, Ph.D. thesis, Université Claude Bernard Lyon 1 (2014).

[121] C. Haurie, D. C. Dale, M. C. Mackey, Cyclical neutropenia and other periodic hematological disorders: a review of mechanisms and mathematical models, *Blood, The Journal of the American Society of Hematology* 92 (8) (1998) 2629–2640.

[122] D. t. Guerry, D. Dale, M. Omine, S. Perry, S. Wolff, et al., Periodic hematopoiesis in human cyclic neutropenia, *The Journal of Clinical Investigation* 52 (12) (1973) 3220–3230.

[123] D. Dale, W. Hammond IV, Cyclic neutropenia: a clinical review, *Blood reviews* 2 (3) (1988) 178–185.

[124] N. Giordano, F. Mairet, J.-L. Gouzé, J. Geiselmann, H. De Jong, Dynamical allocation of cellular resources as an optimal control problem: novel insights into microbial growth strategies, *PLoS computational biology* 12 (3) (2016) e1004802.

[125] H. De Jong, S. Casagranda, N. Giordano, E. Cinquemani, D. Ropers, J. Geiselmann, J.-L. Gouzé, Mathematical modelling of microbes: metabolism, gene expression and growth, *Journal of The Royal Society Interface* 14 (136) (2017) 20170502.

[126] B. I. Escher, P. A. Neale, D. L. Villeneuve, The advantages of linear concentration–response curves for in vitro bioassays with environmental samples, *Environmental toxicology and chemistry* 37 (9) (2018) 2273–2280.

[127] M. S. Salahudeen, P. S. Nishtala, An overview of pharmacodynamic modelling, ligand-binding approach and its application in clinical practice, *Saudi Pharmaceutical Journal* 25 (2) (2017) 165–175.

[128] Q. Zhang, A. M. Schmidt, Y. P. Chaubey, Modeling left-censored skewed spatial processes: The case of arsenic drinking water contamination, *Spatial Statistics* 59 (2024) 100816.

[129] J. W. Little, Threshold effects in gene regulation: When some is not enough, *Proceedings of the National Academy of Sciences* 102 (15) (2005) 5310–5311.

[130] H. F. Nijhout, Dominance, thresholds and boundaries, *The biology of genetic dominance* (2006) 61.

[131] H. F. Nijhout, Stochastic gene expression: Dominance, thresholds and boundaries, in: *Madame Curie Bioscience Database [Internet]*, Landes Bioscience, Austin (TX), 2000, available from: <https://www.ncbi.nlm.nih.gov/books/NBK6366/>.

[132] M. D. Robinson, A. Oshlack, A scaling normalization method for differential expression analysis of rna-seq data, *Genome biology* 11 (3) (2010) R25.

[133] R. Yu, E. Vorontsov, C. Sihlbom, J. Nielsen, Quantifying absolute gene expression profiles reveals distinct regulation of central carbon metabolism genes in yeast, *Elife* 10 (2021) e65722.

[134] E. M. Sanford, B. L. Emert, A. Coté, A. Raj, Gene regulation gravitates toward either addition or multiplication when combining the effects of two signals, *Elife* 9 (2020) e59388.

[135] M. A. Gillespie, C. G. Palii, D. Sanchez-Taltavull, P. Shannon, W. J. Longabaugh, D. J. Downes, K. Sivaraman, H. M. Espinoza, J. R. Hughes, N. D. Price, et al., Absolute quantification of transcription factors reveals principles of gene regulation in erythropoiesis, *Molecular cell* 78 (5) (2020) 960–974.

[136] K. Kuhlmann, M. Cieselski, J. Schumann, Relative versus absolute rna quantification: a comparative analysis based on the example of endothelial expression of vasoactive receptors, *Biological procedures online* 23 (1) (2021) 6.

[137] L. A. Cox Jr, H. B. Ketelslegers, R. J. Lewis, The shape of low-concentration dose–response functions for benzene: implications for human health risk assessment, *Critical Reviews in Toxicology* 51 (2) (2021) 95–116.

- [138] S. W. Jarantow, E. D. Pisors, M. L. Chiu, Introduction to the use of linear and nonlinear regression analysis in quantitative biological assays, *Current Protocols* 3 (6) (2023) e801.
- [139] W. J. Waddell, Dose-response curves in chemical carcinogenesis, *Nonlinearity in Biology, Toxicology, Medicine* 2 (1) (2004) 15401420490426954.
- [140] F. Kappenberg, J. C. Duda, L. Schürmeyer, O. Gül, T. Brecklinghaus, J. G. Hengstler, K. Schorning, J. Rahnenführer, Guidance for statistical design and analysis of toxicological dose-response experiments, based on a comprehensive literature review, *Archives of Toxicology* 97 (10) (2023) 2741–2761.
- [141] FutureLearn, Absolute vs. relative quantification for qPCR, <https://www.futurelearn.com/info/courses/molecular-biology-how-to-detect-pathogens-in-aquaculture/0/steps/372218>, accessed: 2025-08-25.